Self-Assembling Networks in Microemulsions and Dipolar Fluids

Tsvi Tlusty

Supervisor: Prof. Samuel A. Safran

Department of Materials and Interfaces,

Weizmann Institute of Science

Thesis for the degree of Ph. D.

submitted to the scientific council

of the Weizmann Institute of Science

October 2000

Abstract

We use a model of fluctuating networks to link the structure and thermodynamics of two, linearly aggregating, self-assembling systems, microemulsions and dipolar fluids. In the linear aggregation regime, these two systems that consist very different molecular building blocks, exhibit the same basic thermodynamic and structural features.

By modeling microemulsions as fluctuating networks made of interconnected cylinders of oil-in-water or water-in-oil with amphiphilic molecules at the interfaces, we explained their unique thermodynamics, especially the observation of re-entrant phase separations and associated critical points. We show that the interplay between entropy and structure, governed by the statistics of the topological defects, the junctions and "dead-ends" of the network, provides an explanation for the observed universality of both the structure and phase behavior. The theoretical predictions are in agreement with the thermodynamic measurements and with direct, cryo-TEM observations of the network structures.

Our analysis suggests that the same concept of fluctuating networks may resolve the intriguing question concerning the existence of the usual liquid-gas transition in dipolar fluids. We predict a defect induced, critical phase separation that replaces the usual liquid-gas transition driven by the isotropic aggregation of particles. Our model explains for the branched structures, the unusually low critical temperature and density, and the two-phase coexistence "islands" that have been recently observed in simulation.

Contents

ACKNOWLEDEGEMENT. I would first like to sincerely and especially thank my thesis advisor, Prof. Samuel Safran. I have benefited greatly from his profound and constructive advice, about both science and life. His guidance was like a stream of aphorisms and words of wisdom and I see it as a great privilege to have been taught by him for four years. His friendliness and insight opened up new paths for me to explore. Even though he has one of the busiest jobs in Weizmann, dean of the Feinberg college, Sam always found time for lengthy, intensive sessions on science. He has the special talent to carefully navigate the thesis ship by generously sparing stimulating ideas and advice, but at the same time building a feeling of independence and providing a spur to the confidence of his students.

Our research on self-assembling networks of microemulsion has been a consistent collaboration with experimental groups. Prof. Reinherd Strey and Dr. Thomas Sottmann from Cologne provided us with the most detailed and careful thermodynamic and structural measurements, results of and extensive long going study of microemulsions, which inspired our research. Prof. Ishi Talmon and Dr. Anne Bernheim-Grosswasser from the Technion made state of the art cryo-TEM measurements of microemulsions that provided the first direct evidence for the existence of networks in the system, and posed us many other unresolved questions. Thanks to Ishi and Anne, now in Paris, I have learned how exciting a bare electron micrograph can be. The generous Prof. Elisha Moses let me participate me in many of his diverse research activities. It has always been a pleasure to hear his alternative views on the state of humanity and academy while drinking his excellent espressos and steeling books from his rich library. I thank Elisha for the concise manual for survival in Manhattan he gave me. I hope it will help me in the coming years. Elisha is also my examiner together with Prof. David Maukamel. I thank them for their careful guidance of my research.

Prof. Phillip A. Pincus from Santa-Barbara is a pioneer in the research of soft condensed matter and the Weizmann oriental cuisine (he is one of the few living daredevils who survived both the “Ping Pong” restaurant and the “dirty-finger” bistro, not to mention the world infamous ”San-Martin”). Prof. Pincus has encouraged and inspired our work on dipolar fluids while personifying the optimal cursing-friendly environment that young, impolite scientists so desperately need. My friendship with Dr. Roy Bar-Ziv began long ago when we were M. Sc. students. During the following years Roy privileged me by collaborating in many of his studies with Elisha. No one could understand better than him the emotional and intellectual ups and downs that I have been through during these years. During my visits to New-York, Roy has been the perfect host. I hope that I will be able to repay his hospitality. Dr. Becky Menes has started the work on microemulsions that led to the self-assembling network model. I thank her for my scientific initiation in Sam’s group and for more importantly, for being a great friend: her incredible warmth is felt even when she is ten thousand miles away in Los-Angeles. I wish her the best. About my friendship with Uri Alon (a.k.a “il professore”) what can I say. Suffice I mention the names of David and Jonathan, Gilbert and Sullivan, Max und Moritz.

An important appreciation goes to my roommates. They put up with my alternating moods of stress, depression, calculation rage and seclusion. Aharon Weinstein directed me as a freshman in the maze of the Weizmann Ph. D. life. I wish him success in his new career. I shared his experience with Dima Lukatsky and Anton Zilman to whom I wish success in completing their Ph. D. studies. I also thank Pierre Sens, Eugene Gurevich and Ulrich S. Schwarz. Being a member of the Materials and Interfaces Department I cannot but express my deep thanks to Herut Sharan and Zelu Itskovich, an omnipotent yet smile enriched administrative team. Special thanks are dedicated to Prof. Meir Lahav, head of the department, for his generous support in our reasearch. For making every meeting with bureaucracy a pleasure I thank Batya Kfir, Yosefa Givoli and all the members of the Feinberg college administration. I thank the gardeners of the Weizmann Institute, with their Alice in Wonderland golf carts, for keeping this hidden oasis flourishing within the asphalt jungle of the Dan megalopolis.

I had the unique privilege to be the son of Joseph and Geula Tlusty. From childhood they nurtured me and supplied boundless love which was a mighty support that carried me to the end of my education odyssey. Mom’s succulent delicacies that I brought back from Haifa every week fortified my flesh just as the comfort and love which were showered upon me during the weekends visits sustained my spirit. My sisters, Merav and Tal, are my best friends and spread sunshine and laughter in my life. I wish for them both only the best that life can offer. Tagel, my light and my love. The praise you deserve I will tell you myself.

Publications on Self-Assembling Networks

- Chap. 2: **Scaling Laws for Microemulsions Governed by Spontaneous Curvature**
  T. Tlusty, R. Menes, S. A. Safran and R. Strey, *Phys. Rev. Lett.* **78**, 2616 (1997).
- Chap. 3: **Topology, Phase Instabilities and Wetting of Microemulsion Networks**
  T. Tlusty, S. A. Safran and R. Strey, *Phys. Rev. Lett.* **84**, 1244 (2000).
- Chap. 4: **Direct Observation of Phase Separation in Microemulsion networks**
  A. -B. Grosswasser, T. Tlusty, S. A. Safran, Y. Talmon, *Langmuir* **15**, 5448 (1999).
- Chap. 5: **Microemulsion Networks: The Onset of Bicontinuity**
  T. Tlusty, S. A. Safran, *J. Phys.: Cond. Mat.* **12**, A253 (2000).
- Chap. 6: **Defect Induced Phase Separation in Dipolar Fluids**
  T. Tlusty and S. A. Safran, *Science* **290**, 1328-1331 (2000).

1
Introduction

1.1 Self-Assembly of Soft Matter

Soft matter refers to materials that are much more deformable than ordinary solids or fluids. Even relatively weak forces, such as those involved in Brownian motion, are usually sufficient to significantly distort their structure. An extensively studied class of soft materials are systems of amphiphiles, molecules consisting of hydrophilic (water soluble) polar or charged groups covalently bonded to hydrophobic (water insoluble) hydrocarbon chains. Two examples of amphiphiles are surfactants (soaps) and lipids, the main constituent of cell membrane [1, 2]. The physical properties of soft matter vary strongly when observed on different length scales. Typically, the molecules of soft matter are grouped together within larger, more complex structures, such as polymers formed by covalent bonding of monomers, or micelles formed by the hydrophobic interaction between surfactant molecules and the surrounding water. On microscopic length scales, the relative motion of the elementary molecules within such aggregates is fairly constrained. By contrast, on mesoscopic length scales, the set of molecules forming each aggregate can move collectively, via center-of-mass diffusion or long wave-length fluctuations. The basic constituents or "particles" of these *complex fluids*, as they are sometimes called because of their large-scale, fluid-like properties, are not the individual molecules but the aggregates that they form [3, 4].

The softness of matter is deeply related to this complexity. The strength of a certain material is quantitatively characterized by its elastic moduli that scale like $e \sim E/L^d$, where E and L are the typical inter-particle interaction energy and distance, respectively, and d is the dimensionality. In ordinary 3-dimensional atomic solid, the typical distance is of a few angstroms and the typical bond energy is $0.1 - 1eV$ (this cohesive energy is large for ionic bonds and smaller for hydrogen or van der Waals bonds). This results in an elastic moduli of order $e \sim eV/\text{Å}^3$ [6]. In complex fluids, however, the typical distance between the large aggregates is *mesoscopic*, $L \sim 10^2 - 10^4\text{Å}$, which decreases the strength

by 4-10 orders of magnitude. Moreover, the energy scale of inter-aggregate forces is typically much lower than the eV energy scale of molecular forces, further increasing the deformability of soft matter [10]. When the energy scale of interaction exceeds k_BT, the energy scale of thermal fluctuations, the system overcomes the entropic tendency to homogenize and the basic aggregates self-organize and create large-scale, global order.

Self-assembly (or self-organization) occurs when the structure is determined not by external forces in an a priori manner, but rather by internal interactions [3]. In equilibrium, it arises from the interplay between a structure-dependent energy and the thermal fluctuations that drive the self-assembling system towards a state of maximal entropy. Non-equilibrium self-assembly may be driven by kinetic processes such as diffusion limited aggregation of colloidal particles [11, 12]. The properties of self-assembling systems are governed by their collective behavior, in contrast to "simpler" systems, whose basic properties can be understood in terms of two-body interactions. The large-scale properties of self-assembling systems are mainly affected by their universal, geometrical characteristics and less by the chemical details. A prominent example for the collective self-organization is the rich variety of ordered structures exhibited by amphiphilic interfaces [13, 14] and diblock copolymers [15, 16, 17], such as lamellar, hexagonal and cubic phases. The similarity of structures and phase diagrams between these two systems, of very different microscopic building blocks, indicates the influential role of universal properties that govern the thermodynamics of self-assembly. In non-equilibrium systems, another manifestation of this material independent universality is the fractal, scale-invariant structure of diffusion limited colloidal aggregates [12].

The sensitivity of self-assembling systems to physical parameters such as temperature, electric field and concentration provides a fine tuned control of their spatial organization in complex structures of various topologies and sizes, on the nanoscale and beyond. In nature, many components of the living cell that are crucial for its functionality are self-assembled structures, such as the lipid membrane that envelope the cell and its organelles, the DNA complexes that carry its genetic information and the actin and tubulin networks that provide mechanical strength and enable cell motility [1, 2]. Complex fluids have overwhelming industrial importance as detergents, paints, food materials and cosmetics. The nature of self-assembly systems allows the design of sophisticated supramolecular materials that possess novel characteristics unattainable in simpler systems. Among the possible applications are microelectronics and data storage devices. Of special interest are designs that try to mimic the functions of biological materials, such as artificial ion channels, artificial muscles [18], or designed DNA crystals [19].

Often, the inter-aggregate forces are of entropic origin and therefore have an energy scale comparable with the k_BT energy scale of thermal fluctuations. Two significant examples for such entropy driven forces are the repulsion between undulating surfactant membranes, which leads to smectic order of lamellae [20], and the entropic interaction of ionized solutions which leads to the formation of macroscopic crystalline order of colloidal macroions. Entropy driven interactions are of special interest, since

in this case the interplay between the structure dependent energy and thermal fluctuations leads to the formation of complex, random structures.

1.2 Self-Assembling Networks

In the present work we treat two self-assembling systems that under certain conditions show aggregation into linear, polymer-like structures. Most of the work focuses on microemulsions (Chaps. **2**-**5**) , dispersions of polar (oil) non-polar (water) fluids and amphiphile. A related system treated in Chap. **6** are dipolar fluids composed of magnetic colloidal nano-particles. While the microscopic building blocks of these systems have nothing in common, we show that both possess the same basic large-scale structural and thermodynamic features, another manifestation of the universal nature of self-assembly.

Topological defects play a crucial role in the thermodynamics of one-dimensional systems. It is well-known 1D statistical system with short-range interaction, e.g. an Ising ferromagnet or a lattice gas, lacks a first-order phase transition at non-zero temperature due to the proliferations of domain-wall defects [21] (although phase transitions may occur at $T > 0$ when long-range forces are introduced). By analogy, it was shown that self-assembling worm-like micelles do not separate into a coexistence of a phase of infinite and a phase of short micelles, but instead, exhibit a broad exponential length polydispersity [22, 26]. In this case the topological defects are the micelle ends.

Our analysis shows that the global topology of these two linearly aggregating, self-assembling systems, microemulsions and dipolar fluids, is also governed by entropically induced defects. The energetically favorable state of the amphiphilic molecules or magnetic colloidal particles is when they aggregate in linear structures, and defects occur only due to the entropy increase caused by their introduction. Apart from terminating at an end, these linearly aggregating systems may also contain another kind of defects, branch points. When the branch points dominate over the ends the linear branches self-organize to form *large-scale networks*. Our theory focuses on the topologically induced interactions within such fluctuating networks and provides a unified understanding of both their structure and thermodynamics.

1.3 Microemulsions

In the case of microemulsions, dispersions formed by the addition of an amphiphilic agent to a system containing oil and water, the collective character of self-assembling systems is expressed by a rich variety of topologies [3, 26]. Even the presence of small amount of amphiphile can facilitate the local mixing of the usually insoluble polar (water) and non-polar (oil) by creating complex fluids [23, 24, 25]. These ternary mixtures, which are thermodynamically stable, seem to be homogeneous when observed in visible light [27]. However, shorter wave-length scattering experiments [28] and microscopy [29, 31] reveal intricate microstructures: The amphiphile tends to self-assemble at interfaces separating the water

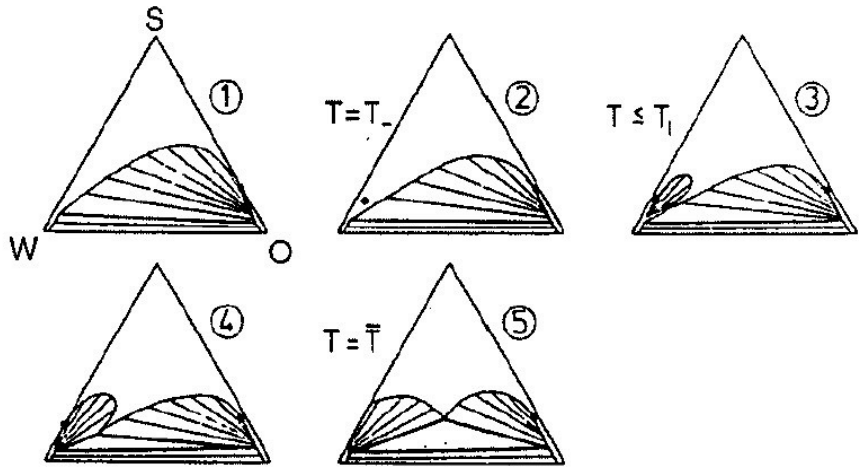

FIGURE 1.1. **Evolution of the two-phase reentrant loops and the subsequent three-phase regions** — The triangles are isothermal cuts through the phase diagram (W- water, O- oil, S - amphiphile) that trace the multi-phase regions as the system approaches the symmetric regime ($c_0 \simeq 0$): The loop appears as a bicritical point (2), expands (3) and collides with the emulsification failure region (4), yielding the three-phase region (4-5) [49].

and oil regions with its polar head residing in the water and its non-polar tail in the oil. Due to this unusual surface activity these molecules are termed *surfactants*. The domains defined by the surfactant interfaces are large compared with the microscopic molecular length scales. Their typical lengths are *mesoscopic*, ranging from tens of nanometers up to few microns while typical surfactant length is only $1 - 4$ nanometer.

The phase diagrams of microemulsions were the main subject of the early experimental studies [32, 33, 34], which originated from the research of solubilization and emulsification properties of soaps. Measurements of microemulsions phase behavior [35] discovered that certain ternary systems exhibit coexistence two- or three-phase coexistence regions around some typical temperature, $\bar{T}$ (Fig. 1.1; detailed description of the phase behavior is found in Refs. [25] and [36].) The systematic research of the last two decades, mainly by Kahlweit, Strey and their co-workers [36, 37, 38], observed that these phase patterns are a generic feature of microemulsion systems, not an accidental material-specific property. They have shown that close to $\bar{T}$ microemulsions exhibit unique thermodynamic behavior, especially the appearance of the critical, reentrant two-phase separation [39, 40] that evolves into a three-phase region as $\bar{T}$ is approached further [41] (Fig. 1.1). Furthermore, recent studies [42, 43] suggest that generality of certain phase behavior characteristics is not merely a qualitative feature of microemulsions; the data from distinct ternary systems collapse onto a single curve revealing quantitative *universality* and *scaling* properties.

The microstructure related to this phase behavior has been studied using either direct microscopy methods [31, 29] or scattering and Fourier-space analysis [28]. The microemulsion scattering structure factor exhibits a characteristic wave-length dependence [44]. A prominent characteristic is the appearance of distinct peaks shown at non-zero wave-vector that depend on the composition and the temperature of the system [44] This indicates the existence of mesoscopic structures [41]: globular phases, bicontinuous sponges, and even ordered phases such as lamellar or cubic. The structure is determined by the detailed interplay between the entropy of the solutes and the energetics of surfactants. In general, if there is enough surfactant the microemulsion exhibits an ordered lyotropic phase. With fewer surfactant molecules there are still oil and water domains separated by an amphiphilic interface but they are *disordered* due to entropic effects [45, 46]. If the amount of surfactant is further reduced, there is not enough interface to create mesoscopic domains and the system tends to reject the excess amount of pure water or oil into a separate phase such that the concentration of surfactant in the rest of system suffices to produce domains of the optimal size [48]. The topology of a given microemulsion phase is determined by the arrangement of the amphiphilic monolayers that separate the oil and water domains. This microstructure is controlled by the composition of the microemulsion and by the value of the spontaneous curvature, c_0, the preferred curvature of the amphiphile monolayer towards water or oil [7], which can be changed by varying temperature, chain length or salinity. One possible classification of microemulsions is according to this topology: *(i)* In the so-called "symmetric" region, where the spontaneous curvature is small, microemulsions at low amphiphile volume fractions typically form sponge-like, multiply connected, *bicontinuous* structures with interwoven water and oil labyrinths that are both continuous. In this region the microemulsion phase can coexist with both aqueous an oil-rich phase (this three phase coexistence is sometimes termed "Winsor III" [33]). (ii) For large values of c_0, the microstructure is typically one of disconnected oil-in-water or water-in-oil globules [22]. In this region, the globular phase can coexist with a bulk oil (Winsor I) or water (Winsor II) phases (Fig.1.1).

The ultra-low interfacial tension. In experiment, the reentrant phase separation and the related formation of bicontinuous phase are accompanied by a decrease of the interfacial tensions between the coexisting phases by 3-5 orders of magnitude (relative to the bare oil/water value [36, 49]). Strey and Sottmann have shown that the tension curves also exhibit universal scaling [50, 52].

Previous theories were able to produce some of the prominent experimental features of microemulsions, but not the reentrant phase separation with its critical points [53]. Chap. **2** describes how our model of microemulsions in this regime as fluctuating networks whose building blocks are cylindrical amphiphilic water-in-oil or oil-in-water tubes [54]. This model relates the physics of the progression of the microemulsion topology to the striking, universal thermodynamics [43]. The observed, re-entrant phase separation, characterized by the closed loops (Fig. 1.1 - phase diagrams 3, 4), is explained as a direct result of the connected topology of the network that induces an effective attraction between junction points in the network. The topologically induced attraction, which is governed by the material-

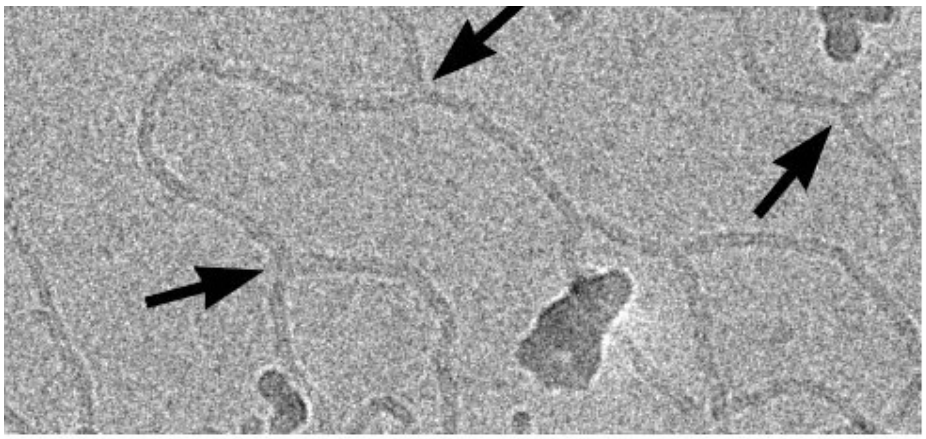

FIGURE 1.2. **Microemulsion network** — Cryogenic transmission electron microscope image of microemulsion shows the formation of the semi-flexible network and its 3-fold junctions [A. Bernheim-Grosswasser and Y. Talmon (to be published)].

independent statistics of the junctions explains the experimentally observed universality demonstrated by the data collapse of phase diagrams of non-ionic microemulsions [42, 50]. In Chap. **3** we calculate the scaling of the ultra-low interfacial tension as a function of the spontaneous curvature and show that this is a direct outcome of the network topology which leads to the 2-phase and 3-phase coexistence. We also predict the related wetting transition [55], in accord with experiment [56].

The fluctuating networks model predicts the existence of bicontinuous structures relatively far from the symmetric sponge regime. The bicontinuous regime spans from the sponge to a region of dilute, highly asymmetric networks formed by interconnected amphiphile cylinders. Chap. **4** describes our collaboration with the experimentalists Anne Bernheim-Grosswasser and Y. Talmon of the Technion, who directly verified this prediction by cryogenic transmission electronic microscopy (cryo-TEM) measurements (Fig. 1.2). The images strongly support the prediction that the critical phase separation of microemulsions is into two coexisting networks which differ in their density of junctions [57].

The cryo-TEM measurement also confirmed that at the boundaries of the bicontinuous regime the networks break up into disconnected cylindrical globules [57]. We have found that this connectivity transition occurs when the curvature energies of both defects, ends and branch points, are approximately equal. This is discussed in Chap. **5**, where we calculate the defect energies by means of a numerical minimization and a simplified analytical approximation. The results show that junctions are preferred at low values of the spontaneous curvature while ends are preferred at larger spontaneous curvature due to their curved spherical cap. The cross over between these two regimes heralds the formation of a connected network [58]. The anomalous reentrant nature of this phase separation in both microemulsion and dipolar fluids results from the non-monotonic dependence of the defect energy on system parameters, as explained in Chap. **2**.

1.4 Dipolar fluids

Dipolar fluids have numerous scientific and industrial applications, mostly related to their strong field-responsive properties [59, 60]. Ferrofluids are stable colloidal dispersions of ferromagnetic particles, such as cobalt, iron oxide (Fe_3O_4) or nickel, coated with stabilizing surfactant or silica layers and dispersed in a host liquid, such as water or paraffin [60]. Applications based on their high magnetic susceptibility include floppy disks, credit cards, video tapes, loudspeakers, rotating shaft seals (as in computer hard disk drives) and exclusion seals [61]. Another class of dipolar fluids, electro-rheological fluids, are colloidal dispersions of highly polarizable particles in solvents with low dielectric constant, whose rheological and mechanical properties change dramatically when an electric field is applied [62].

Dipolar fluids also have theoretical significance as one of the most basic models of statistical mechanics, since they are perhaps the simplest example of an anisotropic fluid. Nevertheless, the physical understanding of this seemingly simple system is far from being complete. One of the fundamental, yet unresolved questions in this field is the existence of a liquid-gas transition [63]. Adopting the basic framework of simple liquids theory, one may first calculate the second virial coefficient of hard spheres with only dipolar interaction to obtain a van der Waals like, $1/r^6$ attraction [64, 65]. This result suggests that one might expect a liquid-gas transition to occur as the temperature is decreased [66].

However, this naive argument seems to contradict with the results of some recent simulation studies which failed to observe such a liquid-gas transition in the phase diagram. Instead, it was found that as temperature decreases, the dipolar interaction, which favors a nose-to-tail alignment of the dipoles, drives the particles to form polymer-like semi-flexible chains [68, 69, 70, 71, 72] as predicted by theories [67]. This chaining process reduces the typical coordination number since a particle in a chain has only two nearest neighbors, much less than a particle in a random, close-packed isotropic aggregate. Thus, the driving force for phase separation, the average attractive interaction per particle, is much weaker in this system. Many studies have attributed the absence of liquid-gas transition to this strongly collective behavior of the dipolar particles which interferes with the isotropic aggregation crucial for such transition to occur [73]-[84]. Due to the one-dimensionality of the chains, defects proliferate and prevent phase separation [21, 22]. Of course, if an enough isotropic attraction is present (e.g. the usual van der Waals dispersion interaction), the usual isotropic aggregation and the resulting liquid-gas separation can occur [74, 85, 86, 87]. However, the interesting and controversial point is whether phase separation can be driven by the dipolar interaction alone. Recent computer simulations have found evidence for a liquid-gas transition in a system of hard spheres with solely dipolar interactions [89]. Near the critical point, the spheres assemble in chains that form networks with apparent branch points. Thermodynamic measurements found evidence for a critical [90] liquid-gas transition [91] in magnetic fluids consisting of ferric oxide nano-spheres. However, in this colloidal fluid it is difficult to separate the effect of the dipolar interaction from the short-range, isotropic attraction [92].

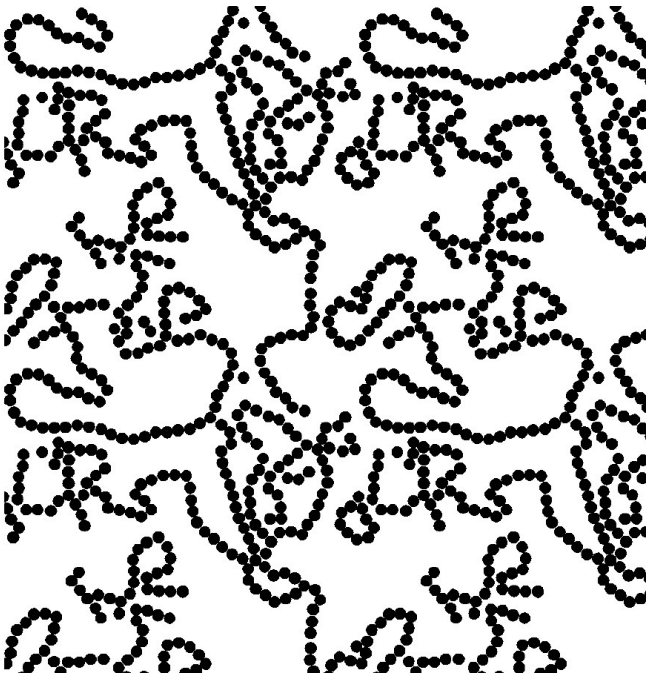

FIGURE 1.3. **Dipolar network** — A simulation of a self-assembling network (2D) composed of dipolar hard spheres by Davis et al. [93].

Motivated by this preliminary evidence, we apply, in Chap. **6**, the concepts of the network model to dipolar fluids. In this case, it is the anisotropic dipolar interaction that drives the linear chaining of the particles and the subsequent formation of networks when the chains are interconnected by junctions (Fig. 1.3) [93, 94, 95]. Our analysis suggests a resolution of the intriguing question concerning the existence of the critical liquid-gas transition. We propose a novel, defect-induced liquid-gas transition that is driven by the formation of dipolar networks [88], in accord with recent evidence for the occurrence of such a transition in computer simulations. The model also explains the existence of closed, two-phase coexistence "islands" in the phase diagram of sphero-cylindrical dipoles [89, 96, 97], an analogue of the reentrant behavior of microemulsions. Noteworthy, in the context of this deep analogy, are recent experimental studies on combined systems of magnetic nano-particles within self-assembling amphiphiles [64, 80].

In Chap. **7** we summarize the results of the theory in the context of recent experimental findings and suggest directions for future work.

2

Scaling Laws for Microemulsions Governed by Spontaneous Curvature

Scaling Laws for Microemulsions Governed by Spontaneous Curvature

T. Tlusty,[1] S. A. Safran,[1] R. Menes,[1] and R. Strey[2]
[1]*Department of Materials and Interfaces, The Weizmann Institute of Science, Rehovot 76100, Israel*
[2]*Max-Planck-Institut für Biophysikalische Chemie, Postfach 2841, 37018 Göttingen, Germany*
(Received 30 September 1996)

We introduce a model for microemulsions whose basic building blocks are cylindrical tubes connected by spherical junctions forming a network. The model predicts analytic scaling laws which quantitatively reproduce several prominent experimental features of the phase diagram, including the closed loops of 2-phase coexistence and the 3-phase body. The interfacial nature of our model, which takes into account only the curvature energy and the entropy of the interface, explains the observed water/oil symmetry and the collapse of the experimental data onto a single universal scaling curve. [S0031-9007(97)02840-8]

PACS numbers: 82.70.Kj, 64.70.Ja, 64.75.+g

Recent studies of nonionic microemulsions (ME) have provided systematic experimental knowledge concerning their structure and phase behavior. The phase diagrams of these simplest ternary systems, which contain water, oil, and a nonionic surfactant, are fairly universal. Among the prominent features is the coexistence of either two or three phases in a temperature regime around $\bar{T}$, the temperature where the average curvature of the surfactant interfacial film vanishes [1]. The progression of the multiphase regions as a function of temperature exhibits a remarkable water/oil symmetry: As the temperature is increased above a critical value, $T_- < \bar{T}$ a two-phase closed loop with two critical points appears in the water-rich corner of the phase diagram (the oil volume fraction $\phi \sim 0.1$). A symmetrical loop appears in the oil-rich corner when the temperature is decreased below the critical value $T_+ > \bar{T}$ [2]. When the temperature further approaches $\bar{T}$ (increasing in the water side and decreasing in the oil side) the loops start to expand. At certain temperatures the loops ($T_l > T_-$ on the water side, $T_u < T_+$ on the oil side) intersect the emulsification failure line (EF) associated with the coexistence of globules and an excess phase [3]. This results in the creation of the three-phase body which exists in the temperature regime $T_l < T < T_u$ [4].

The microstructure of ME has been studied using NMR [5], neutron and x-ray scattering [6], and freeze fracture electron microscopy (FFEM) [7]. The experiments suggest that the ME near the closed loops and three-phase regions is locally cylindrical. However, the global geometry of the ME has not yet been established. There is some evidence (FFEM, x-ray scattering [8], viscosity, and conductivity experiments) that supports the existence of a connected structure [9].

Much effort has been directed at developing a theoretical understanding of ME which can explain in a unified manner both the phase equilibria patterns and microstructure observed in experiments [10]. The random interface models [10,11] which describe the sponge phase do not reproduce the typical phase behavior of the closed loops and the critical points near the asymmetrical three-phase body, where the microstructure of the ME is asymmetric bicontinuous or globular. The important length scale in these asymmetric phases, far from $\bar{T}$, is the radius of curvature while the natural length scale in these models is the persistence length arising from the random collisions of fluctuating sheets.

In another class of ME models which treat more dilute ME phases composed of compact objects such as spherical droplets [3] or cylinders [12] the basic length scale is the spontaneous curvature. This approach was used in the work of Menes *et al.* [13] in order to explain the closed loops in terms of an interplay between a shape transformation and a postulated attraction between globules. In order to reproduce the observed closed loops the model had to assume that these short-ranged, material-specific interactions were in a particular window of attraction strengths. The loops obtained from this model were not as symmetrical as those observed in experiments [9]; moreover the shape dependent attraction mechanism required the assumption that the interactions of water globules in oil and oil globules in water be of the same order of magnitude.

Motivated by the experimental evidence we propose a theory based on a picture of branched tubular ME. The connected topology enables a unified description of both dilute systems in the vicinity of the loops, and the bicontinuous dense sponge ($\phi \sim 0.5$). By modifying the compositions, the radius of the cylindrical tubes changes and the system continuously transforms from a dilute network composed of long narrow cylinders connected by remote junctions to a very dense network in which the radius of the cylinders is comparable with their length and the junctions are very close, which can very well represent the asymmetric bicontinuous sponge phase [8]. We show that the interplay between entropy and curvature energy which are coupled through the connected topology of the network can produce an effective attraction between the junctions. This, inherent, material independent entropic interaction is balanced by the steric repulsion of the undulating cylinders. We show that the observed phase

 0031-9007/97/78(13)/2616(4)$10.00 © 1997 The American Physical Society

behavior that stems from the detailed balance of these curvature-entropy interactions reproduces quantitatively many experimentally observed features of the closed loops and three-phase body. The water-oil symmetry is a generic feature of this model due to the entropic and interfacial character of the interactions.

We treat the branched ME as a network of self-assembling, semiflexible polymers [12,13] interconnected by z-fold junctions [14]. The curvature energy associated with the creation of each junction, $\epsilon(r)$, to be calculated below, is a function of the cylinder radius, $r \sim \delta\phi/\phi_s$, where ϕ and ϕ_s are the volume fractions of the internal phase and surfactant, respectively, and δ the surfactant chain length. The junctions connect an ensemble of cylindrical branches whose length distribution is proportional to $X(m)$, the number density of branches of length m. The free energy per unit volume of the self-assembling network, F_N (in units of k_BT), includes three contributions,

$$F_N = \int X(m) \ln X(m)\, dm - (z-1)\rho \ln \rho + \rho\epsilon, \tag{1}$$

where $\rho = \frac{2}{z}\int X(m)\, dm$ is the number density of the junctions. The first term is the Flory-type translational entropy of the free cylinders, the second term accounts for the entropy loss of the cylinders' free ends when they are constrained to meet at a junction, and the third term is the curvature energy of the junctions, that also includes the curvature energy of the cylinders which is independent of $X(m)$ [15].

The end-cap energy of a free cylinder is generally large compared to that of a junction, hence the system prefers to pay the entropy penalty of a junction in order to avoid free ends [16]. The optimal geometry of the network is found by minimizing F_N with respect to $X(m)$. This procedure yields an exponential length distribution of the cylinders with an average cylinder length, $\bar{m}$, which scales like $\bar{m} \sim \phi^{1-z/2} e^{\epsilon}$. Substituting the optimal distribution $X(m)$ results in

$$F_N = -\rho = \frac{2}{z}\frac{\phi}{\bar{m}} \sim -\phi^{z/2} e^{-\epsilon}. \tag{2}$$

This is just the free energy of an ideal gas of junctions, whose density, ρ, is determined by the network volume fraction and the Boltzmann factor of the junction energy, $e^{-\epsilon}$. The $\phi^{z/2}$ dependence of F_N indicates that high-z junctions are less probable [14]. We therefore consider only the case $z = 3$. The nonlinear $\phi^{3/2}$ dependence of F_N represents an effective attraction between the junctions.

As we show below, we find that the curvature energy of a junction, $\epsilon(c_0 r)$ is a nonmonotonic function of the tube radius, r and the spontaneous radius of curvature, c_0^{-1}. This nonmonotonic behavior is responsible for the trend of phase separation followed by remixing which produces the closed loops and three-phase body in the phase diagram.

We use a variational model to simplify the calculation of the curvature energy of the junction characterized by a bending modulus $\kappa(T)$. We consider a junction composed of three "horns" connected to a spherical core. The radius, r, of the cylindrical part of the horns is determined by the composition, and the parameter to be minimized is the curvature of the horn near the spherical core [17]. The minimized junction energy exhibits a nonmonotonic dependence on the tube radius, which has the approximate form [18],

$$\epsilon(r,T) \simeq \frac{\kappa(T)}{T}\,\epsilon_0\left[1 + \epsilon_2\left(c_0 r - \frac{1}{2}\right)^2\right], \tag{3}$$

where $\epsilon_0 \simeq 2; \epsilon_2 \simeq 10$, thus there is a deep minimum at $c_0 r = 1/2$ (r is measured in units in which the EF is at $c_0 r = 1$). As a result, Eq. (2) indicates that the effective attraction between the junctions, whose magnitude is proportional to $e^{-\epsilon}$, exhibits a steep maximum at $c_0 r = 1/2$. Hence, increasing r from the lower side of this maximum increases the effective attraction eventually driving the system to phase separate into two phases. A further increase in the radius decreases the attraction so that entropy tends to remix the phases. As shown below this phenomenon results in the creation of closed loops.

The effective attraction, $F_N = -\rho$, competes with two repulsive terms: One term arises from the restriction of the thermal fluctuations of the flexible tubes by neighboring cylinders resulting in an entropy decrease and an effective repulsion. Scaling arguments show that this repulsion behaves like $F_H = \frac{27}{16}\phi^{4/3}$, where the geometrical prefactor is found by a more detailed calculation [19]. The second term is a quadratic excluded-volume steric repulsion, $(1-\phi)\ln(1-\phi) \sim \phi^2/2$. The dependence on the tube radius, $r \sim \delta\phi/\phi_s$, enters only in the attraction term, through the Boltzmann factor, $e^{-\epsilon(r,T)}$. The total free energy possesses a critical point where the attraction F_N is large enough for the ME to phase separate. The phase of lower volume fraction is a dilute network with fewer junctions and the higher volume fraction is a dense network with many junctions [20]. The critical composition and junction energy are $\phi_c \simeq 1/8; e^{-\epsilon_c} \simeq 0.2$, respectively. The location of the critical point, which is far from the binary-mixture sides of the phase triangle, indicates that the system phase behavior is governed by the swollen network interactions and is not directly connected to the micellar binary systems. The nonmonotonic behavior of $\epsilon(r)$ indicates that there are two critical radii, r_c, at which the system phase separates. This provides an inherent mechanism for reentrant phase separation [13] which does not involve any material-specific interactions. The corresponding phase diagram is the closed loop with two critical points (Fig. 1).

The temperature dependence enters exponentially through the prefactor $\kappa(T)/T$ of the Boltzmann factor argument of the attraction. $\kappa(T)$ is the renormalized bending modulus [21]: $\kappa(T) \simeq \kappa_0[1 - (3/4\pi)(T/\kappa_0)\ln(r/a)]$. When we approach $\bar{T}$, the temperature at

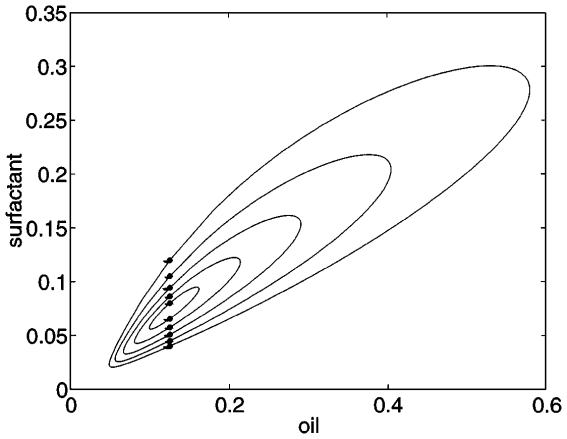

FIG. 1. Spinodal curves: each expanding loop has two critical points at $\phi = \phi_c \simeq 1/8$. The small loops are symmetrical, and as they grow the lower ϕ side of the loop sharpens. The axis of the loops is at $c_0 r = 1/2$ in accord with experiment [1,9].

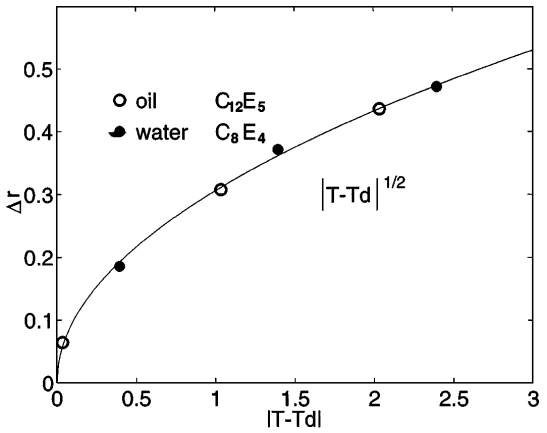

FIG. 2. Expansion of the closed loop: the experimental data from Ref. [7] for the water-rich side of C_8E_4 system and the oil-rich side of $C_{12}E_5$ is plotted along the scaling result $\Delta r \sim |T - T_d|^{1/2}$. The prefactors for the oil-rich and the water-rich sides are almost the same indicating the water-oil symmetry.

which c_0 vanishes, both from above and below the length scale, c_0^{-1}, increases as $c_0^{-1} \sim |T - \bar{T}|^{-1}$. Thus, the junctions become larger and, due to the renormalization of the bending modulus, softer, so that the entropy induced attraction between the junctions overcomes the curvature energy cost of their creation. Consequently, there are two double-critical temperatures, $T_d = T_-, T_+$, where the attraction reaches a critical value and the closed loops appear. The water side loop appears at T_-. As the temperature is increased the double-critical point splits into two separate critical points with radii below and above $c_0^{-1}/2$, both at the same volume fraction $\phi = \phi_c \simeq 1/8$. The oil side loop exhibits an analogous behavior with an opposite temperature dependence: they shrink with increasing temperature and disappear at T_+. The difference between the critical radii, r_c, and the axis of the loop, $c_0 r = 1/2$, which is proportional to the width of the closed loops in the isothermal cuts, scales like [23]

$$c_0 |r_c - r_0| \simeq \left[\epsilon_2 \frac{\kappa_0}{\bar{T}} \left(\frac{T_+ - T_-}{\bar{T}} \right) \right]^{1/2} \left| \frac{T - T_d}{\bar{T}} \right|^{1/2}, \tag{4}$$

where $T_d = T_-$ on the water-rich side and $T_d = T_+$ on the oil-rich side. This temperature dependence is plotted in Fig. 2 along with the experimental data. The oil-rich side data is for a ternary system whose surfactant is $C_{12}E_5$ and the water-rich side of a system with C_8E_4. These ternary systems have almost equal values of $\kappa_0(T_+ - T_-)$ [9]. As predicted from Eq. (4), both curves exhibit the square root temperature dependence with *almost equal* prefactors demonstrating the water-oil symmetry. This indicates that the phase-separation mechanism is identical for both the water and oil systems and is very unlikely to be related to specific attractive interactions.

This branched ME picture also explains the creation of the three-phase triangle as a result of the intersection of the EF, $c_0 r = 1$, with the closed loop, as seen experimentally [1]. As shown above, when the temperature approaches $\bar{T}$ the closed loop expands. The ratio between the angles of the axis of the loop $c_0 r = 1/2$ and the EF $c_0 r = 1$ remains constant. Eventually, the expanding loop intersects the EF and forms a three-phase triangle. There are two intersection temperatures at which the three-phase body appears, $T_l < \bar{T}$ for the water side and $T_u > \bar{T}$ for the oil side. When the loop further expands its contact point with the EF splits into two phases with volume fractions above and below ϕ_c which coexist with the excess phase rejected by the globules that have already reached their optimal size. As the temperature approaches $\bar{T}$, the volume fraction of the dense network, usually termed "the middle phase," increases and it becomes an asymmetric sponge phase. At temperatures lower than $\bar{T}$ the asymmetric sponge is composed of connected oil tubes. As the temperature increases the middle phase becomes a symmetric sponge exactly at $\bar{T}$, and after a further temperature increase the asymmetric sponge becomes a net of water tubes.

The interfacial, material-independent nature of our model provides *universal* scaling laws which are in agreement with a data collapse of several ternary systems onto a single curve when they are described by appropriate reduced variables [22]. Employing the scaling laws which approximate the expansion of the loop (4) and the curvature energy of the junction (3) one derives a universal scaling for the composition of the middle phase, ϕ_μ, which shows a sigmoidal temperature dependence [23],

$$\bar{\phi} = \mathrm{sgn}(t) \{ [\sqrt{(q+1)^2/4 - q|t|} - (q-1)/2]^{1/2} - 1 \}, \tag{5}$$

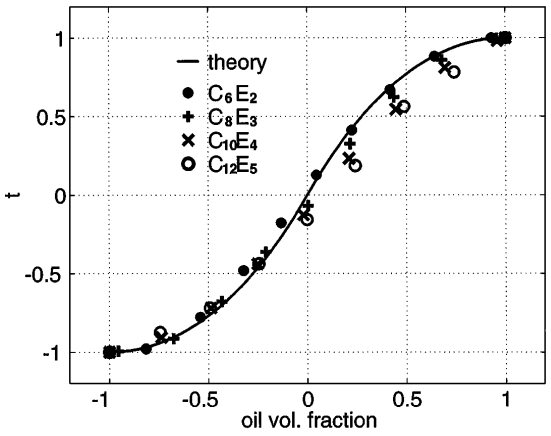

FIG. 3. The middle phase trajectory: the experimental data of several C_iE_j systems from Ref. [22] collapse onto the theoretical scaling result when plotted in the normalized variables $t = (T - \bar{T})/(\bar{T} - T_l) = (T - \bar{T})/(T_u - \bar{T})$ and $\bar{\phi} = (\phi_\mu - 1/2)/(1/2 - \phi_c)$.

where $q \simeq 5$ is a universal constant and the reduced variables are $t = (T - \bar{T})/(\bar{T} - T_l) = (T - \bar{T})/(T_u - \bar{T})$ and $\bar{\phi} = (\phi_\mu - 1/2)/(1/2 - \phi_c)$. The middle-phase trajectory (5) exhibits the same water-oil symmetry observed in the closed loops (4). As can be seen from Fig. 3 the theoretical universal curve (5) is in good agreement with the data collapse obtained for four different C_iE_j surfactants taken from [22]. It is important to note that although the network picture is not valid very close to $\bar{T}$ the scaling for the middle-phase composition passes smoothly through the symmetric sponge phase; thus, indicating that branched ME model is applicable for most of the phase space.

The authors thank B. Widom and P. Pincus for the useful discussions. They are grateful to the Israel Science Foundation and to the Israel Ministry of Science under the joint Israel-French cooperation program.

[1] For a review of experiments R. Strey, Ber. Bunsen-Ges. Phys. Chem. **100**, 182 (1996).

[2] P. Kilpatrick *et al.*, J. Phys. Chem. **90**, 5292 (1986); M. Kahlweit, R. Strey, and G. Busse, Phys. Rev. E **47**, 4197 (1993).

[3] S. A. Safran and L. A. Turkevich, Phys. Rev. Lett. **50**, 1930 (1983); M. S. Leaver and U. Olsson, Langmuir **10**, 3449 (1994).

[4] In ionic systems the existence of extra degree of freedom, the concentration of the salt, complicates the phase diagram. Nevertheless, when the ratio water/oil is kept constant and the control parameter is the salinity (analogous to the temperature in nonionic systems) it exhibits a similar progression of the phase behavior, including the appearance of closed loops and three-phase body.

[5] M. S. Laver, U. Olsson, H. Wennerström, and R. Strey, J. Phys II (France) **4**, 515 (1994).

[6] O. Glatter, R. Strey, K.-V. Schubert, and E. W. Kaler, Ber. Bunsen-Ges. Phys. Chem. **100**, 323 (1996).

[7] R. Strey, Colloid Polymer Sci. **272**, 1005 (1994).

[8] I. S. Barnes, S. T. Hyde, B. W. Ninham, P. J. Derian, M. Drifford, and T. N. Zemb, J. Phys. Chem. **92**, 2286 (1988).

[9] R. Strey (unpublished).

[10] G. Gompper and M. Schick, *Self-Assembling Amphiphilic Systems* (Academic, New York, 1994).

[11] S. T. Milner, S. A. Safran, D. Andelman, M. E. Cates, and D. Roux, J. Phys. (Paris) **49**, 1065 (1988); P. Pieruschka and S. A. Safran, Europhys. Lett. **31**, 207 (1995).

[12] S. A. Safran, L. A. Turkevich, and P. Pincus, J. Phys. (Paris) Lett. **45**, L-69 (1984).

[13] R. Menes, S. A. Safran, and R. Strey, Phys. Rev. Lett. **74**, 3399 (1995).

[14] Systems with negative saddle-splay modulus, $\bar{\kappa} < 0$ prefer minimal number of arms, $z = 3$. This is in accordance with the observation of "Y-like" structures by Strey *et al.* [7] which suggests 3-fold junctions.

[15] T. J. Drye and M. E. Cates, J. Chem. Phys. **96**, 1367 (1992). The statistical mechanics of the network are treated by a method similar to what they use for micellar networks. The entropy penalty is $-(z\rho \ln z\rho - \rho \ln \rho) \simeq -(z - 1)\rho \ln \rho$. It vanishes in the limit $z = 1$ where Eq. (1) reproduces the result for wormlike micelles. The different underlying microscopic properties are taken into account in the dependence of the junction bending energy, ϵ, on the swelling radius, r, leading to a phase separation unique for ME networks.

[16] This assumption fails for thick cylinders in the vicinity of the EF, where the junction energy, ϵ, is comparable with the end-cap energy and the network is unstable to the formation of nearly spherical drops.

[17] W. Wintz, H.-G. Dobreiner, and U. Seifert, Europhys. Lett. **33**, 403 (1996).

[18] This approximates the bending energy, $\kappa \int (H - c_0)^2 \, dA$, of the junction. The Gaussian curvature contribution to the junction bending energy is $-4\pi\bar{\kappa}(z/2 - 1) = -2\pi\bar{\kappa}$ [Z. Wang and S. A. Safran, Europhys. Lett. **11**, 425 (1990)]. This contribution does not depend on the cylinder radius and therefore affects only the values of the coefficients, ϵ_0 and ϵ_2, with no qualitative change in the phase behavior.

[19] D. Roux and C. Coulon, J. Phys. (Paris) **47**, 1257 (1986); J. V. Selinger and R. F. Bruinsma, Phys. Rev. A **43**, 2910 (1991). The energy per unit length associated with the entropy of a cylinder fluctuating inside a tube of radius d scales like $(\kappa r d^2)^{-1/3}$. In our model conservation implies $\phi \sim (d/r)^2$. The cylinder length per unit volume scales like ϕ/r^2. Employing these scalings we find the $\phi^{4/3}$ dependence of F_H.

[20] In dense networks, when the junctions are close, they strongly interact via the elastic deformations imposed by their dense packing. However, this extra repulsion is minor in the vicinity of the critical point.

[21] For example, L. Peliti and S. Leibler, Phys. Rev. Lett. **54**, 1690 (1985).

[22] T. Sottmann and R. Strey, J. Phys. Condens. Matter **8**, A39 (1996).

[23] T. Tlusty, S. A. Safran, R. Menes, and R. Strey (to be published).

3

Topology, Phase Instabilities and Wetting of Microemulsion Networks

Topology, Phase Instabilities, and Wetting of Microemulsion Networks

T. Tlusty,[1] S. A. Safran,[1] and R. Strey[2]
[1]*Department of Materials and Interfaces, The Weizmann Institute of Science, Rehovot 76100, Israel*
[2]*Institut für Physikalische Chemie, Luxemburger Strasse 116, D-50939 Köln, Germany*
(Received 16 August 1999)

We predict theoretically the gradual formation of fluctuating, connected microemulsion networks from disconnected globules as the spontaneous curvature is varied, in agreement with recent direct measurements of these topological transitions. The connectivity induced instability together with emulsification failure of the network relate the ultralow tensions and wetting transition to the changing microstructure.

PACS numbers: 64.75.+g, 68.10.Cr, 82.70.–y

The interplay between structural energy and entropy that characterizes the self-assembly of microemulsions (ME) leads to an extremely rich variety of geometries. Among these, the multiply connected sponge, in which the water and oil domains are both continuous, has been extensively studied [1]. These bicontinuous structures are observed around the inversion temperature, $\bar{T}$, where the mean curvature of the surfactant film vanishes. In the very same region, ME systematically exhibit striking thermodynamic features, especially the critical, reentrant two-phase separation and the subsequent formation of a three-phase region [2], where the ME is composed of a surfactant-rich lens that generally wets the interface between the water-rich and oil-rich phases only partially [3]. The behavior of the ultralow tensions at these three interfaces as a function of temperature exhibits a wetting transition, where the lens spreads all over the oil-water interface [4]. Recent experimental studies by Strey and Sottmann on 19 different non-ionic surfactant ME have shown that both the phase diagrams [5] and tensions [6] obey similar universal scaling properties.

Previous theories [7] that focused on the symmetric sponge, where the amphiphilic random interface has equal probabilities to curve towards oil or water, could not reproduce the critical, reentrant phase behavior nor the subsequent criticality near the three-phase region. Motivated by the unexplained reentrance phenomena, we proposed a model for ME based on thermally fluctuating *asymmetric* bicontinuous networks, whose building blocks are cylinders interconnected by junctions [8]. The cylinders are stabilized by the finite spontaneous curvature, c_0, above or below $\bar{T}$ [9]. Recently, these networks with their three-fold "Y-like" junctions have been directly observed by transmission electron microscopy (TEM) [10] (Fig. 1a).

In this paper, we show how a unified explanation of the connection between microstructure and interfacial properties naturally emerges from the fluctuating network model. It consistently predicts the topological transitions of the ME with decreasing spontaneous curvature, c_0 (which is controlled by temperature in non-ionic systems): The ME evolves from spherical globules to long cylinders of radius R that subsequently interconnect by threefold junction, leading to the formation of the bicontinuous network. We introduce the concept of emulsification failure (EF) of networks that allows for the optimization of the *local* curvature energy through rejection of the excess internal phase. In the region of the reentrant phase separation the

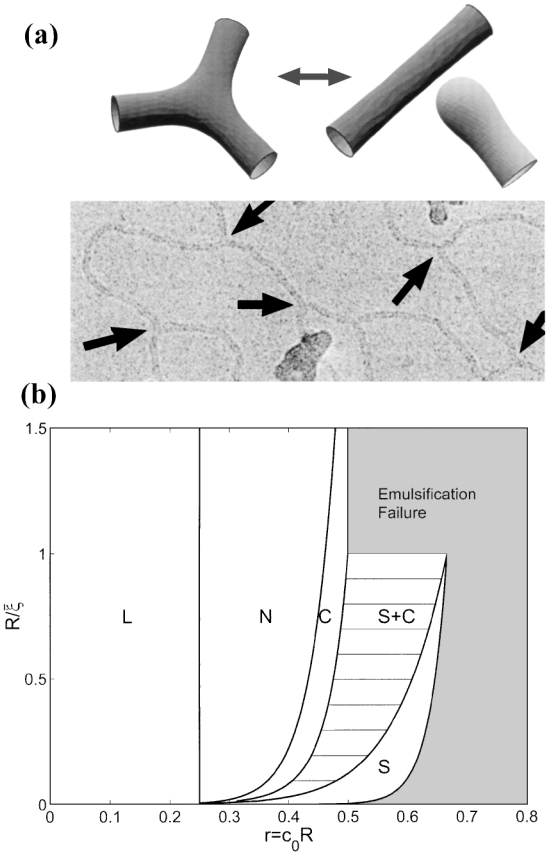

FIG. 1. (a) The formation of a threefold "Y-like" junction. The theoretical shape of the junction, as calculated by numerical minimization, has a lamellar core, while the cylinder terminates with an enlarged spherical end cap. The cryo-TEM image of the Habon G system shows the semiflexible network formed by such junctions [A. B. Grosswasser and Y. Talmon (to be published)]. (b) The phase stability diagram of spheres (S), cylinders (C), lamellae (L), and the network (N) made of interconnected cylinders. Note the series of topological transitions, S → S + C → C → N as c_0R decreases.

 0031-9007/00/84(6)/1244(4)$15.00 © 2000 The American Physical Society

global, large-scale network topology is optimized via adjustment of the typical distance, L, between its junctions. The appearance of the three-phase coexistence of ME with almost pure oil and water phases, when the EF and the reentrance loops overlap, therefore signifies the capability of the system to simultaneously tune its structure on *both local and global* length scales. We trace the progression of the microstructure from the curvature-governed dilute network, $L \gg R \sim c_0^{-1}$, to the strong fluctuation regime, where the typical distance between junctions is comparable with their size, $c_0^{-1} \gg L \sim R$, and they form a dense sponge. We predict the consequent dependence on c_0 of the interfacial tension and the resulting wetting transition in agreement with experiment.

We first discuss the sequence of topological transitions that ME show on the way to the formation of bicontinuous networks. At high spontaneous curvature, far from $\bar{T}$ (lower part of the phase diagram in Fig. 1b), one can neglect the thermal fluctuations. The dominant contribution to the free energy (per unit volume) is the local elastic curvature energy, $f_e = \phi r^{-3} E(r)$, where ϕ is the volume fraction of the inner phase (oil or water), $r = c_0 R$ is the ratio of the radius to the optimal radius of curvature; $E(r)$ is the scale invariant curvature energy. Previous studies have dealt with the details of the phase diagram in this regime and we describe only the main results [9]: In a single phase, the radius is determined by the volume to surface ratio $R = 2\delta(\phi/\phi_s)$, where the volume fraction of the surfactant is ϕ_s and δ is the surfactant chain length (R is the cylinder radius, 2/3 of the sphere radius). The curvature energy of cylinders is $E_c(r) = \kappa(1 - 4r)$, where κ is the bending modulus. For spheres, the curvature energy, $E_s(r) = \frac{8}{9}[2\kappa(1 - 3r) + \bar{\kappa}]$, includes a topological contribution proportional to the saddle-splay modulus, $\bar{\kappa}$ (E_s and E_c are measured relative to the curvature energy of lamellae $E_l = 0$). Comparing the energies of the three possible local geometries, one finds that lamellae are optimal in the symmetric regime $r < \frac{1}{4}$ (Fig. 1b). As r increases, there occurs a transition to cylinders, followed by a transition to a region where they coexist with spheres, and finally to a pure phase of spheres. When r is further increased, the free energy becomes unstable with respect to the EF phase separation: In this type of instability the *local* curvature energy, E, is optimized by the rejection of the excess, internal phase to optimize the curvature energy and still obey the geometrical constraints set by composition [11,12]. Coexistence with an excess phase takes place when the osmotic pressure of the material outside the globules vanishes. Expressed in the free energy $f(r, \phi)$, this condition takes the form

$$f + (1 - \phi)\partial_\phi f + (r/\phi)\partial_r f = 0, \qquad (1)$$

or in the scaled form of the curvature energy, $r\partial_r E = 2E$.

The global structure of the ME, and especially the *connectivity* transition from separate cylinders to the bicontinuous network [13], is governed by thermal fluctuations. The cylindrical local geometry [9] is determined by the relatively large curvature energy while all other scales are governed by the smaller free energy of fluctuations, ranging from the stringlike undulation of the branches to the longer wavelength translational entropy of the junctions [8]. To estimate the free energy, consider the network formed when the cylindrical branches are interconnected by z-fold junctions that each cost an energy ϵ (relative to the cylinders) due to their curvature. The junctions behave as an ideal gas of defects in the sense that the entropy is $k_B T$ per junction. The connectivity of the network implies that the number density of junctions, ρ_z, scales nonlinearly with ϕ, the network volume fraction, $\rho_z \sim \phi^{z/2} e^{-\epsilon}$ [14] resulting in an effective attraction (for $z \geq 3$). For disconnected cylinders ($z = 1$), the ideal gas of junctions is replaced by a gas of end caps of number density ρ_1 that each cost curvature energy ϵ_1. This attraction between the junctions is the driving force leading to the connectivity transition from cylinders to network around the line $\rho_3 = \rho_1$. Apart from a logarithmic correction, this transition occurs when the energies of both defects are equal, $\epsilon - \epsilon_1 \simeq \ln\phi$. Figure 1a describes the creation of a junction by the fusion of an end cap and a cylinder with the topological cost of one handle; its contribution to the integral over the Gaussian curvature is $\bar{\kappa} \int K\, dS = -4\pi\bar{\kappa}$. The difference in the mean curvature contribution to the elastic energy, as calculated by numerical or variational minimization, scales approximately linearly with r, $2\kappa \int dS\,(H - c_0)^2 \simeq 4\pi\kappa(Pr - Q)$, with $P \simeq 2.14$ and $Q \simeq 1.04$ [15]. Junctions are optimal for small values of the normalized spontaneous curvature due to their flat lamellar core, while end caps are preferred at larger r by their spherical cap (Fig. 1a). The resulting transition line,

$$r_n = \frac{1}{P}\left(Q + \frac{\bar{\kappa}}{\kappa} + \frac{1}{4\pi\kappa}\ln\phi\right), \qquad (2)$$

is depicted in Fig. 1b. We include the effects of short wavelength fluctuations by the renormalized bending modulus $\kappa(R) = -(\alpha/4\pi)\ln(R/\xi)$, and saddle-splay modulus $\bar{\kappa}(R) = (\bar{\alpha}/4\pi)\ln(R/\bar{\xi})$; the corresponding membrane thermal persistence lengths are $\xi = \delta\exp(4\pi\kappa_0/\alpha)$ and $\bar{\xi} = \delta\exp(-4\pi\bar{\kappa}_0/\bar{\alpha})$, where κ_0 and $\bar{\kappa}_0$ are the bare values of the moduli and the exponents are $\alpha = 3$, $\bar{\alpha} = \frac{10}{3}$ [16]. As the temperature approaches the inversion temperature, $\bar{T}$, the curvature determined length scale increases as $R \sim 1/c_0 \sim 1/|T - \bar{T}|$, and $\bar{\kappa}$ increases logarithmically from its typical negative nominal value, $\bar{\kappa}_0 < 0$. This leads to the expansion of the network region (Fig. 1b), since higher values of $\bar{\kappa}$ favor the saddlelike shape of the junction [17]. This theoretical prediction for the topological transition, spheres $\rightarrow$ spheres + cylinders $\rightarrow$ cylinders $\rightarrow$ network, was recently substantiated by direct cryo-TEM measurements of non-ionic ME [10].

We also anticipate that the network will be unstable with respect to EF similar to that of globules. Motivated by the experimental phase diagrams, which exhibit straight, constant-r EF lines, we neglect the small effect of the entropic contribution in the free energy of the network and substitute in Eq. (1) only the dominant curvature contribution, $\phi r^{-3} E_c(r)$. Since this local energy is not sensitive to connectivity, we obtain an identical result for both disconnected cylinders and networks for the optimal radius,

$$c_0 R_c = \frac{2\ln(R_c/\xi) - 1}{4\ln(R_c/\xi) - 1}. \quad (3)$$

R_c has two limits; the curvature-governed regime ($h = c_0\xi \ll 1$), shown in Fig. 1b, $R_c = 1/(2c_0)$, while in the entropy-governed regime ($h \sim 1$) it crosses over to $R_c \sim \xi$. The suggested EF of cylinders followed by EF of networks, at lower values of c_0 (Fig. 1b), is in accord with experiment [10].

Apart from the local EF instability, which is also common to globules, the bicontinuous network exhibits a unique instability which directly results from its global connectivity: The entropic part of the free energy is unstable to phase separation when the effective attraction, $-\rho_z \sim -\phi^{z/2} e^{-\epsilon}$, overcomes the repulsion. This occurs for values of the junction energy lower than a critical value. Since $\phi^{z/2}$ represents an effective attraction only if the exponent is higher than linear (or $z \geq 3$), we find that this type of phase separation is unique to the connected structures. Within the network picture, the reentrant phase separation loops and the subsequent three-phase coexistence emerge as direct results of the nonmonotonic behavior of the junction energy, $\epsilon(r)$ [8]. The curvature energy of the junction exhibits a minimal value at r_* [15] which corresponds to a steep maximum of the attraction $\sim e^{-\epsilon}$. When the maximal attraction exceeds a critical value, the ME phase separates into two networks of the same cylindrical radius r, which differ in the density of junctions, as verified by experiment [10]. In the phase diagram, this *global* instability is manifested by the appearance of a two-phase coexistence loop bounded by two critical points with a width that expands as $\Delta r = |r - r_*| \sim (1 - h/h_*)^{1/2}$ [8] (h_* refers to the double critical points where the loops first appear).

As T approaches the inversion temperature, $\bar{T}$ (where $h = c_0 = 0$), the loops expand until the increasing radius of their cylinders make the networks unstable to the local EF [Eq. (3)], and they reject the excess phase. The consequent three-phase coexistence between two ME networks, dense and dilute, together with an excess phase, is therefore the outcome of the simultaneous action of two distinct mechanisms for phase separation [12]; the local EF is characterized by the radius of curvature, R_c [Eq. (3)], and governs the coexistence of the network with its excess phase, while the global attraction of the junctions is characterized by the typical junction-junction correlation length and governs the two-network coexistence. The experimental phase diagrams [6] and tension curves [5] of many non-ionic ME systems, in both the two-phase and three-phase temperature regimes, exhibit a universal data collapse. We suggest that the source of this universality is purely geometrical; it is the connectivity of the ME network that provides an inherent, material independent, topological mechanism for attraction. Recent cryo-TEM experiments [10] which prove our structural understanding of the three-phase region, have also confirmed this theoretical proposal that indeed the bicontinuity is sustained even up to the highly asymmetric regime where the reentrant phase separation first occurs.

In the emulsification failure (EF) scenario, the macroscopic interface between the ME and the excess phase is a well-defined monolayer [18]. For this case, the experimentally measurable, macroscopic interfacial tension, σ, is simply the free energy per unit area required to unfold a segment of the ME network to a planar monolayer when the surfactant molecules are transferred to the newly formed interface. Far from $\bar{T}$ ($h \gg 1$), the dominant contribution is the elastic energy of the flattened interface due to the difference between its curvature energy and the optimal value at the network EF. This scales as $\kappa(R)c_0^2$ and therefore vanishes at $\bar{T}$. An additional contribution to the interfacial tension, which dominates in the strong fluctuation regime, accounts for the loss of network entropy, and this contribution determines the finite, ultralow value of the tensions at $\bar{T}$, where the curvature contribution vanishes. To estimate σ we employ an expansion of the reentrance loop and the EF around the critical end points $h = h_3 \simeq 0.9$, where the three-phase body first appears, with respect to the critical parameter $\Delta h = 1 - |h|/h_3$ [8]. The resulting values for the interfacial tensions between the two networks and their excess phase are (in units of $k_B T \xi^{-2}$)

$$\sigma_{\pm}(h) = \kappa(R_c)h^2 + (\xi/R_c)^2(A \pm B\Delta h^{1/2}), \quad (4)$$

where the constants $A \simeq 0.4$ and $B \simeq 0.02$ are found by expansion of the network free energy. The higher value, σ_+, corresponds to the dilute network phase, due to its higher entropy (weaker repulsion forces), and the lower value, σ_-, corresponds to the dense ME phase. In Fig. 2 the experimental curves $\sigma_+(h)$ measured for 19 ternary systems [6] collapse onto the universal theoretical prediction of Eq. (4), when normalized by $k_B T \xi^{-2}$, where ξ was independently measured by small-angle neutron scattering (SANS) [19]. The data shows an asymptotic h^2 behavior with a deep decrease, over 3 orders of magnitude, to the ultralow nonvanishing value $A + B \simeq 0.42$ at the entropy-governed symmetric sponge.

By contrast, when the two coexisting phases are both networks, the corresponding interface is a continuous transition layer separating regions where the branches have the same radius but their local density (or the density of junctions) differs. Near the critical end point where the two networks merge, the thickness of this transition layer

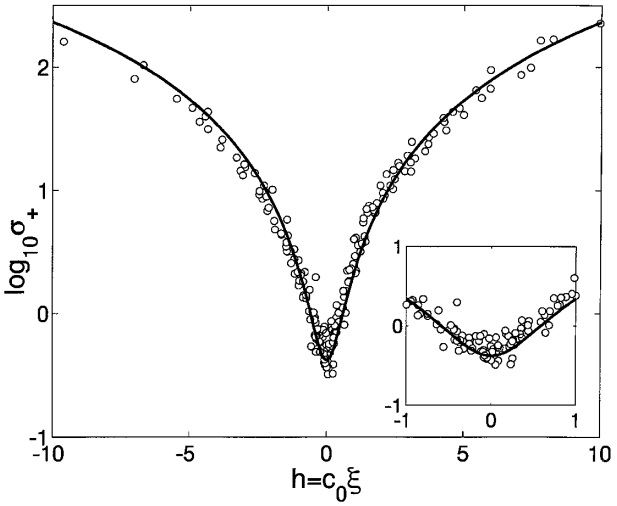

FIG. 2. The tension at the interface between the dilute network and the excess phase, σ_+, of 19 non-ionic microemulsions [6] collapse onto the scaling result (4) when plotted in units of $k_B T \bar{\xi}^{-2}$, where $\bar{\xi}$ was measured independently by SANS [19]. The data crosses over from the curvature governed regime, $h \gg 1$, to the ultralow nonvanishing value at the symmetric sponge, $h \ll 1$ (inset).

increases. Recalling that the phase separation is along constant-r tie lines, we consider only inhomogeneities of the network volume fraction by adding a term proportional to the square of its local gradient, $(\nabla\phi)^2$. Within a mean-field approximation, this approach yields an interfacial tension that vanishes as $\sigma_c \sim \Delta h^{3/2}$ at the critical points. Following the experiments, we assume that the boundary crosses over from a monolayer to a continuous transition layer in the vicinity of $\bar{T}$ ($h \ll 1$), where the thickness of the interface is comparable to the radius of the cylinders, $\sigma_- = \sigma_c$ [18]. This is typical of the symmetric sponge, where the global length scale becomes comparable to the size of the domains. The resulting tension takes the following form:

$$\sigma_c(h) = (\bar{\xi}/R_c)^2 (A - B)\Delta h^{3/2}. \tag{5}$$

The consequent balance of the three surface forces, given by Eqs. (4) and (5), determines the wetting properties of the ME: A generalized Young's law implies that the contact angle of a nonwetting lens [3] of the dense network phase floating between the dilute network and the excess phase is $\cos\theta = (\sigma_+^2 - \sigma_-^2 - \sigma_c^2)/(2\sigma_c\sigma_-)$. The tensions of the symmetric sponge at $h = 0$ are almost equal $\sigma_+ \simeq \sigma_- = \sigma_c$, and the theory predicts a lens with a contact angle $\theta \simeq 2\pi/3 - 4B/\sqrt{3}A \simeq 0.63\pi$. As the ME becomes asymmetric and approaches the critical end points, $h = h_3$, the tension between the merging phases vanishes as $\sigma_c \sim \Delta h^{3/2}$, which is faster than the vanishing of the difference between the tensions at the monolayers separating these phases and the excess phase, that scales as $\sigma_+ - \sigma_- \sim \Delta h^{1/2}$. Consequently, close enough to the critical end points, it is energetically favorable to avoid creating an interface between the dilute network and the excess phase by spreading an intervening layer of the dense network phase. Consistent with experiment [4], we predict a wetting transition at the points, $h = h_W$, which are defined by the complete wetting condition, $\sigma_+ = \sigma_- + \sigma_c$, leading to $h_W/h_3 \simeq 1 - 2B/A \simeq 0.9$. In this vicinity the theory predicts that the contact angle vanishes as $\theta \sim (h_W - h)^{1/2}$. We note that the entropic residue of the free energy due to the thermal fluctuations of the network is essential to obtain this wetting transition as well as the ultralow nonvanishing tensions at $\bar{T}$.

The authors thank T. Sottmann, who collaborated in the measurements, and K. Brakke and U. Schwarz for their help in using the SURFACE EVOLVER software. We are indebted to A. Bernheim-Grosswasser and Y. Talmon for generously allowing us to use the micrograph. We are grateful to the Israel Science Foundation Center for Self-Assembly and the Minerva Gerhard Schmidt Center.

[1] *Micelles, Membranes and Microemulsions and Monolayers*, edited by W. M. Gelbart, A. Ben-Shaul, and D. Roux (Springer-Verlag, Berlin, 1994).
[2] M. Kahlweit, R. Strey, and G. Busse, J. Phys. Chem. **94**, 3881 (1990).
[3] B. Widom, Langmuir **3**, 12 (1987).
[4] M. Aratono and M. Kahlweit, J. Chem. Phys. **95**, 8578 (1991); M. Kahlweit, R. Strey, and G. Busse, Phys. Rev. E **47**, 4197 (1993).
[5] T. Sottmann and R. Strey, J. Chem. Phys. **106**, 8606 (1997).
[6] T. Sottmann and R. Strey, J. Phys. Condens. Matter **8**, A39 (1996).
[7] G. Gompper and M. Schick, *Self-Assembling Amphiphilic Systems* (Academic, New York, 1994).
[8] T. Tlusty, S. A. Safran, R. Menes, and R. Strey, Phys. Rev. Lett. **78**, 2616 (1997).
[9] S. A. Safran, L. A. Turkevich, and P. A. Pincus, J. Phys. (Paris), Lett. **45**, 19 (1984).
[10] A. Bernheim-Grosswasser, T. Tlusty, S. A. Safran, and Y. Talmon, Langmuir **15**, 5448 (1999).
[11] M. S. Leaver and U. Olsson, Langmuir **10**, 3449 (1994).
[12] S. A. Safran and L. A. Turkevich, Phys. Rev. Lett. **50**, 1930 (1983).
[13] Y. Bohbot, A. Ben-Shaul, R. Granek, and W. M. Gelbart, J. Chem. Phys. **103**, 8764 (1995).
[14] T. J. Drye and M. E. Cates, J. Chem. Phys. **96**, 1367 (1992).
[15] T. Tlusty and S. A. Safran, J. Phys. Condens. Matter **12**, 253 (2000).
[16] F. David, in *Statistical Mechanics of Membranes and Surfaces*, edited by D. Nelson, T. Piran, and S. Weinberg (World Scientific, Singapore, 1989).
[17] D. C. Morse, Phys. Rev. E **50**, R2423 (1994); L. Golubović, Phys. Rev. E **50**, R2419 (1994).
[18] D. Langevin and J. Meunier, in *Micelles, Membranes and Microemulsions and Monolayers* (Ref. [1]).
[19] T. Sottmann, R. Strey, and S.-H. Chen, J. Chem. Phys. **106**, 6483 (1997).

4

Direct Observation of Phase Separation in Microemulsion networks

Direct Observation of Phase Separation in Microemulsion Networks

A. Bernheim-Groswasser,[†] T. Tlusty,[‡] S. A. Safran,[‡] and Y. Talmon*,[†]

Department of Chemical Engineering, Technion-Israel Institute of Technology, Haifa 32000, Israel, and Department of Materials and Interfaces, Weizmann Institute of Science, Rehovot 76100, Israel

Received March 15, 1999

Direct evidence by cryogenic temperature transmission electron microscopy shows the existence of networks in microemulsions near the two-phase closed loops. Networks formed by interconnected oil-swollen cylinders were observed in the water-rich regions of the phase diagram of the $C_{12}E_5$ /water/*n*-octane system. The coexisting phases within the loops were shown to be concentrated and dilute networks. Similar micellar networks were also found in the binary system. These observations substantiate the suggested theoretical link between the structural bicontinuity and the unique phase separation and criticality of microemulsions: All these regimes are governed by the entropic attraction between network junctions.

Introduction

Bicontinuous, multiply connected shapes are a widespread, almost generic feature of microemulsions (ME) and are associated with ultralow interfacial tensions. The typical spongelike microstructure of these phases consists of two-dimensional layers of amphiphiles separating oil and water domains that are both continuous.[1] These *dense symmetric sponges* (at almost equal volume fractions of oil and water) have been observed mainly in the vicinity of the inversion temperature ($\bar{T}$), where the preferred curvature of the amphiphile monolayer toward water or oil (the spontaneous curvature) is small.[2,3] The bicontinuity disappears at higher spontaneous curvatures, away from $\bar{T}$, where the monolayers tend to form disconnected globules containing water or oil surrounded by a continuous domain of the other component.[4−7]

Preliminary measurements by self-diffusion NMR and conductivity suggested the existence of connected structures at temperatures relatively far from $\bar{T}$, where one would have expected a phase of disconnected globules.[8,9] A recent theory predicted that those structures are *dilute, highly asymmetric networks* formed of interconnected semiflexible cylinders.[10] Moreover, it suggested a direct link between the structural bicontinuity and the unique thermodynamics of ME: The generic two-phase closed loops, their critical points, and the subsequent formation of the three-phase body (Figure 1A[1]) are all explained as a direct result of an effective entropic attraction induced by the network fluctuations. This attraction governs ME from dense sponges down to dilute (even *micellar)* networks; all these regimes can be understood as different limits of the same network picture.

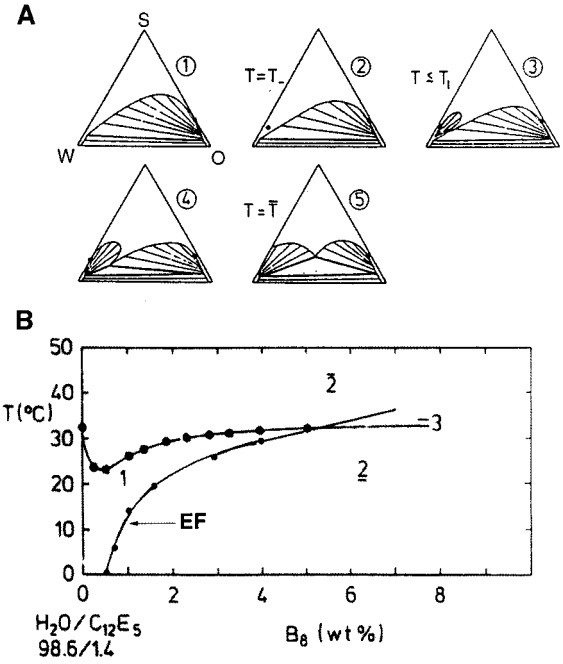

Figure 1. (A) Evolution of the three-phase triangles (water (W), oil (O), and surfactant (S)) with rising temperature, demonstrating the evolution of the isothermal closed loops, their critical points, and the subsequent formation of the three-phase body ($T = T_l$). (B) Evolution of the one-phase channel (1) defined by the EF line (2) as we measured (small dots), and line of critical points ($\bar{2}$) (dots after Kahlweit et al.[1]), for fixed $C_{12}E_5$/water weight ratio of $\phi_s/\phi_w = 1.4/98.6$, as function of temperature and *n*-octane weight percent, ϕ_o.

Here we report the first direct evidence, by cryogenic temperature transition electron microscopy (cryo-TEM) imaging of the existence of these dilute, semiflexible networks in the nonionic, ternary ME, $C_{12}E_5$/water/*n*-octane, in the water-rich corner of the phase diagram. Disconnected spheres or even cylinders were indeed

* To whom all correspondence should be addressed.

† Technion-Israel Institute of Technology.

‡ Weizmann Institute of Science.

(1) Kahlweit, M.; Strey, R.; Busse, G. *Phys. Rev. E* **1993**, *47*, 4197.
(2) (a) Scriven, L. E. In *Micellization, Solubilization and Microemulsion*; Mittal, K., Ed.; Plenum: New York, 1977. (b) De Gennes, P. G.; Taupin, C. *J. Phys. Chem.* **1982**, *86*, 2294.
(3) Kahlweit, M.; Strey, R.; Haase, D.; Kunieda, H.; Schmeling, T.; Faulhaber, B.; Borkovec, M.; Eicke, H.-F.; Busse, G.; Eggers, F.; Funck, Th.; Richmann, H.; Magid, L.; Söderman, O.; Stilbs, P.; Winkler, J.; Dittrich, A.; Jahn, W. *J. Colloid Interface Sci.* **1987**, *118*, 436.
(4) Strey, R. *Colloid Polym. Sci.* **1994**, *272*, 1005.
(5) Leaver, M. S.; Olsson, U.; Wennerström, H.; Strey, R. *J. Phys. II (France)* **1994**, *4*, 515.
(6) Strey, R.; Glatter, O.; Schubert, K. V.; Kaler, E. W. *J. Chem. Phys.* **1996**, *105*, 1175.
(7) Kahlweit, M.; Strey, R.; Sottmann, T.; Busse, G.; Faulhaber, B.; Jen, J. *Langmuir* **1997**, *13*, 2670.
(8) Strey, R. Unpublished.
(9) Lipgens, S.; Schübel, D.; Schlicht, L.; Spilgies, J. H.; Ilgenfritz, G.; Eastoe, J.; Heeman, R. K. *Langmuir* **1998**, *14*, 1041.
(10) Tlusty, T.; Safran, S. A.; Menes, R.; Strey, R. *Phys. Rev. Lett.* **1997**, *78*, 2616.

10.1021/la990301q CCC: $18.00 © 1999 American Chemical Society
Published on Web 07/31/1999

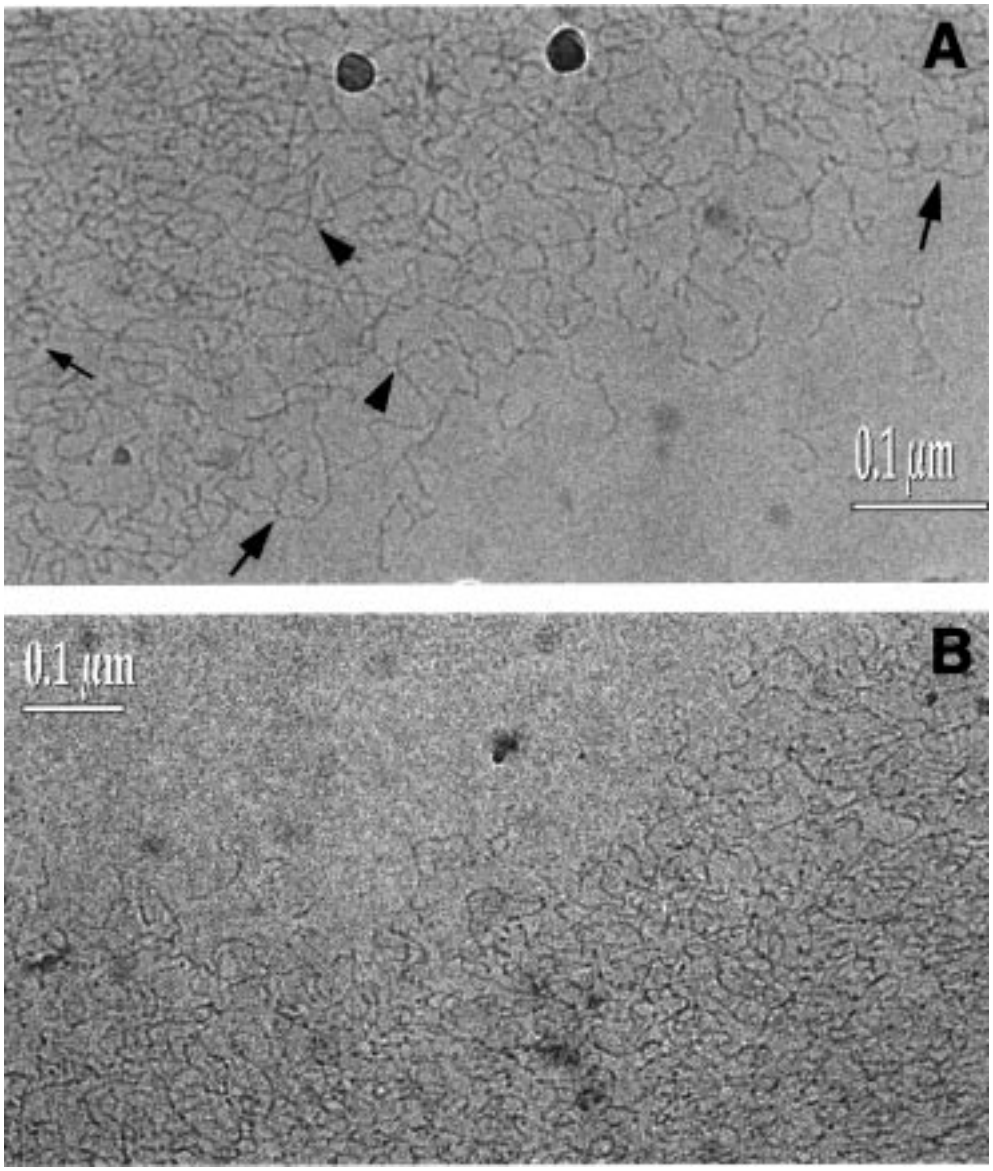

Figure 2. (A) Cryo-TEM image of a microemulsion at $\phi_o = 3\%$ and $T = 30$ °C showing swollen oil-in-water cylindrical tubes. One can identify 3-fold junctions (large arrows), entanglement points, or 4-fold junctions (arrowheads). Black dots indicate cylinder ends pointing outside the image plane or a folded thread (noted by a small arrow). (B) Cryo-TEM image of a microemulsion at $\phi_o = 0.7\%$ and $T = 23$ °C. The swollen oil-in-water cylindrical tubes are thinner in comparison to Figure 2A due to the lower oil content.

observed when lowering the temperature increased the spontaneous curvature. However, we find that all the important thermodynamic links between the symmetric, bicontinuous phase at temperatures close to $\bar{T}$ and those phases with finite spontaneous curvatures at temperatures relatively far from $\bar{T}$ occur via network topology. These networks are observed in the proximity of both the two-phase closed loop and the emulsification failure (EF) line, where they are in equilibrium with a rejected excess phase.[11] Moreover, the phase separation within the closed loop results in coexistence of concentrated and dilute networks. The three-phase equilibrium of the symmetric sponge ME with excess water/oil phases arises from the confluence of the EF instability and the two-phase loops,[10,12] both of which involve network structures. All these observations experimentally substantiate the theoretical link between ME phase separation, the entropic attraction, which leads to the formation of networks at temperatures away from $\bar{T}$, and the symmetric, bicontinuous phase at $\bar{T}$.[10] In the dilute limit, we observed similar network topology in the corresponding binary $C_{12}E_5$/water system.[13]

Experimental Section

Materials. We used $C_{12}E_5$ (Nikko, Japan) that had been stored under nitrogen atmosphere at about −20 °C, *n*-octane (Riedel-de Haën, Germany, 99% purity), and Millipore water. The solvents and the surfactant were used without further purification. Solutions were prepared at constant surfactant-to-water weight ratio of $\phi_s/\phi_w = 1.4/98.6$ at various *n*-octane contents ($\phi_o \leq 3\%$) and temperatures.

Cryo-TEM. Specimens were prepared in a controlled environment vitrification system (CEVS[14]), at controlled temperature and relative humidity to avoid loss of volatile components (water and *n*-octane). The microemulsion drop was placed on a TEM grid covered by a holey carbon film. The drop was then blotted with filter paper to form a thin liquid film on the grid, which was

(11) Safran, S. A.; Turkevich, L. A. *Phys. Rev. Lett.* **1983**, *50*, 1930.
(12) Kahlweit, M.; Strey, R.; Busse, G. *J. Phys. Chem.* **1990**, *94*, 3881.
(13) Bernheim-Groswasser, A.; Wachtel, E.; Talmon, Y. To be submitted for publication.
(14) Bellare, J. R.; Davis, H. T.; Scriven, L. E.; Talmon, Y. *Electron Microsc. Technol.* **1988**, *10*, 87.

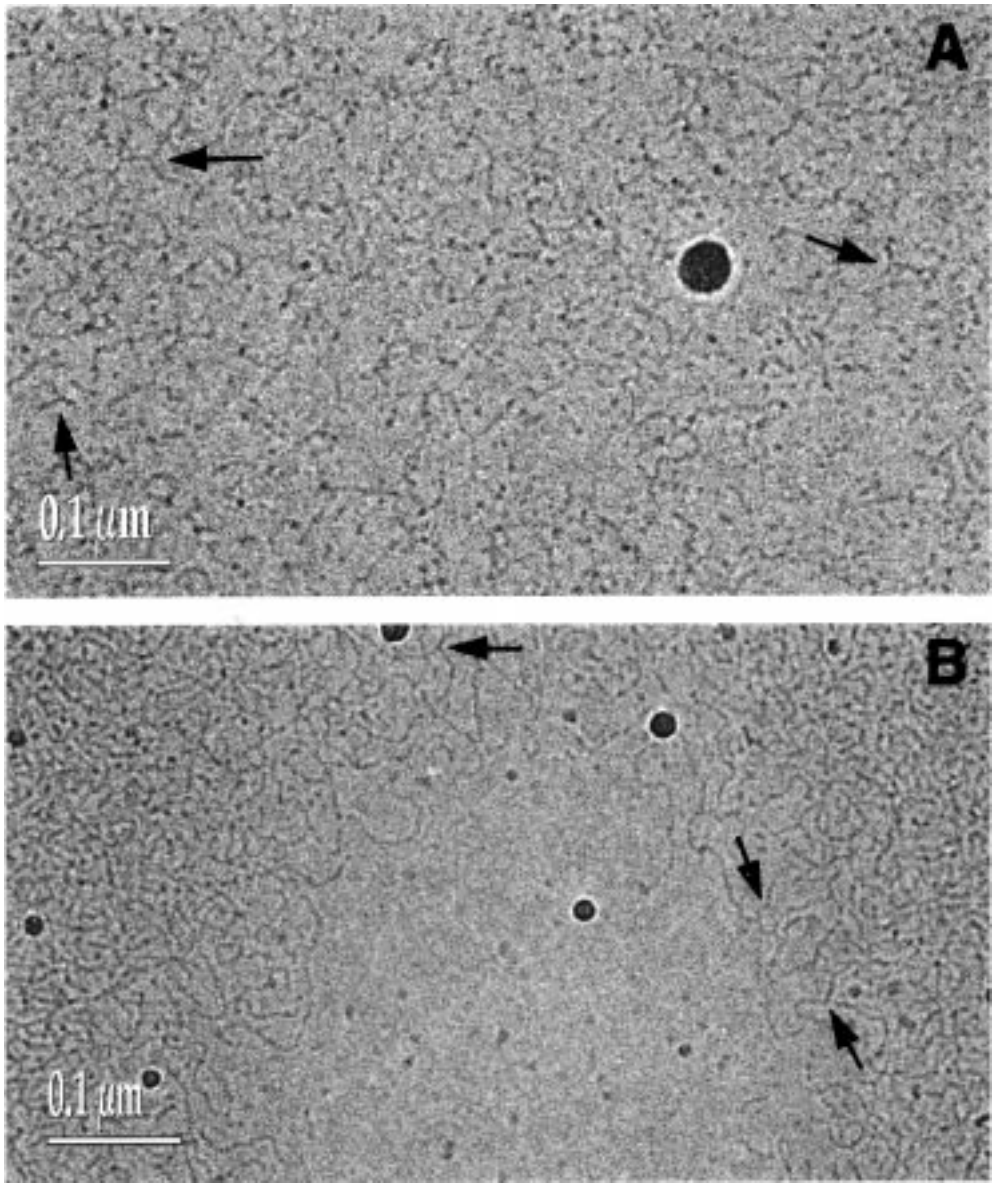

Figure 3. Cryo-TEM images of coexisting microemulsion networks at $T = 24.4$ °C: (A) dilute (high water content) and (B) concentrated (low water content) phase. In both images one can identify 3-fold junctions (arrows).

then immediately plunged into liquid ethane at its freezing temperature. The vitrified specimens were observed in a Philips CM120 transmission electron microscope at an accelerating voltage of 120 kV. The specimens were kept in the microscope at better than −175 °C by an Oxford Instruments cryo-specimen holder. Low-electron-dose images were digitally recorded by a Gatan MultiScan 791 CCD camera at about 4 μm underfocus to enhance phase contrast.

Results and Discussion

The ME network topology was observed by cryo-TEM in a large region that was probed in the one-phase channel defined by the EF line and the two-phase boundary as shown in Figure 1B[1]. Only at lower temperatures, where the spontaneous curvature is large, was a transition to disconnected globules observed. Following ref 1 we worked at a fixed $C_{12}E_5$/water weight ratio of $\phi_s/\phi_w = 1.4/98.6$, at various temperatures and *n*-octane weight percent, ϕ_o. Closed, two-phase coexistence loops are found[1] throughout the temperature regime where the upper phase boundary line ($\bar{2}$) is nonmonotonic. These loops first appear at the minimum of $\bar{2}$ (which we refer to as $T = T_-$) and then expand as temperature becomes higher. Their evolution as function of temperature is presented in Figure 1A, where the dotted line is a cut at fixed $C_{12}E_5$/water weight ratio. The width of the loop between its two critical points is approximately the difference in oil content ϕ_o, between the two branches of the $\bar{2}$ line. Another phase separation occurs at the EF line (2) where the ME coexists with excess, almost pure oil, phase.[15] The single-phase channel bounded by these two lines shrinks as one increases the oil content and vanishes at the critical end point ($T_l = 31.8$ °C) where the two lines intersect to form the three-phase body.[12]

According to the network model,[10] this unique phase-behavior is intimately related to the interconnected structure of the ME in this region: The ternary system forms networks of oil-in-water cylindrical tubes (of radius $r \sim \phi_o/\phi_s$) connected by 3-fold junctions. The closed loops

(15) This defines a plane through the phase prism that cuts the binodal surface ($\bar{2}$) close to the line of critical points. Throughout the temperature regime where the binodal line ($\bar{2}$) is nonmonotonic the isothermal cuts exhibit closed two-phase coexistence loops. These loops disappear at the double critical point located at the minimum of the binodal surface and the line of critical points. The EF surface located at the 2 line where the ME coexists with an excess phase, thus defining a single-phase channel.

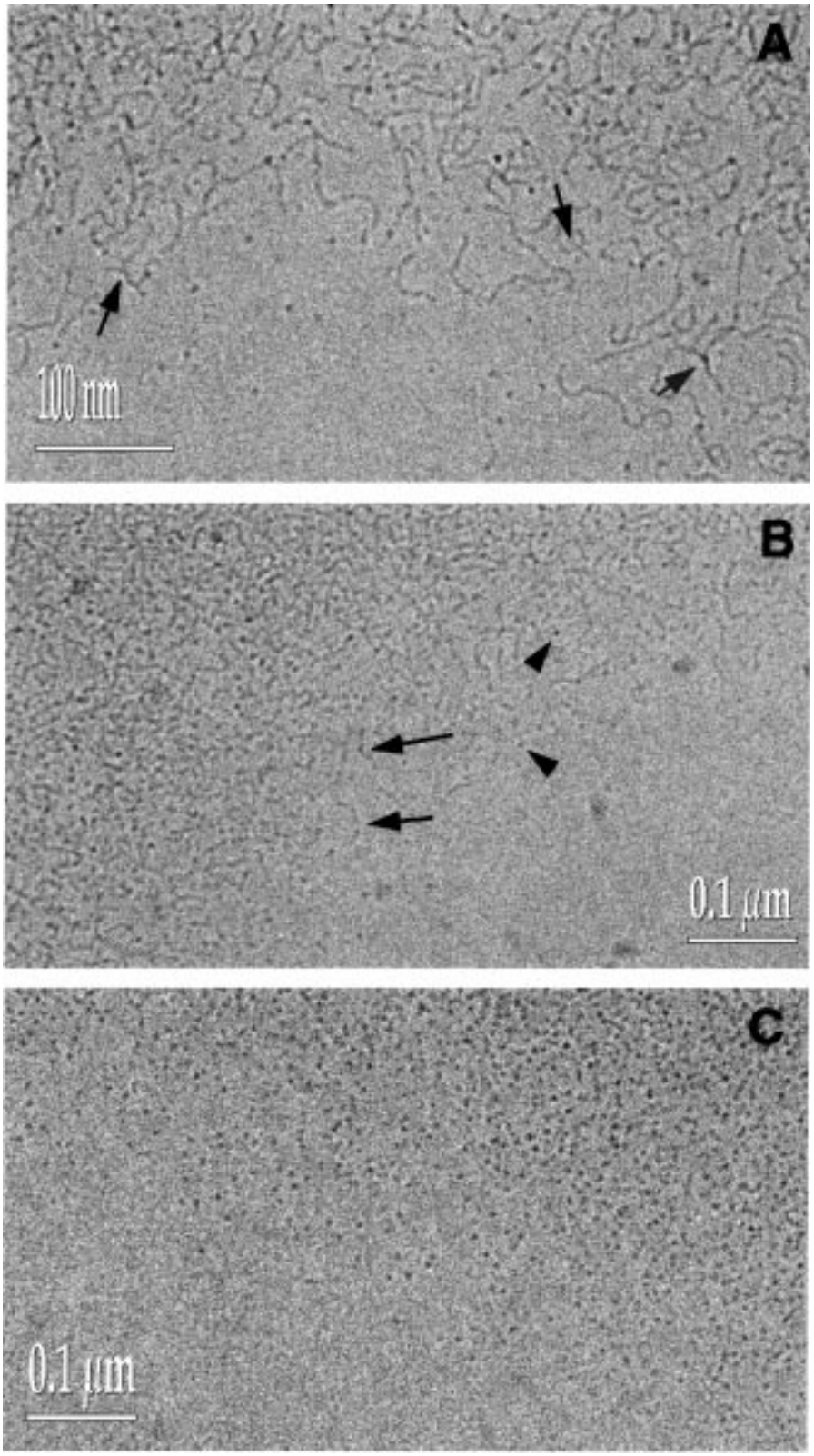

Figure 4. Cryo-TEM images of microemulsion micrsotructures along the EF line: (A) at $\phi_o = 3\%$ and $T = 26.5$ °C, where the structure is oil-swollen cylindrical micelles connected by 3-fold junctions (arrows); (B) the system at $\phi_o = 0.755\%$ and $T = 5$ °C is made of disconnected spherical oil-swollen globules (arrowheads) coexisting with relatively short (a few tens of nanometers) cylindrical threads (arrows); (C) at a very low temperature of $T = 2$ °C and at $\phi_o = 0.613$ the observed microstructure is that of monodisperse oil-swollen spheres.

are a direct consequence of an effective attraction within the ME networks due to the translational entropy of the junctions. This attraction is proportional to the number density, ρ, of the junctions which scales exponentially with their curvature energy, ϵ, like $\rho \sim \phi_o^{3/2} e^{-\epsilon/T}$. The ME separates into two network phases when the junction curvature energy is below a critical value $\epsilon_c \sim 2$ corresponding to a critical junction density $\rho_c \sim 0.03$ (in units of $1/r^3$), where attraction first overcomes the repulsion between neighboring fluctuating cylinders. Due to the

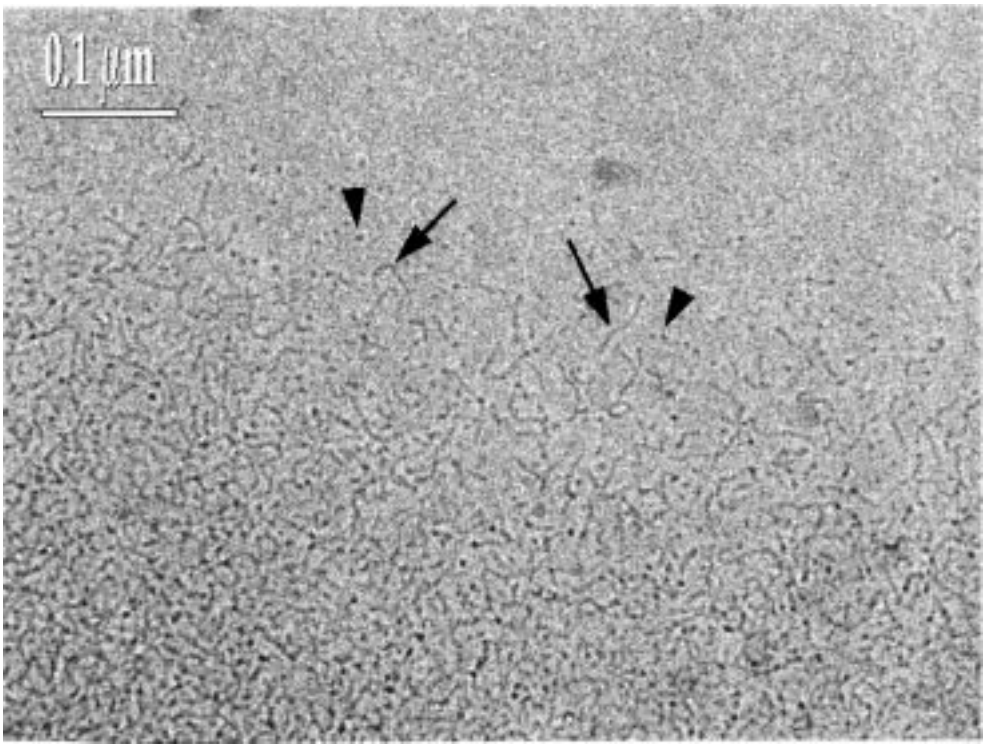

Figure 5. Approaching the binary micellar system ($\phi_o = 0.028$) at $T = 2$ °C, the system is comprised of cylindrical structures (arrows) in coexistence with spheres (arrowheads), as seen by cryo-TEM.

nonmonotonic dependence of the curvature energy $\epsilon(r)$ on the cylinder radius, r (which scales such as $r \sim \phi_o/\phi_s$), the resulting phase separation region is a closed loop bounded by two critical points.[10]

Consistent with this picture, we observe ME networks along the $\bar{2}$ line from the critical end point (Figure 2A at $\phi_o = 3\%$, $T = 30$ °C) through the double critical point (Figure 2B, at the minimum in Figure 1B, $\phi_o = 0.7\%$, $T = 23$ °C) toward a binary solution. A typical cryo-TEM micrograph of network phase is shown in Figure 2A: swollen oil-in-water cylindrical tubes describe the local structure. One can easily identify many 3-fold junctions (large arrows) connecting these semiflexible tubes, thus forming a network. The typical length of the tubes (distance between neighboring junctions) is a few tens of nanometers with a rather broad distribution, in accord with the exponential distribution suggested by theory. The radius of the tubes is about 5 nm, close to the theoretical value determined by volume and surface conservation. The tubes in the picture are semiflexible with a persistence length of about 10−20 nm. Although much less numerous, one can find disconnected network fragments that may be related to shearing during specimen preparation. The few four-way "crossroads" mark entanglement points or the rare 4-fold junctions (arrowheads). The black dots indicate cylinder ends pointing outside the image plane or a folded thread (noted by a small arrow). Following the $\bar{2}$ line to lower oil content (Figure 2B) the topology of local cylindrical structures connected by 3-fold branching points is unchanged. Note that the cylinders are now thinner due to lower oil content. Since the planar cut defined by the constant weight ratio is close to the line of critical points, the number density of the junctions along the $\bar{2}$ line is expected to scale as the critical value, $\rho_c r^{-3} \sim \rho_c(\phi_s/\phi_o)^3$. This is qualitatively supported by the measurements that indicate denser networks as we approach the binary system ($\phi_o \rightarrow 0$).

Within the two-phase closed loop, the predicted coexistence into concentrated (upper) and dilute (lower) network phases was indeed observed. This continuous phase separation occurs close to the double critical point, T_-, where the closed loop is relatively small (the minimum of $\bar{2}$). Figure 3 shows the coexisting ME networks of a system whose temperature is slightly above this double critical point, at $T = 24.4$ °C and $\phi_o = 0.76\%$. In both cryo-TEM micrographs of the lower (Figure 3A) and the upper (Figure 3B) phases one can identify the network topology formed of 3-fold junctions (arrows) interconnecting the oil-in-water cylindrical tubes. As predicted, the two networks in Figure 3 are of equal cylinder radius, r, and differ only in their junction density, ρ. At higher temperatures, where the closed loop has already widened, the network topology was observed in both concentrated and dilute phases, but in the dilute phase we also found disklike shapes. If the temperature is further increased, a three-phase body is formed. In the dilute (lower) phase, we found only disconnected structures, due to their higher entropy. Their shapes range from spherical to disklike shapes due to the small spontaneous curvature. Similar bicontinuous ME networks were observed even along the EF line, where previous theoretical studies predicted a discontinuous topology of spherical droplets.[11] The EF of networks, as manifested experimentally by observation of networks coexisting with an excess phase, agrees with the prediction of the network model: It suggests that the same mechanism leading to the rejection of excess phase by droplets at their optimal curvature, far from $\bar{T}$, induces EF also in a ME network. The model shows that EF results from the optimization of the local geometry (i.e., the mean curvature of the surfactant monolayers) and is therefore insensitive to the global geometry of disconnected globules or connected network.[16] Figure 4A shows a typical cryo-TEM image in the one-phase channel slightly above the EF line at $\phi_o = 3\%$ and $T = 26.5$ °C. The structure is similar to that of Figure 2, with oil-swollen cylindrical

(16) Tlusty, T.; Safran, S. A.; Strey, R. To be submitted for publication.

micelles connected by 3-fold junctions (arrows). Similar networks were observed down to $T = 9$ °C where the EF line is at $\phi_o = 1\%$ (Figure 1B).

Following the EF line to lower temperatures induces a topological transition: Figure 4B shows the microstructure of the ME on the EF at $T = 5$ °C and $\phi_o = 0.755\%$; the system is comprised of disconnected spherical oil-swollen globules (arrowheads) coexisting with relatively short (a few tens of nanometers) cylindrical threads (arrows). This is in qualitative agreement with theory that predicts a network breakup in regions where the higher entropy of the disconnected cylinders overcomes the higher curvature energy of their end-caps relative to the network junctions.[16] Finally, when we further decreased the temperature to $T = 2$ °C (at $\phi_o = 0.613$) the observed structure is that of rather monodisperse oil-swollen spheres (Figure 4C) as predicted by comparison of their curvature energy to that of the cylinders.[16,17] This is in accord with previous experimental studies of EF using freeze-fracture electron microscopy,[4] NMR,[5] small angle neutron scattering (SANS),[6] and light scattering.[7] Approaching the binary micellar system (by decreasing the oil content down to $\phi_o = 0.028\%$) while keeping the same temperature as in Figure 4C ($T = 2$ °C), we return to cylindrical structures (arrows) in coexistence with spheres (arrowheads) (Figure 5) as observed in the pure binary system.[13] In the binary system, networks were observed at higher temperatures, below the two-phase separation curve (with critical temperature $T_c = 31.5$ °C). This roughly locates a connected/disconnected topological transition line departing from the EF line at a temperature between 5 and 8 °C and increasing with T as oil content is lowered (Figure 1B).

(17) NMR and SANS measurements indicate a cylinder to sphere transition at higher temperatures, but still below the loops (Strey, R.; Glatter, O. Private communication).

Conclusions

The theoretical model predicts that the same physics of entropic interactions within semiflexible networks that govern swollen ME may also determine the structure and phase behavior of certain binary micellar solutions. Our study supports this prediction experimentally by the observation of network topology in the vicinity of the binary critical point. In contrast to past theories that explained phase separation and criticality as resulting from increasing attraction between growing micelles,[18] we suggest an explanation within the same context of ME networks:[19] The binary critical point and the phase separation are naturally described as the $\phi_o \rightarrow 0$ limit of the ME critical point and two-phase coexistence region.

Acknowledgment. We thank Professors O. Glatter and R. Strey for useful discussions. This work was supported in part by a "Center of Excellence" grant from the Israel Academy of Sciences and Humanities.

LA990301Q

(18) Blankschtein, D.; Thurston, G. M.; Benedek, G. B. *J. Chem. Phys.* **1986**, *85*, 7268.
(19) Drye, T. J.; Cates, M. E. *J. Chem. Phys.* **1992**, *92*, 1367.

5

Microemulsion Networks: The Onset of Bicontinuity

J. Phys.: Condens. Matter **12** (2000) A253–A262. Printed in the UK PII: S0953-8984(00)09283-3

Microemulsion networks: the onset of bicontinuity

T Tlusty and S A Safran

Department of Materials and Interfaces, The Weizmann Institute of Science, Rehovot 76100, Israel

Received 4 November 1999

Abstract. We predict theoretically the gradual formation of fluctuating, connected microemulsion networks from disconnected cylinders as the spontaneous curvature and the radius are varied, in agreement with recent direct measurements of these topological transitions. We discuss the role of the topological defects, the network junction and the end-cap of the disconnected cylinders, in the connectivity transition. The optimal shapes and curvature energies of the junctions and end-caps are calculated numerically and compared with analytic approximations.

1. Introduction

Microemulsions (ME), dispersions of polar (water) and non-polar (oil) fluids and amphiphile, exhibit an extremely rich variety of geometries. This behaviour is attributable to the amphiphilic molecules which reside at the interfaces between water and oil, thus reducing the bare water–oil tension by 3–5 orders of magnitude; this drastic reduction enables the formation of mesoscopic water and oil domains defined by amphiphilic interfaces which can assemble in many different shapes and sizes. Among these topologies, the multiply-connected *symmetric* sponge, in which the water and oil domains are both continuous, has been extensively studied [1]. These bicontinuous structures are observed around the inversion temperature, $\bar{T}$, where the preferred curvature of the amphiphilic monolayer towards water or oil (the spontaneous curvature) vanishes. Away from $\bar{T}$, this bicontinuity disappears and the amphiphilic monolayers were traditionally thought to form disconnected globules surrounded by a continuous domain of the other component.

Preliminary data from self-diffusion NMR and conductivity measurements [2,3] suggested the existence of bicontinuous structures even far from $\bar{T}$, where one would have expected a phase of disconnected globules [4]. Recently, we proposed a model for ME based on thermally fluctuating *asymmetric bicontinuous networks*, whose building blocks are cylinders interconnected by junctions [5]. Our model provides a direct link between the structural bicontinuity and the striking thermodynamic features that ME exhibit around $\bar{T}$: the generic, critical, re-entrant two-phase separation and the subsequent formation of a three-phase region [6] together with its remarkable ultra-low values of the three tensions at the interfaces [7] are all direct results of an entropic attraction induced by the network fluctuations. Moreover, the model explains the universal scaling properties observed in recent experimental studies by Strey and Sottmann, that show data collapse of both the phase diagrams [8] and tensions [9] of 19 different non-ionic ME systems. The latest, most conclusive evidence to support the network picture was provided by Bernheim-Grosswasser and Talmon who used cryogenic transmission

0953-8984/00/SA0253+10$30.00 © 2000 IOP Publishing Ltd

electron microscopy (cryo-TEM) to directly observe the dilute, semi-flexible networks with their typical threefold 'Y-like' junctions [10], in both the single-phase and two-phase regions.

The fluctuating network model consistently predicts the topological transitions observed in ME when the spontaneous curvature, c_0, is decreased (in non-ionic ME, c_0 is controlled by the temperature as $c_0 \sim T - \bar{T}$): first, the ME evolves from spherical globules to long cylinders that subsequently interconnect via threefold junctions, leading to the formation of the bicontinuous network. The junctions interconnecting the cylindrical branches of the network are one type of topological defect of the infinite cylinders with a defect energy cost of the junction curvature energy, ϵ_3, relative to the cylinder bending energy. As usual, the defects are stabilized by the additional entropy that they afford the system since they increase the possible configurations of the ME network. We show below how this interplay between curvature energy and the network configurational entropy determines the network topology and the related free energy. Similarly, in ME composed of disconnected cylinders, the length distribution is determined by the balance between the curvature energy required to form the end-caps of the cylinders, ϵ_1, and their translational entropy. Moreover, we show that the *connectivity* transition when the network is formed from disconnected cylinders takes place when the junction and the end-cap energies are comparable, $\epsilon_3 \simeq \epsilon_1$ [11]. All this makes an accurate estimate of the curvature energies of these two types of topological defects a crucial ingredient of our theory, essential for understanding the relation between structure and thermodynamics and for comparison with experiment. In this paper, we briefly discuss the main concepts and results of the model, and present for the first time a calculation of the end-cap and junction curvature energies.

2. Network free energy and phase behaviour

Within the network, one can identify two length scales: the *local* length scale is the radius of the cylinders, R, that is governed by the curvature energy of the amphiphile interface. The *non-local, large-scale* length is the typical distance, L, between the network junctions, which is governed by the translational entropy of the junctions. Our theory traces the progression of the microstructure from the curvature-governed dilute network, $L \gg R \sim c_0^{-1}$, to the strong-fluctuation regime, where the junction defects proliferate, the typical distance between junctions becomes comparable with their size, $L \sim R \ll c_0^{-1}$, and they form a dense sponge.

As predicted by theory and confirmed by experiment [10], the bicontinuous ME network first appears at high spontaneous curvature, far from $\bar{T}$. In these regions, one can neglect the effect of short-wavelength thermal fluctuations and the *local* geometry of the ME is determined solely by the curvature energy of the amphiphile interface:

$$F_e = \frac{1}{2}\kappa \int \mathrm{d}S \left(\frac{1}{R_1} + \frac{1}{R_2} - 2c_0 \right)^2 + \bar{\kappa} \int \mathrm{d}S \left(\frac{1}{R_1} \frac{1}{R_2} \right) \tag{1}$$

where R_1 and R_2 are the principal radii of curvature, κ is the bending modulus and $\bar{\kappa}$ is the saddle-splay modulus. We discuss the sequence of transitions leading to the formation of the cylinders and then focus on their interconnection to form a bicontinuous network, a process governed by the entropy and the energetics of the junctions and the end-caps.

For bending constants, $\kappa \gg k_B T$, the curvature energy dominates and the free-energy density scales as $f_e = F_e/V = \phi r^{-3} E(r)$, where ϕ is the volume fraction of the inner phase (oil or water) and $r = c_0 R$ is the ratio of the radius to the optimal radius of curvature; $E(r)$ is the scale-invariant curvature energy. To find the stable local structure we compare the curvature energy of three possible geometries, spherical, cylindrical and lamellar. In a single phase the

radius is determined by the volume-to-surface ratio:

$$R = 2\delta \frac{\phi}{\phi_s} \tag{2}$$

where the volume fraction of the surfactant is ϕ_s and δ is the surfactant chain length (R is the cylinder radius, which is two-thirds of the sphere radius, and twice the inter-lamellar distance). The curvature energy of the cylinders is

$$E_c(r) = \kappa(1 - 4r) \tag{3}$$

while for spheres $E_s(r) = \frac{8}{9}(2\kappa(1 - 3r) + \bar{\kappa})$, where E_s and E_c are measured relative to the curvature energy of the lamellae $E_l = 0$. Comparing the curvature energies, one finds that the lamellae are optimal for $r < \frac{1}{4}$ (this region may be accessed by approaching the inversion temperature, $\bar{T}$, or alternatively by reducing the radius, R). As r increases there occurs a transition to cylinders, followed by a transition to a region where they coexist with spheres (around $r \simeq \frac{7}{12} + \frac{2}{3}\bar{\kappa}/\kappa$), and finally to a pure phase of spheres [4, 11].

The global structure of the cylindrical ME [4] is governed by entropy, due to the thermal fluctuations of its topological defects, the junctions and the end-caps [12]. To estimate the free energy, consider the network formed by an ensemble of cylinders of various lengths. The number density of cylinders of length m is $X(m)$, which obeys the volume conservation, $\int mX(m)\ \mathrm{d}m = \phi$. The branches are interconnected by z-fold junctions that each cost an energy ϵ_z (relative to the cylinders) due to their curvature. The number density of the junctions is z times smaller than the number density of free ends of the disconnected cylinders:

$$\rho_z = \frac{2}{z} \int X(m)\ \mathrm{d}m.$$

To obtain the free-energy density (in units of $k_B T$), one needs to take into account, apart from the translational entropy of the free cylinders (the first term of equation (4)), the curvature energy of the junctions (the second term) and the entropy (the last term) lost when each set of z free ends is constrained to form a junction [13]:

$$f_n = \int X(m)(\ln X(m) - 1)\ \mathrm{d}m + \rho_z \epsilon_z - (z - 1)\rho_z \ln \rho_z. \tag{4}$$

Minimizing the free energy (equation (4)) with respect to the length distribution $X(m)$, one finds that the junctions behave as an ideal gas of defects, in the sense that the entropy is $k_B T$ per junction, $f_n = -\rho_z$. The connectivity of the network together with the conservation laws for $X(m)$ imply that the number density of junctions, ρ_z, and the free energy scale as follows [13]:

$$f_n = -\rho_z \sim \phi^{z/2} \mathrm{e}^{-\epsilon_z}. \tag{5}$$

The $z = 1$ case corresponds to disconnected cylinders terminating at end-caps. The $z = 2$ 'junctions' may describe a one-dimensional system of defects along one infinite cylinder. These perturbations are taken into account by the thermal fluctuations of the cylinders, and become important only close to the cylinder $\leftrightarrow$ sphere transition, where the curvature energy of cylinders exceeds that of spheres. Connected networks are formed only for $z \geqslant 3$. Hereafter we consider only $z = 3$, Y-like junctions and $z = 1$ end-caps. In general, junctions of higher coordination number, $z > 3$, are also feasible, but occur very rarely [10]. This results from the $\phi^{z/2}$-scaling of the network free energy that favours low-z networks when the system is dilute, $\phi \ll 1$. High-genus junctions are also unfavourable due to the saddles introduced by their shape (topologically, each junction corresponds to $z/2 - 1$ handles). For the connected network ($z = 3$) the exponent ($\frac{3}{2}$) governing the dependence of the free energy on the volume fraction is higher than linear, resulting in an effective attraction. When the network is broken

into free cylinders ($z = 1$), the ideal gas of junctions is replaced by an ideal gas of end-caps, of number density ρ_1, that each cost curvature energy ϵ_1.

The network starts to form when the number of junctions exceeds the number of end-caps, at $\rho_1 \simeq \rho_3$. Comparing the topology-dependent part of the network free energy (equation (5)) for junctions and end-caps, we find that apart from a logarithmic correction, the network forms when the energies of the two defects are equal. The critical volume fraction for the cylinder-to-network transition is thus given by [11]

$$\epsilon_3 - \epsilon_1 \simeq \ln \phi. \tag{6}$$

The contribution of the Gaussian curvature, $K = 1/(R_1 R_2)$, to the elastic energy (equation (1)) is, by the Gauss–Bonnet theorem, a topological invariant determined solely by the total number of junctions and end-caps. The threefold junction and the end-cap have opposite topological contributions of $-4\pi\bar{\kappa}(z/2 - 1) = \pm 2\pi\bar{\kappa}$ [11]. The resulting $4\pi\bar{\kappa}$ difference between the curvature energies of the two defects may have implications for the ME structure and phase diagram, as discussed below.

3. Junction and end-cap shapes and energies

Apart from the difference in topology of the end-caps and junctions and the consequent saddle-splay energies, one needs to minimize the curvature energy due to the deviation of the mean curvature, $H = \frac{1}{2}(1/R_1 + 1/R_2)$, from its preferred value, the spontaneous curvature, $2\kappa \int (H - c_0)^2 \, \mathrm{d}S$. The construction of a defect requires amphiphilic molecules and an inner phase which need to be taken from the cylinders. This is taken into account by considering the cylinders as a large reservoir coupled to the defects by its chemical potentials (surface tension and osmotic pressure):

$$\epsilon_z = F_z - \left(\frac{\partial F_c}{\partial S}\right)_V S_z - \left(\frac{\partial F_c}{\partial V}\right)_S V_z \tag{7}$$

where F_z is the curvature energy of the defect (equation (1) for a junction or end-cap), V_z its volume and S_z its surface area; the chemical potentials are derivatives of the cylinder curvature energy, $F_c = \phi r^{-3} E_c(r) V$ with respect to change in their surface and volume. Substituting the cylinder curvature energy E_c (equation (3)) in the potentials of equation (7) results in a scale-invariant defect energy:

$$\epsilon_z = 2\kappa \int \mathrm{d}s_z \, (h^2 - 2rh) - \kappa\left(\frac{3}{2} - 4r\right)s_z - \kappa(4r - 2)v_z \tag{8}$$

where $r = c_0 R$, $h = HR$, $s_z = S_z R^{-2}$ and $v_z = V_z R^{-3}$ are the normalized spontaneous curvature, mean curvature, surface area and volume, respectively. The effective osmotic pressure, $\Pi = \kappa(2 - 4r)$, becomes negative for $r > \frac{1}{2}$. This manifests the instability of the cylinders to emulsification failure—that is, the rejection of the excess internal phase to optimize the curvature energy [14]. Functional minimization of equation (8) yields cumbersome Euler–Lagrange equations which were numerically solved only for the simplified case of axial symmetry [15]. Below, we describe the results of a direct numerical minimization using the optimization code SURFACE EVOLVER [16] and compare them to those obtained by a simplified single-parameter variation approach, which provides some physical insight into the exact results of the simulation. The structures of both junction and end-cap were confirmed in recent measurements by Bernheim-Grosswasser and Talmon [10, 11].

Two typical, numerically optimized junctions are depicted in figure 1. The amphiphile interface is represented by an open triangulated grid of points which evolve under the influence

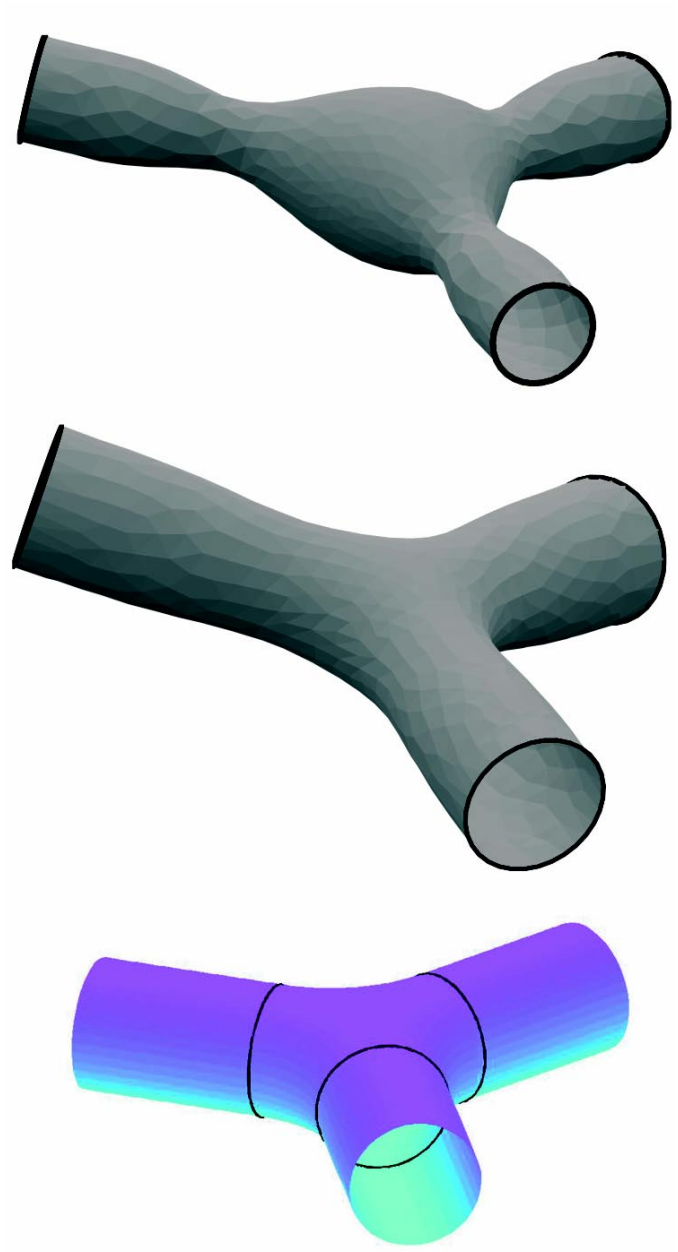

Figure 1. *The optimal shape of the threefold 'Y-like' junction.* Numerical optimization at high curvatures, $r = c_0 R = 0.5$, shows that the junction develops an enlarged spherical core with necks connecting to the cylinders (top). At smaller spontaneous curvatures, $r = c_0 R = 0.3$, we find that the junction develops a lamellar core, reflecting the fact that the system approaches the region where flat lamellae are the preferred local geometry (middle). This shape is similar to the analytic approximation (bottom), a lamellar core smoothly attached to three semi-toroidal segments. Each semi-toroidal segment is a sixth of the inner part of the torus. The smooth connections to the cylinders are denoted by dark rings.

of pseudo-forces derived from the energy integral (equation (8)) [16]. The boundary conditions are smooth connections of the minimized junction interface to three coplanar cylinders of radius $R = 1$ (since the problem is scale invariant) meeting at angles of $\frac{2}{3}\pi$. Observing the progression of the shape of the junction as the spontaneous curvature is changed, we find two regimes. At small spontaneous curvatures, $r = c_0 R < 0.3$, we find that the junction develops a lamellar core, reflecting the fact that the system approaches the region where flat lamellae are the preferred local geometry. At higher curvatures, $0.3 \leqslant r < 0.5$, we approach the region of spherical local geometry and the junction develops a spherical core with necks connecting to the cylinders. When we further increase the curvature, to $r > 0.5$, we find that the junction is unstable with respect to emulsification failure. In simulation, this instability is manifested by the 'explosion' of the core. The numerical minimization yields an approximately linear scaling of the junction energy with the spontaneous curvature (figure 2):

$$\epsilon_3 \simeq 4\pi\kappa(\alpha_3 r + \beta_3) \tag{9}$$

with $\alpha_3 \simeq 1.3$ and $\beta_3 \simeq -0.5$. We note that the ϵ_3 becomes negative for $r < -\beta_3/\alpha_3 \simeq 0.38$, even before the stable local geometry becomes lamellar. In simulation, junctions in this region tend to split into three junctions by puncturing the middle core. However, these negative-energy junctions may still be stabilized by three additional effects:

(i) For small enough saddle-splay modulus, $\bar{\kappa}$, the topological 'charge' of the junction, $-2\pi\bar{\kappa}$, may overcome the negative ϵ_3.

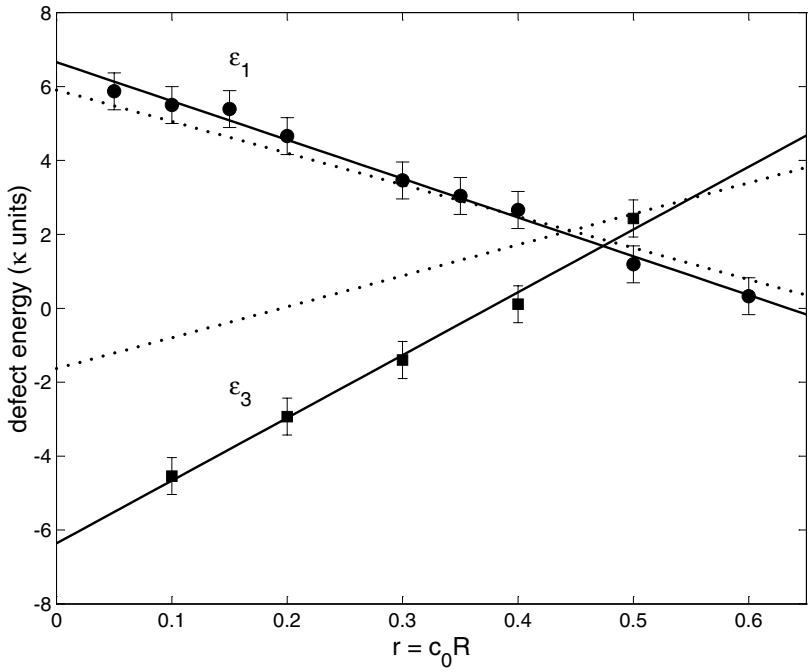

Figure 2. *Curvature energy of the defects.* Numerical optimizations of the curvature energy of junctions (ϵ_3—solid squares) and end-caps (ϵ_1—solid circles) exhibit an approximately linear scaling in $r = c_0 R$ (linear fits—solid lines). Junctions are optimal for small values of the normalized spontaneous curvature, r, due to their flat lamellar core, while end-caps are preferred at larger r because of their spherical cap. The numerical results are compared to the analytic approximations (dotted lines).

(ii) When the junctions proliferate they repel each other due to the curvature energy cost of the finite-length cylinders whose shape and energies have been modified by the nearby junctions.

(iii) As we discuss below, when the radius of the cylinders becomes comparable with the thickness of the amphiphile interface, one should introduce higher-order terms into the curvature energy.

An analytical approximation to the junction interface is depicted in figure 1: the junction is constructed from a lamellar core smoothly attached to three semi-toroidal segments of inner radius $R = 1$ and outer radius R_T, which is the parameter to be optimized. Each semi-toroidal segment is a sixth of the inner part of the torus. Integrating equation (8) over the surface of the junction we obtain

$$\epsilon_3 = \pi\kappa\left(\frac{2\tau^2}{\sqrt{\tau^2-1}}\arctan\sqrt{\frac{\tau+1}{\tau-1}} + \left(\frac{\sqrt{3}}{\pi} - \frac{1}{2}\right)\tau^2 - \frac{1}{2}\pi\tau + \frac{1}{3}(8r-7)\right)$$

where $\tau = R_T/R$ is the ratio of the outer and inner radii of the torus. Minimizing the latter expression, we find that optimal outer radius, and thus the junction shape, is independent of c_0, with $\tau = R_T/R \simeq 2.59$. The resulting junction energy is $\epsilon_3 \simeq 4\pi\kappa(\frac{2}{3}r - 0.13)$. This analytical approximation (figure 2) exhibits the same qualitative behaviour as the numerical solution of equation (9). The energy reflects the interplay between the tendency to enlarge the preferred lamellar core and the need to keep the outer radius of the torus small enough to compensate by its negative curvature, $0 \geqslant 1/R_1 \geqslant -1/R_T$, the positive curvature of the circular cross section, $1/R_2 = 1/R$. However, the approximation strongly deviates from the numerical solution for small r, mainly because the lamellar core cannot adjust its thickness, which is constrained to be equal to the diameter of cylinders. One may improve the poor agreement with simulation by relaxing this constraint, adding the ratio of core and cylinder widths as a second variational parameter [12].

The optimized shape of the end-cap, ϵ_1, exhibits an opposite dependence on the parameter $r = c_0R$ (figure 2): due to their enlarged spherical cap (figure 3) the end-caps cost more curvature energy at small r, where the preferred geometry is lamellar. The numerical minimization yields

$$\epsilon_1 \simeq 4\pi\kappa(\alpha_1 r + \beta_1) \tag{10}$$

with $\alpha_1 \simeq -0.84$ and $\beta_1 \simeq 0.54$. To obtain an analytical approximation we describe the end-cap as composed of two parts: a semi-spherical cap smoothly connected to the cylinder by a constant-mean-curvature, trumpet-like interface (figure 3). The axially symmetric interface is described by the profile of the radius $y(z)$ determined by the constant-mean-curvature constraint [15]:

$$\sin\theta = (1 + (\partial_z y)^2)^{-1/2} = (y + R_s R/y)/(R + R_s)$$

where R_s is the radius of the spherical cap to be optimized; the principal curvatures are $1/R_1 = \sin\theta/y$ and $1/R_2 = d_y \sin\theta$. The resulting curvature integral (equation (8)) is

$$\epsilon_1 = \frac{1}{3}\pi\kappa\left[\mu\left(\frac{\mu}{\mu+1}(4\mu^2+\mu-8) - 4[\mu(2\mu-3)+2]r + 7\right)E\left(\sqrt{1-\mu^{-2}}\right)\right.$$
$$\left. + \left(\mu(4\mu-9) - 8[(\mu-3)\mu+3]r\right) + 2\mu(2r-1)K\left(\sqrt{1-\mu^{-2}}\right) + 12\right]$$

where $\mu = R_s/R$ is the ratio of the sphere and cylinder radii. Optimizing the radius of the spherical cap, we obtain from the latter expression $\epsilon_1 = 4\pi\kappa(-0.68r + 0.47)$, in good agreement with the numerical solution (equation (10)), as depicted in figure 2. Here, the small

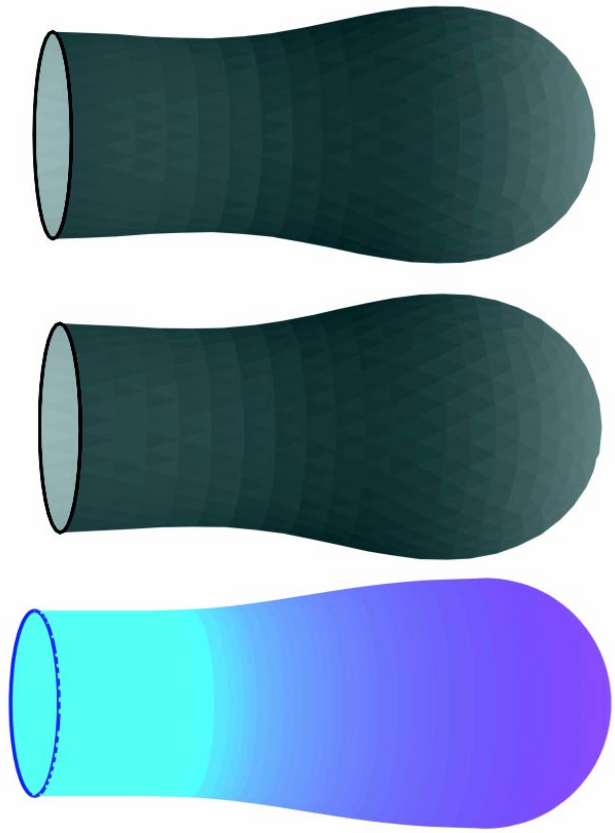

Figure 3. *The optimal shape of the end-cap.* The typical enlarged spherical cap is smoothly connected to the cylinder by a trumpet-like interface (these connections are denoted by dark rings). The numerical optimization shows no significant difference between the shapes of the optimal end-caps at high curvature (top—$r = c_0 R = 0.5$) and low curvature (middle—$r = 0.2$). The analytic, constant-mean-curvature approximation yields a similar shape (bottom).

deviations occur mainly because of a neck between the 'trumpet' and the cylinder that develops in simulation in the small-r region (figure 3).

The difference in elastic energy of the junction and end-cap, as calculated by the numerical or variational minimization described above, scales approximately linearly with r:

$$\epsilon_3 - \epsilon_1 = 4\pi\kappa((\alpha_3 - \alpha_1)r + (\beta_3 - \beta_1)) - 4\pi\bar{\kappa}$$

where the last term accounts for the opposite topological 'charge'. Junctions are optimal for small values of the normalized spontaneous curvature due to their flat lamellar core, while end-caps are preferred at larger r because of their spherical cap (figures 1–3). Substituting in equation (6) produces an expression for the value of $r = c_0 R$ at the cylinders-to-network transition at $r = r_n$ with [11]

$$r_n = \frac{1}{\alpha_3 - \alpha_1}\left((\beta_1 - \beta_3) + \frac{\bar{\kappa}}{\kappa} + \frac{1}{4\pi\kappa}\ln\phi\right). \tag{11}$$

The theoretical prediction described above, for the series of topological transitions leading to the formation of a network, spheres $\rightarrow$ spheres + cylinders $\rightarrow$ cylinders $\rightarrow$ network, was

recently substantiated by direct cryo-TEM measurements on non-ionic ME [10].

To accurately describe the elastic energy of ME systems with relatively small radii of curvature $R \sim \delta$, and especially to approach the limit of binary micellar ME (with no internal phase), one needs to take into account the details of the molecular interactions [12]. Here we approximate these effects by adding to the harmonic bending energy the next-order term, of third order in the principal curvatures. Expanding the elastic energy (equation (1)) for curvatures at a parallel surface, we find that the third-order term is proportional to $\kappa\delta(c_0 - H)(H^2 + c_0 H - K)$. We consider only the surface integral over H^3 and HK, since all other third-order terms contain powers of c_0 and therefore vanish in the binary limit, $r = c_0 R = 0$; for large values of r these terms are negligible compared to the harmonic bending energy. Using our results for the typical shapes of the end-cap and junctions, we find that this contribution, $2\kappa\delta \int \mathrm{d}S\ (KH - H^3)$, is negative for the end-cap and positive for the junction and scales as

$$\bar{\epsilon}_z = \gamma_z \kappa \frac{\delta}{R} = \gamma_z \kappa \frac{c_0 \delta}{r} \tag{12}$$

with $\gamma_1 < 0$ and $\gamma_3 > 0$, both of order unity. The third-order term, $\bar{\epsilon}_z$, inverts the behaviour of ϵ_z close to the binary limit, $r = 0$ (the actual radius at the binary limit is the molecular length, $r \simeq c_0\delta$). We therefore find a maximum in ϵ_1 and a minimum of ϵ_3 at typical radii which scale like $R_* \sim (\delta/c_0)^{1/2}$ (or $r_* \sim (c_0\delta)^{1/2}$).

The minimum in ϵ_3 has important implications for the ME phase diagram. The bicontinuous network exhibits a unique instability which directly results from its global connectivity: the entropic part of the free energy is unstable to phase separation when the effective attraction, $f_n = -\rho_z \sim -\phi^{z/2}\mathrm{e}^{-\epsilon}$, overcomes the repulsion. This occurs for values of the junction energy lower than a critical value. Since $\phi^{z/2}$ represents an effective attraction only if the exponent is higher than linear (or $z \geqslant 3$), we find that this type of phase separation is unique for the connected structures. The curvature energy of the junction exhibits a minimal value at r_* which corresponds to a steep maximum of the attraction due to its exponential dependence $\sim\mathrm{e}^{-\epsilon_3}$. When the maximal attraction exceeds the critical value, the ME phase separates into two networks of the same local geometry, cylindrical of radius r, which differ in the density of junctions, as verified by experiment [10]. This explains the re-entrant phase separation loops and the subsequent three-phase coexistence, which emerge as direct results of the non-monotonic behaviour of the junction energy, $\epsilon_3(r)$ [5]. In the phase diagram this *global* instability is manifested by the appearance of a two-phase coexistence loop bounded by two critical points.

Acknowledgments

The authors thank R Strey, T Sottmann, A Bernheim Grosswasser and Y Talmon for fruitful collaboration and inspiring discussions. We thank K Brakke and U S Schwarz for their help in using SURFACE EVOLVER, the numerical minimization software. We are grateful to the Research Centre on Self-Assembly of the Israel Science Foundation and the Minerva Gerhard Schmidt Centre for Supramolecular Architecture.

References

[1] Gelbart W M, Ben-Shaul A and Roux D (ed) 1994 *Micelles, Membranes and Microemulsions and Monolayers* (Berlin: Springer)
[2] Strey R, unpublished
[3] Lipgens S, Schūbel D, Schlicht L, Spilgies J H, Ilgenfritz G, Eastoe J and Heeman R K 1998 *Langmuir* **14** 1041

[4] Safran S A, Turkevich L A and Pincus P A 1984 *J. Physique Lett.* **45** L19
[5] Tlusty T, Menes R, Safran S A and Strey R 1997 *Phys. Rev. Lett.* **78** 2616
[6] Kahlweit M, Strey R and Busse G 1990 *J. Phys. Chem.* **94** 3881
[7] Aratono M and Kahlweit M 1991 *J. Chem. Phys.* **95** 8578
Kahlweit M, Strey R and Busse G 1993 *Phys. Rev.* E **47** 4197
[8] Sottmann T and Strey R 1997 *J. Chem. Phys.* **106** 8606
[9] Sottmann T and Strey R 1996 *J. Phys.: Condens. Matter* **8** A39
[10] Grosswasser A B, Tlusty T, Safran S A and Talmon Y 1999 *Langmuir* **15** 5448
[11] Tlusty T, Safran S A and Strey R 2000 *Phys. Rev. Lett.* **84** 1244
[12] May S, Bohbot Y and Ben-Shaul A 1997 *J. Phys. Chem.* B **101** 8649
[13] This mean-field approach was applied to micellar solutions:
Drye T J and Cates M E 1992 *J. Chem. Phys.* **96** 1367
and for a spin $n \to 0$ approach see
Elleuch K, Lequeux F and Pfeuty P 1995 *J. Physique* I **5** 465
[14] Safran S A and Turkevich L A 1983 *Phys. Rev. Lett.* **50** 1930
Leaver M S and Olsson U 1994 *Langmuir* **10** 3449
[15] Deuling H J and Helfrich W 1976 *J. Physique* **37** 1335
[16] K Brakke's Manual and Code for SURFACE EVOLVER may be downloaded at
http://www.susqu.edu/facstaff/b/brakke/evolver/evolver.html
http://www.geom.umn.edu/software/download/evolver.html

6

Defect Induced Phase Separation in Dipolar Fluids

dance. But, if we assume that the true iron abundance of the hot interstellar medium is solar, then we might be forced to infer that only 30% of the diffuse emission is actually thermal. Despite the observation of thermal line emission, it is thus difficult to rule out a component of diffuse emission from inverse Compton scattering. Assuming that the hard diffuse emission contains a major component of thermal origin (30 to 100% of the total) and integrating over the Gaussian elliptical region, we estimate that the plasma has a temperature of $\sim T \simeq 40$ MK and pressure of the order of $P/k \simeq 10^9$ cm^{-3}.

It seems quite likely that the hot component is not in hydrostatic equilibrium and is the basic driving force for the galactic wind outflowing perpendicular to the plane of M82. This hot x-ray–emitting gas is thus overpressurized as compared to the galaxy's gravitational potential well and is thus probably the principal driving mechanism for the hot outflow of chemically enriched material into the intergalactic medium. Such high-temperature plasmas in the cores of starburst galaxies may be the basic drivers for the chemical enrichment of the intergalactic medium and the intracluster medium within clusters of galaxies.

References and Notes

1. D. W. Weedman *et al.*, *Astrophys. J.* **248**, 105 (1981).
2. Y. Sofue, Ed., *The Central Regions of the Galaxy and Galaxies*, *IAU Symp. 184* (Kluwer, Dordrecht, Netherlands, 1998).
3. K. A. Van der Hucht, G. Koenigsberger, P. R. Eenens, Eds., *Wolf-Rayet Phenomena in Massive Stars and Starburst Galaxies*, *IAU Symp. 193* (Astronomical Society of the Pacific, San Francisco, 1999).
4. J. E. Barnes, D. B. Sanders, Eds., *Galaxy Interactions at Low and High Redshift*, *IAU Symp. 196* (Kluwer, Dordrecht, Netherlands, 1999).
5. S. Holt, E. Smith, Eds., *After the Dark Ages: When Galaxies Were Young* (AIP Press, New York, 1999).
6. W. Freedman *et al. Astrophys. J.* **427**, 628 (1994).
7. P. Kronberg, in *Galactic and Extragalactic Star Formation*, R. E. Pudritz, M. Fich, Eds. (Reidel, Boston, 1988), pp. 391–399.
8. R. E. Griffiths, M. D. Johnson, D. A. Schwartz, J. Schwarz, J. C. Blades, *Astrophys. J.* **230**, L21 (1979).
9. M. G. Watson, V. Stanger, R. E. Griffiths, *Astrophys. J.* **286**, 144 (1984).
10. J. N. Bregman, E. Schulman, K. Komisaka, *Astrophys. J.* **439**, 155 (1995).
11. T. G. Tsuru, H. Awaki, K. Koyama, A. Ptak, *Publ. Astron. Soc. Jpn.* **49**, 619 (1997).
12. E. C. Moran, M. D. Lehnert, *Astrophys. J.* **478**, 172 (1997).
13. I. R. Stevens, D. K. Strickland, K. A. Wills, *Mon. Not. R. Astron. Soc.* **308**, 123 (1999).
14. A. Ptak, R. E. Griffiths, *Astrophys. J.* **517**, L85 (1999).
15. M. C. Weisskopf, S. L. O'dell, L. P. van Speybroeck, *Proc. SPIE* **2805**, 2 (1996).
16. G. Garmire *et al.*, in preparation.
17. ACIS on the CXO provides sub–arc second imaging across a wide spectral band, low instrumental background rates permitting study of extended structures, and moderate spectral resolution at every pixel for astrophysical modeling.
18. The displayed images required several steps of data processing. With level 1–processed detected "event" lists, several types of events that were probably dominated by cosmic ray primary and secondary particles rather than imaged x-rays were removed: (i) event energies above 8 keV and below 0.2 keV; (ii) events split between pixels, except for standard ASCA grades; (iii) "hot columns" and other low-quality events; and (iv) brief periods of high background. The ACIS-I chips suffered radiation damage early in the Chandra mission, producing an increase in its charge-transfer inefficiency (CTI) during readout. To compensate for this effect, we recalibrated the ADU (analog-to-digital unit)-to-energy conversion for each photon as a function of its CCD pixel coordinate in the *y* direction (CHIPY) location using the calibration data set acisf1310. This correction is similar to that in (*29*) and produces individual photon energies accurate to ~10%. Our analysis here concentrates on events extracted from CHIPY > 700 in CCD I3, where most of the events detected from M82 are found. The resulting count-rate map was subject to adaptive kernel smoothing, which permits simultaneous viewing of compact and extended structures (*29*). Point sources were located with a multiscale wavelet analysis of the image (*30*). Although this procedure reliably detects isolated sources down to about seven photons, its sensitivity within the bright diffuse emission pervading the core of M82 is lower and difficult to determine quantitatively.
19. A. Collura, F. Reale, E. Schulman, J. N. Bregman, *Astrophys. J.* **420**, L63 (1994).
20. G. H. Rieke, M. J. Lebovsky, R. I. Thompson, F. J. Low, A. T. Tokunaga, *Astrophys. J.* **238**, 24 (1980).
21. D. Barret, J. E. McClintock, J. E. Grindlay, *Astrophys. J.* **473**, 963 (1996).
22. K. A. Wills, A. Pedlar, T. W. B. Muxlow, I. R. Stevens, *New Astron. Rev.* **43**, 633 (1999).
23. R. W. O'Connell, J. S. Gallagher, D. A. Hunter, W. N. Colley, *Astrophys. J.* **446**, L10 (1995).
24. L. Townsley *et al.*, in preparation.
25. These fits were performed with XIMGFIT, which is available at http://snooker.phys.cmu.edu/ximgfit. Photons from the sources in Table 1 were removed by replacing pixels where the contrast between the source model (Gaussian) and background model exceeded 50% by a Poisson deviate with a mean value given by the background model at that position.
26. H. V. D. Bradt, J. E. McClintock, *Annu. Rev. Astron. Astrophys.* **21**, 13 (1983).
27. A. P. Cowley *et al.*, in *The Stellar Content of Local Group Galaxies*, *IAU Symp. 192*, P. A. Whitelock, R. D. Cannon, Eds. (Astronomical Society of the Pacific, San Francisco, 1999), pp. 100–103.
28. We caution that the calibration of the ACIS spectral response is still evolving because of the CTI problem (*18*), and spectral fitting for extended structures is likely to improve beyond the work presented here.
29. L. Townsley *et al.*, *Astrophys. J.* **534**, L139 (2000).
30. H. Ebeling, D. A. White, V. N. Rangarajan, *Mon. Not. R. Astron. Soc.*, in press.
31. R. W. O'Connell, J. J. Mangano, *Astrophys. J.* **221**, 62 (1978).
32. P. E. Freeman, V. Kashyap, R. Rosner, D. Q. Lamb, in preparation.
33. H. Kaneda *et al.*, *Astrophys. J.* **491**, 638 (1997).
34. S. Satyapal *et al.*, *Astrophys. J.* **483**, 148 (1997).
35. Z. P. Huang, T. X. Thuan, R. A. Chevalier, J. J. Condon, Q. F. Yin, *Astrophys. J.* **424**, 114 (1994).
36. R. de Grijs, R. W. O'Connell, G. D. Becker, R. A. Chevalier, J. S. Gallagher III, *Astron. J.* **119**, 68 (2000).

37. We express our appreciation for the many scientists and engineers who brought Chandra to fruition, in particular those at the Massachusetts Institute of Technology, Penn State University, and Lockheed Martin who contributed to the ACIS instrument. This research was funded by NASA contract NAS8-38252 to Penn State University.

27 July 2000; accepted 10 October 2000

Defect-Induced Phase Separation in Dipolar Fluids

T. Tlusty* and S. A. Safran*

A defect-induced, critical phase separation in dipolar fluids is predicted, which replaces the usual liquid-gas transition that is driven by the isotropic aggregation of particles and is absent in dipolar fluids due to strong chaining. The coexisting phases are a dilute gas of chain ends that coexists with a high-density liquid of chain branching points. Our model provides a unified explanation for the branched structures, the unusually low critical temperature and density, and the consequent two-phase coexistence "islands" that were recently observed in experiment and simulation.

The critical liquid-gas phase transition (LGT) is a generic feature of simple fluids. When the temperature is decreased below the critical temperature, the simple fluid phase separates into a low-density gas that coexists with a high-density liquid. The phase separation is well understood as the consequence of a temperature-dependent interplay between the entropy loss due to hard-core repulsion and a short-range isotropic attraction, as was first formulated by van der Waals in his equation of state. In contrast, the basic thermodynamics of dipolar fluids, where the attraction is due to long-range anisotropic dipolar forces, are still obscure, including the basic question of whether the LGT exists at all.

Dipolar fluids have numerous scientific and industrial applications, mostly related to the strong field-responsive properties of colloidal ferrofluids (*1*) or electro-rheological fluids (*2*). For these applications, it is crucial to know whether the system exists in a single homogenous phase. Dipolar fluids also have theoretical significance as a fundamental model of statistical mechanics, perhaps the simplest example of an anisotropic fluid, which may provide physical insight for polar fluids such as hydrogen fluoride or even water.

The mean dipolar interaction between two particles is attractive (with a Boltz-

Department of Materials and Interfaces, Weizmann Institute of Science, Rehovot, Israel.

*To whom correspondence should be addressed. E-mail: cptsvi@weizmann.ac.il (T.T.); sam.safran@weizmann.ac.il

mann weighted average due to mutual orientation), which may lead one to conclude within a mean-field theory that a LGT similar to that exhibited by isotropic fluids should also occur in dipolar fluids (*3*). However, simulation studies (*4*–*7*) reveal a completely different and more complex scenario: The anisotropic dipolar interaction, which favors a nose-to-tail alignment of the dipoles (Fig. 1A), drives the particles to self assemble in polymer-like chains (Fig. 1B) (*8*, *9*). The linear aggregation of the chains is a one-dimensional process in which no phase transition is expected to occur. The absence of the LGT has been attributed to the strong chaining that interferes with the isotropic aggregation (*7*, *10*–*12*).

Large-scale computer simulations have found evidence for the occurrence of a critical liquid-gas transition in a system of hard spheres with solely dipolar interactions (*13*); however, the estimated critical temperature and density are unusually low in comparison to simple fluid values. In the proximity of the critical point, the simulated dipolar spheres assemble in chains with apparent branching points. Thermodynamic measurements found evidence for a critical liquid-gas transition in magnetic fluids consisting of ferric oxide nanospheres (*14*). However, in this colloidal fluid it is difficult to separate the effect of the dipolar interaction from the short-range isotropic attraction (*15*).

Motivated by these experimental and simulation studies, we consider a model whose basic components are not the dipolar spheres themselves but the ensemble of self-assembling chains they form, allowing us to focus on the collective large-scale features of the system. The dipolar fluid consists of identical spheres of diameter D carrying a magnetic moment of amplitude μ. The dipolar interaction between two spheres whose dipoles are $\vec{\mu}_1$, $\vec{\mu}_2$, and are separated by a distance $\vec{r}$ is

$$U = \frac{1}{r^3}(\vec{\mu}_1 \cdot \vec{\mu}_2) - \frac{3}{r^5}(\vec{\mu}_1 \cdot \vec{r})(\vec{\mu}_2 \cdot \vec{r}) \qquad (1)$$

The natural dipolar energy unit is that of two spheres at contact, $u_d = \mu^2/D^3$, which defines the reduced temperature, $T^* = T/u_d$. The maximal possible dipole-dipole attraction is $-2u_d$, obtained when the two spheres touch at nose-to-tail alignment, which is twice the attraction of antiparallel side-by-side dipoles (Fig. 1A). At low temperatures, $T^* \ll 1$, this strong anisotropy favors the linear aggregation of the spheres that are concatenated in the chains (Fig. 1B). The dipolar interaction is also long-range due to its r^{-3} decay. Nevertheless, in the absence of external magnetic field a thermodynamic limit exists (*16*) and the interaction becomes "nearly short range" for one-dimensional objects (*17*). Thus, we treat the chains as an ensemble of self-assembling, "living" polymers that are free to break, reform, and exchange spheres.

In a certain regime of relatively low temperatures and densities, the chains will further organize and will interconnect via threefold junctions into a network. This branching occurs when it is energetically favorable to construct junctions from chain ends at the expense of the reduction of their translational entropy (Fig. 1C). Both topological defects, ends and junctions, cost dipolar interaction compared with the lower energy state of an infinite chain. However, the introduction of either kind of defect increases the entropy and is therefore favored at finite temperature. The energy cost of a free end, ε_1, is larger than that of a junction, ε_3. At low temperatures, this energy difference drives the formation of a network (*18*).

Our model of dilute dipolar fluids at low temperatures as self-assembling networks enables us to apply theoretical tools that were originally developed to treat living polymers (*19*), micellar solutions (*20*), and, recently, microemulsion networks (*21*, *22*). The starting point of the model is the probability that a chain starts or terminates at a point $\vec{r}$, $\psi(\vec{r})$ (*23*). The probability for a chain crossing through $\vec{r}$ is proportional to $\psi(\vec{r})^2$, because one may think of each monomer as the confluence of two chain ends. Within our mean-field model, it directly follows that the volume fraction of spheres scales like $\phi \sim \psi^2$. The concentration of ends is ψ multiplied by a Boltzmann factor that accounts for the energetic cost of an end defect, $\rho_1 \sim \psi e^{-\varepsilon_1/T^*} \sim \phi^{1/2} e^{-\varepsilon_1/T^*}$, where the defect energies are measured in units of u_d. Similarly, we find that the concentration of threefold junctions, that require the confluence of three ends, scales like $\rho_3 \sim \psi^3 e^{-\varepsilon_3/T^*} \sim \phi^{3/2} e^{-\varepsilon_3/T^*}$. Calculation of the free energy yields the standard result for systems governed by an interplay between the energy and entropy of topological defects. Each defect, whether it is a threefold junction or an end, contributes $-k_B T$ (where k_B is the Boltzmann constant) to the free energy density (*24*)

$$f = -\rho_1 - \rho_3 + 1/2\phi^2 = -(2\phi)^{1/2} e^{-\varepsilon_1/T^*} - 1/3(2\phi)^{3/2} e^{-\varepsilon_3/T^*} + 1/2\phi^2 \qquad (2)$$

where the third term accounts for the excluded volume repulsion between chains. Examining the osmotic pressure, $p = \phi^2 \partial_\phi (f/\phi) = 1/2\phi^2 + 1/2(\rho_1 - \rho_3)$, we find two opposing, topologically induced thermodynamic forces, a repulsion due to ends and an attraction due to junctions.

The dipolar fluid phase separates when the attraction of the dipolar junctions overcomes the repulsion due to ends and the excluded volume entropy loss. This phase separation occurs only below a critical temperature, T_c^*, located at the point where the coexistence curve meets the spinodal curve, the boundary of thermodynamic stability, $\partial_\phi^2 f = 0$ (Fig. 2). Analysis of the free energy yields the critical temperature and volume fraction

$$T_c^* = \frac{\varepsilon_1 - 3\varepsilon_3}{3 \ln 3 - 2 \ln 2},$$
$$\ln \phi_c = -\frac{\varepsilon_1(2 \ln 3 - \ln 2) - \varepsilon_3 \ln 2}{\varepsilon_1 - 3\varepsilon_3} \qquad (3)$$

The critical point has a remarkable topological significance. In analyzing f we find that the number of ends and junctions are equal $\rho_1 = \rho_3$ at the critical point, which is thus a point of connectivity transition in the system (*25*, *26*).

Indeed, the dipolar fluid separates into two isotropic phases, but the nature of the "liquid" and "gas" phases is different from

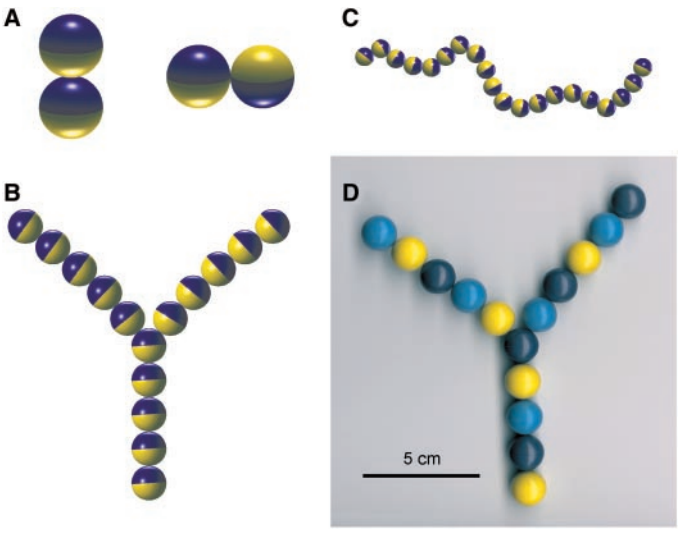

Fig. 1. (**A**) The dipolar attraction between two spheres in nose-to-tail alignment (left) is twice the attraction of side-by-side spheres (right). (**B**) At low temperatures and densities, this anisotropy drives the particles to self assemble in thermally fluctuating polymer-like chains. (**C**) The numerically optimized shape of the threefold junction. The "Y-like," almost symmetrical fork shape of the junction has lower energy than the end defect, leading to the formation of connected networks. (**D**) A photograph of a similar configuration that is obtained when one brings three chains of magnetic marbles ($D \simeq 1.5$ cm) in close proximity; they attract and form a stable junction.

that of simple fluids. The basic "particles" in our model are not the individual dipolar spheres but the topological defects—the network junctions and free ends. Whereas the free energy of an individual sphere saturates to an almost constant value due to the strong dipolar attraction in the chains, the global structure and thermodynamics are governed by the entropy of the defects in accord with the isotherms of Camp *et al.*, which exhibit approximately constant free energy per sphere over almost one decade of increasing density in the regime of phase separation. The liquid-gas transition is, therefore, analogous to the demixing of a binary fluid consisting of junctions and ends. In the low density "gas" there are more ends than junctions ($\rho_1 > \rho_3$) whereas the high density "liquid" is dominated by junctions ($\rho_1 < \rho_3$). Hence, the liquid network is connected in the sense discussed above, whereas the gas is composed of disconnected chains. In the phase diagram, these two regions are separated by the connectivity transition line ($\rho_1 = \rho_3$) (Fig. 2).

To further substantiate our proposal that the origin of the critical phase separation is a connectivity transition, we demonstrated that the energy cost of an end defect is indeed higher than that of a threefold junction. The estimates from the simulations of Camp *et al.* for the critical temperature and volume fraction are $T_c^* \simeq 0.15 - 0.16$ and $\phi_c \simeq 0.05 - 0.07$, which correspond to defect energies of $\varepsilon_1 \simeq 0.67$ and $\varepsilon_3 \simeq 0.12$, respectively (Fig. 2). We then compared these values to numerical estimates. The end energy cost is simply half the energy required to cut a continuous chain. Within the nearest neighbor approximation, this energy is $\varepsilon_1 = 1$, and the upper limit obtained for straight, infinite chain is $\varepsilon_1 = \zeta(2) \simeq 1.65$. The excess energy and the "Y-like" fork shape of the optimal threefold junction are calculated by numerical minimization (Fig. 1C). A similar shape is obtained when one assembles three chains of magnetic marbles ($D \simeq 1.5$ cm) that form an energetically stable junction (Fig. 1D). Upon its formation, the junction gains one additional bond but loses more energy due to deviations from the optimal nose-to-tail alignment. This tunable balance results in a junction energy, which is lower than the end energy, as required. The estimate for the junction energy, $\varepsilon_3 \simeq 0.2 - 0.5$, reflects the analytical difficulties in minimizing the long-range dipolar interaction among the three finite, thermally fluctuating branches. The lower limits for ε_1 and ε_3 yield reasonable critical parameters, $T_c^* \simeq 0.20$ and $\phi_c \simeq 0.03$, whereas the upper limits give an unrealistically small critical density.

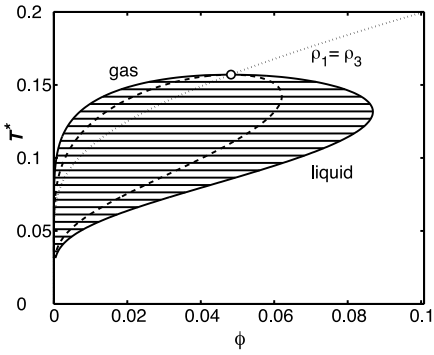

Fig. 2. The phase diagram of the dipolar network calculated for defect energies of $\varepsilon_1 = 0.67$ and $\varepsilon_3 = 0.12$. At the critical point (circle), the coexistence curve (thick solid line), the phase stability boundary (dashed line), and the connectivity transition (dotted line) meet. The lines denote the coexistence of the end-rich "gas" with the junction-rich "liquid." At low temperatures, the coexistence region narrows to very low densities.

The densities of both junctions and ends decrease exponentially with decreasing temperature, leading to exponentially longer branches. The junction density, $\rho_3 \sim e^{-\varepsilon_3/T^*}$, decreases slower than the end density, $\rho_1 \sim e^{-\varepsilon_1/T^*}$, due to the lower defect energy. Therefore, in the proximity of the critical point, the junction attraction overcomes the end repulsion and the coexistence region expands. As temperature is further decreased, there are not enough junctions to balance by their attraction the excluded volume repulsion and the coexistence region narrows to very low densities (Fig. 2). This reentrance might be masked by the coexistence of the low-density gas with a solid-like phase or a high-density magnetic liquid (*27*). At low temperatures, we predict that the thermodynamically stable structure is that of a dilute network with many junctions and hardly any ends, in accord with the branched structures exhibited in simulations (*4*, *6*). A crucial test of our model in experiment or simulation may be the observation of dipolar networks in the vicinity of the critical point in both coexisting phases (*22*).

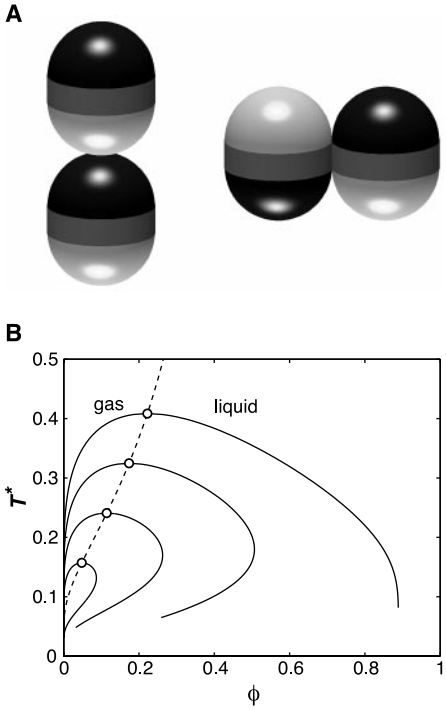

Fig. 3. (**A**) The sphero-cylindrical particles are composed of two hemispheres of diameter D separated by a cylinder of length L. The interaction energies of optimal sphero-cylinders ($L/D \simeq 1/4$) at nose-to-tail and side-by-side alignments are equal, which reduces the defect energies and leads to isotropic aggregation and a critical phase separation similar to that of isotropic fluids. (**B**) A similar effect is achieved by the introduction of a short-range attraction, δ. The series of the calculated coexistence lines (solid) shows the progression, as the contact energy is increased (for $\delta = 0$, 0.08, 0.16, 0.24) from the reentrant coexistence curve (lowest value of T_c^*) to a parabolic shape, typical to isotropic fluids (highest value of T_c^*). The dashed line follows the trajectory of the critical point.

The LGT of dipolar hard spheres is difficult to observe in simulations due to the small scales of density and entropy and the long relaxation times that stem from anisotropic chaining (*28*). One can overcome the strong anisotropy with the use of sphero-cylindrical particles composed of two hemispheres of radius D separated by a cylinder of length L (Fig. 3A). In this system, the degree of anisotropy of the nearest-neighbor interaction can be tuned by varying the aspect ratio L/D. At the optimal aspect ratio, $L/D = 2^{1/3} - 1 \simeq 1/4$, the interaction energies of the nose-to-tail and side-by-side alignments become equal. As a result, the defect energies are reduced to $\varepsilon_1 \simeq \zeta(2)/4 \simeq 0.41$ and $\varepsilon_3 \simeq -0.10$. The negative junction energy indicates that the proliferating junctions are no longer thermal defects but the dominant structural element, so our picture does not apply. The attractive interaction, which is proportional to number junctions, is also amplified and the resulting LGT occurs more easily. The optimal sphero-cylinders retain the ability to cluster isotropically in three-dimensional aggregates like simple liquid particles, as seen in simulations (*29*). As the aspect ratio L/D shifts from its optimal value, the energy of the junctions increases, which exponentially decreases their number, and the phase separation eventually disappears. In the phase diagram, this nonmonotonic behavior is manifested by the appearance of reentrant two-phase coexistence "islands" (*28*, *29*).

A similar enhancement of junction formation may be achieved by the introduction of a short-range attraction. Junctions ac-

quire an additional contact point whereas ends lose one when chains are broken. Accounting for the contribution of the cohesive energy, δ (in units of u_d) the defect energies shift like $\varepsilon_3 \rightarrow \varepsilon_3 - 1/2\delta$ and $\varepsilon_1 \rightarrow \varepsilon_1 + 1/2\delta$. In particular, the critical temperature increases like $T_c^* \rightarrow T_c^* + 1.05\delta$ and the reentrant coexistence curve evolves to a parabolic shape, typical of isotropic fluids (Fig. 3B). The crucial influence that the shape of the particles, their short-range interaction, and polydispersity have on their phase behavior can therefore be tested by measurement of the shape of the coexistence curve.

References and Notes

1. R. E. Rosensweig, *Science* **271**, 614 (1996).
2. T. C. Halsey, *Science* **258**, 761 (1992).
3. Of course, if enough isotropic attraction is added (e.g., van der Waals dispersion interaction), the usual isotropic three-dimensional aggregation is restored, and the resulting LGT does occur. However, the interesting and controversial point is whether phase separation can be driven by the dipolar interaction alone.
4. M. E. van Leeuwan, B. Smit, *Phys. Rev. Lett.* **71**, 3991 (1993).
5. M. J. Stevens, G. S. Grest, *Phys. Rev. Lett.* **72**, 3686 (1994).
6. D. Levesque, J. J. Weis, *Phys. Rev. E* **49**, 5131 (1994).
7. J. M. Tavares, J. J. Weis, M. M. Telo da Gama, *Phys. Rev. E* **59**, 4388 (1999).
8. P. G. de Gennes, P. A. Pincus, *Phys. Kondens. Mater.* **11**, 189 (1970).
9. A. P. Gast, C. F. Zukoski, *Adv. Colloid Interface Sci.* **30**, 153 (1989) .
10. R. P. Sear, *Phys. Rev. Lett.* **76**, 2310 (1996).
11. R. van Roij, *Phys. Rev. Lett.* **76**, 3348 (1996).
12. Y. Levin, *Phys. Rev. Lett.* **83**, 1159 (1999).
13. P. J. Camp, J. C. Shelley, G. N. Patey, *Phys. Rev. Lett.* **84**, 115 (2000).
14. E. Dubois, V. Cabuil, F. Boué, R. Perzynski, *J. Chem. Phys.* **111**, 7147 (1999).
15. In their system, the particles are relatively small and the resulting dipolar interactions are weak. The formation of long chains is thus not likely, and our model of defect-induced phase separation may not apply.
16. S. Banerjee, R. B. Griffiths, M. Widom, *J. Stat. Phys.* **93**, 109 (1998).
17. This may be demonstrated by considering one spherical particle that belongs to an infinite, straight chain. The interaction of one sphere with the rest of the chain is

$$-2u_d \sum_{n=1}^{\infty} n^{-3} = -2u_d\zeta(3)$$

which is only $\zeta(3) - 1 \simeq 20\%$ larger than the interaction of the sphere with its two nearest neighbors, $-2u_d$.
18. Although junctions of even higher coordination number are also possible, they occur very rarely due to their higher energetic cost and lower entropy.
19. J. C. Wheeler, P. Pfeuty, *J. Chem. Phys.* **74**, 6415 (1981).
20. T. J. Drye, M. E. Cates, *J. Chem. Phys.* **96**, 1367 (1992).
21. T. Tlusty, R. Menes, S. A. Safran, R. Strey, *Phys. Rev. Lett.* **78**, 2616 (1997).
22. A. Bernheim-Grosswasser, T. Tlusty, S. A. Safran, Y. Talmon, *Langmuir* **15**, 5448 (1999).
23. P. G. de Gennes, *Scaling Concepts in Polymer Physics* (Cornell Univ. Press, Ithaca, NY, 1979), chaps. IX–X.
24. Minimizing the ideal-gas free energy of noninteracting defects, $f_d = k_BT\rho_d(\ln\rho_d - 1) + \rho_d\varepsilon_d$, where ρ_d is the density of the defects and ε_d their energy cost, one finds the optimal density $\rho_d^* = e^{-\varepsilon_d/k_BT}$ and the minimal free energy, $f_d^* = -k_BT\rho_d^*$.
25. Thinking of the self-assembling chains as the edges of a graph whose vertices are either junctions or ends, one finds that the density of vertices is $v = \rho_1 + \rho_3$ whereas the density of edges is $e = 1/2\rho_1 + 3/2\rho_3 = v + 1/2(\rho_1 - \rho_3)$. This implies that at the critical point $e = v = 2\rho_1 = 2\rho_3$, the minimal graph connecting v vertices, a tree with $e = v$ edges, becomes thermodynamically feasible.
26. T. Tlusty, S. A. Safran, R. Strey, *Phys. Rev. Lett.* **84**, 1244 (2000).
27. K. Sano, M. Doi, *J. Phys. Soc. Jpn.* **52**, 2810 (1983).
28. J. C. Shelley, G. N. Patey, D. Levesque, J. J. Weis, *Phys. Rev. E* **59**, 3065 (1999).
29. S. C. McGrother, G. Jackson, *Phys. Rev. Lett.* **76**, 4183 (1996).

30. We acknowledge fruitful discussions with J. Klein, R. E. Rosensweig, P. A. Pincus, and A. Zilman and support from The Israel Science Foundation center on Self-Assembly and the donors of the Petroleum Research Fund, administrated by the American Chemical Society.

9 August 2000; accepted 22 September 2000

Macroscopic Fibers and Ribbons of Oriented Carbon Nanotubes

Brigitte Vigolo,[1] Alain Pénicaud,[1] Claude Coulon,[1] Cédric Sauder,[2] René Pailler,[2] Catherine Journet,[3]* Patrick Bernier,[3] Philippe Poulin[1]†

A simple method was used to assemble single-walled carbon nanotubes into indefinitely long ribbons and fibers. The processing consists of dispersing the nanotubes in surfactant solutions, recondensing the nanotubes in the flow of a polymer solution to form a nanotube mesh, and then collating this mesh to a nanotube fiber. Flow-induced alignment may lead to a preferential orientation of the nanotubes in the mesh that has the form of a ribbon. Unlike classical carbon fibers, the nanotube fibers can be strongly bent without breaking. Their obtained elastic modulus is 10 times higher than the modulus of high-quality bucky paper.

Theoretical predictions (*1*, *2*) and measurements on individual objects (*3*–*5*) suggest that single-walled carbon nanotubes (SWNTs) (*6*) could form the basis of materials with exceptional mechanical and electromechanical properties. Despite their intrinsic rigidity and high anisotropy, the currently available macroscopic forms of SWNTs are isotropic and rather fragile. These forms mainly consist of raw powder-like materials originating from synthesis (*7*, *8*), suspensions in solvents (*9*), and thin mats, known as bucky paper, obtained by drying SWNT suspensions (*10*). Processing nanotubes on macroscopic scales to obtain materials with more practical uses is a major challenge. Here we report a simple and versatile approach that can create rigid fibers and ribbons of preferentially oriented SWNTs (*11*). Our processing consists of dispersing the nanotubes in surfactant solutions and then recondensing the nanotubes in the stream of a polymer solution. In contrast to most ordinary carbon fibers, SWNT fibers can be strongly bent and even tightly tied without breaking. Although they are still weak under tension, these recently obtained SWNT fibers are already 10 times stronger than high-quality bucky paper, the main macroscopic form of SWNT nanotubes used so far (*12*).

The raw material we used was produced with the electric-arc technique (*8*). This technique produces SWNTs in the form of bundles of a few nanotubes, along with a certain fraction of carbon impurities and catalysts. This material was sonicated in aqueous solutions of sodium dodecyl sulfate (SDS), a surfactant that adsorbs at the surface of the nanotube bundles. At low surfactant concentrations, large and dense clusters of the initial material were still found after sonication. The amount of surfactant was too low to produce an efficient coating and induce electrostatic repulsions that could counterbalance van der Waals attractions (*13*). At higher SDS concentrations, black and apparently homogeneous suspensions were obtained. These suspensions did not coarsen or phase-separate macroscopically over several weeks. However, as revealed by optical microscopy (Fig. 1), dielectric measurements, and electron microscopy of freeze-fractured samples, these systems can in fact exhibit distinct phases. At intermediate concentrations of SDS, SWNTs were homogeneously dispersed and formed a single phase. The viscosity of these systems was almost that of pure water. In this regime, the electrostatic repulsion provided by adsorbed surfactants stabilized the nanotubes against van der Waals attraction. However, at higher SDS concentrations, a texture that reflected the formation of light clusters was observed. The clusters, which did not coarsen over several weeks,

[1]Centre de Recherche Paul Pascal/CNRS, Université Bordeaux I, Avenue Schweitzer, 33600 Pessac, France. [2]Laboratoire des Composites Thermostructuraux, Allée de la Boëtie, 33600 Pessac, France. [3]Groupe de Dynamique des Phases Condensées, Université de Montpellier II, 34095 Montpellier, France.

*Present address: Université Claude Bernard, Lyon I, 43 boulevard du 11 novembre 1918, 69622 Villeurbanne, France.

†To whom correspondence should be addressed. E-mail: poulin@crpp.u-bordeaux.fr

7

Summary and Outlook

7.1 Summary of Theory and Results

The framework of our model is a self-assembling network whose building blocks are linear branches interconnected by z-fold junctions. The physically relevant coordination numbers are $z = 3$ for the network junctions and $z = 1$ for the "end-caps" of disconnected globules. In the case of microemulsions, the branches are semi-flexible amphiphile tubes of water-in-oil or oil-in-water (Fig. 1.2), while in the case of dipolar fluids they are linear chains of dipolar, colloidal particles (Fig. 1.3). The model is solved by a mean field treatment [98] or by an equivalent spin $n \to 0$ approach [99, 100, 101] to give the same result: Each topological defect, whether it is a 3-fold junction or an end-cap, yields a contribution of $-k_BT$ to the free energy, f. Nevertheless, the number density of such defects, ρ, scales differently for connected or disconnected topologies: $\rho \sim e^{-\epsilon}\phi^{z/2}$, where ϵ is the energy cost of the defect and ϕ is the volume fraction of the network. It follows directly that the osmotic pressure, $\pi = \phi\partial_\phi f - f \sim 1 - z/2$, is positive for free branches ($z = 1$) while for networks ($z \geq 3$) the osmotic pressure is negative, a clear indication for the topologically induced attraction.

The effective attraction due to the entropy of the network junctions competes with the repulsion between the fluctuating branches. Another relevant contribution to the free energy arises from occurrence of "dead-ends" in the network. Since the aforementioned interactions are all purely geometrical the thermodynamic behavior is universal, in accord with experiment [43]. Indeed, material specific interactions may cause slight deviations from universality in the two systems studied here, nevertheless the substantial structural and thermodynamic features remain common to both systems.

Microemulsions

The large-scale topology of the network is characterized by the typical distance, L, between the 3-fold junctions which is governed by the translational entropy of the junctions. Within the microemulsion network one can identify an additional *local* length scale, the radius of the cylinders, R, that is governed by the curvature energy of the amphiphile interface. Our theory traces the progression of the microstructure from the curvature-governed, dilute network, $L \gg R$, to the strong fluctuation regime, where the junction defects proliferate. Consequently, the typical distance between junctions becomes comparable with their size, $L \sim R$, and they form a dense sponge. We have explained the microemulsion thermodynamics as the outcome of the simultaneous action of two distinct mechanisms: The large-scale, global network statistics and the local curvature energy [56].

Topological transitions – . Our theory predicts a series of topological transitions with changing spontaneous curvature, c_0: At high spontaneous curvature the stable phase is of spherical globules. As c_0 decreases, the microemulsion evolves from spherical globules to long cylinders that subsequently interconnect by 3-fold junctions, leading to the formation of a bicontinuous network as the system approaches the symmetric region, $c_0 = 0$ [56, 58]. The connectivity transition, from separate cylinders

to the bicontinuous network, is governed by thermal fluctuations of the topological defects. We have found that this transition occurs around the line where the junction and end-cap densities are equal. This theoretical prediction for the topological transition, spheres → spheres + cylinders → cylinders → network (Fig.1 Chap. 3), was recently substantiated by direct cryo-TEM measurements of non-ionic microemulsion [57].

Phase instabilities and reentrance – . Within the fluctuating network model we have identified two distinct phase instabilities corresponding to the local and global contributions to the free energy: In the *emulsification failure* instability [48] it is the local curvature energy that is optimized at a particular globule size (related to the oil, water and amphiphile volume fractions) and is characterized by the rejection of an excess phase. By rejecting the excess phase, the microemulsion tunes the radius of the cylinders to minimize their curvature energy. Since the local energy is not sensitive to connectivity, we suggested that the emulsification failure observed in disconnected globules [103] also occurs in networks, in accord with experiment [57]. Apart from this local instability, the bicontinuous network exhibits a unique instability which results directly from the fluctuations of the junctions. Due to the connectivity of the network, these fluctuations lead to a polydispersity of the lengths of the cylindrical branches; when the resulting effective attraction of the network, $-\rho \sim -\phi^{3/2}e^{-\epsilon}$, overcomes the excluded volume repulsion between the branches, the network becomes unstable to phase separation.

The reentrant phase separation loops and the subsequent 3-phase coexistence are direct consequences of the non-monotonic dependence of the junction energy on the cylinder radius. The curvature energy of the junction exhibits a minimal value at an optimal radius, R^*, which corresponds to a steep maximum of the attraction [58] and to the strongest tendency to phase separate. If this maximal attraction exceeds a critical value, the microemulsion phase separates into two networks of the same cylindrical radius which differ in the density of junctions, as verified by experiment [57]. For either larger radii or smaller radii than R^* the attraction may become less than its critical value and the system becomes single phase, which is the origin of the closed loop. In the phase diagram this *global* instability is manifested by the appearance of a 2-phase coexistence loop bounded by two critical points (Fig. 1 Chap. 2).

As the spontaneous curvature is decreased, the loops expand until cylinder radius increase and the networks become unstable to emulsification failure, in which the system rejects an additional excess phase. The consequent 3-phase coexistence between two microemulsion networks, dense and dilute, together with an excess phase, signifies the simultaneous occurrence of both global and local instabilities. The resulting scaling laws are in good agreement with the universal phase-diagrams [50, 51] in both the 2-phase and 3-phase temperature regimes (Fig. 3 Chap. 2). The source of this universality is purely geometrical; it is the connectivity of the microemulsion network that provides an inherent, material independent, topological mechanism for attraction. Recent cryo-TEM experiments proved our prediction that indeed the coexisting phases are two microemulsion networks in the closed loop, accompanied by an excess phase in the 3-phase region (see Fig. 3 Chap. 4).

Interfacial tension – . The network model provides insight into the physics underlying the microemulsion ultra-low tension. We have found that the interfacial tension between a microemulsion network and an excess phase may be explained, and easily calculated as the free energy per unit area required to unfold a segment of the fluctuating network to a planar monolayer. For large spontaneous curvature, c_0, the dominant contribution to the microemulsion free energy is the elastic energy of the flattened interface due to the difference between its curvature energy and the optimal value at the network. This scales like c_0^2 and therefore vanishes at the symmetric point $c_0 = 0$. In this strong fluctuation regime an additional contribution due to the loss of network entropy determines the finite, ultra-low value of the tension. The universal, theoretical prediction of the interfacial tension between a network and its excess phase (Fig. 2 3) were found to be in good agreement with the experimental data collapse of Sottmann and Strey [50].

In another scenario, when the two coexisting phases are both networks, the corresponding interface is a continuous transition layer separating regions where the branches have the same radius but their local density (or the density of junctions) differs. We have treated this case within a mean field theory and found that the consequent balance of the three surface forces (between the two networks and between each network and the mutual excess phase) leads to the wetting transition that was measured close to the appearance of the 3- phase coexistence [38, 55].

Shape and energy topological of defects – . As mentioned above, a connected network forms when the number of junctions exceeds the number of end-caps (Fig. 7.2). This transition occurs when the curvature energies of both defects are approximately equal. An accurate estimate of the energies is therefore a crucial ingredient of our theory. The curvature energy of these two types of defects includes two contributions: (i) A topological invariant proportional to the number of "handles" in the system which is exactly the difference between the number of junctions and end-caps $\rho_3 - \rho_1$; the junction and the end-cap therefore have opposite topological contributions . (ii) A contribution due to the deviation of the mean curvature of the amphiphilic surface from its preferred value, the spontaneous curvature, c_0. To optimize this shape-dependent part of the defect curvature energy, we have used a numerical minimization code [102] and compared the results with a simplified analytical approximation. We have found that junctions are preferred at low values of the spontaneous curvature due to their flat lamellar core, while end-caps are preferred at larger c_0 due to their curved spherical cap (Fig. 2 Chap. 5). The cross over between these two regimes defines the cylinder $\rightarrow$ network transition line [58].

Dipolar Fluids

Liquid-gas transition – . Our work suggests an alternative mechanism for liquid-gas transition in dipolar systems even in the absence of any extrinsic non-dipolar interactions. The basic components of our model are not the dipolar spheres themselves but the ensemble of self-assembling chains that they form [84]. This approach allows us to focus on the many-body, large-scale features of the system that are inaccessible to "microscopic" treatments. We suggest that the same topologically induced attraction responsible for phase separation in microemulsions can lead to a to liquid-gas transition in dipolar fluids. We have found that in zero external magnetic field, 3-fold junctions have defect energies that are lower than those of the end-caps and the dipolar chains therefore tend to form networks. This difference in energy increases as the particles become more anisotropic (e.g. sphero-cylinders [96, 97]). There is some preliminary evidence for branched structures from simulations and experimental studies of ferrofluids [93, 94, 95]. The attraction and phase separation in our network formalism are not related to the individual dipolar spheres, but rather to the topological defects of the chains – the network junctions. The proposed phase separation, which is driven by effective attraction within the fluctuating networks results in an equilibrium between two dipolar networks with differing density of junction points. Simulation studies of dipolar fluids in the low-temperature, dilute regime encounter severe numerical difficulties due the strongly collective nature of the thermal fluctuations which imposes very long relaxation times. Despite these difficulties, recent studies [89] has found some preliminary evidence supporting our suggestion that junction attraction is indeed the mechanism underlying the liquid-gas transition of dipolar systems.

Reentrant phase separation – . As mentioned above, the evasive liquid-gas transition of dipolar hard spheres is difficult to observe due to the small scales of density and free energy scales and the long relaxation times that stem from the anisotropic chaining (in our network picture the relevant parameters are the dilute junction density and entropy) [73]-[84]. However, one can overcome the strong anisotropy by relaxing the spherical symmetry using sphero-cylindrical particles. In this system, the degree of anisotropy of the nearest-neighbor interaction can be tuned by varying the aspect ratio of the sphero-cylinders. As a result, the sphero-cylinder fluid exhibits an optimal aspect ratio where the energy cost of a junction is minimal. Around this optimal point, the junctions proliferate, their attractive interaction is amplified and the resulting liquid-gas transition is more easily observed (Fig. 7.1). This is analogous to the optimal, tunable cylinder radius of the microemulsion network. Similarly, our theory reproduces reentrant liquid-gas separation regions in the phase diagram; these same "islands" were observed in recent numerical simulations [96, 97]. Motivated by this deep analogy between microemulsions and dipolar fluids, we suggest that the physical features mentioned above, the formation of a fluctuating network with its effective attraction and the resulting phase separation, are generic to linearly aggregating systems and may be a key to the understanding of other basic physical features such as rheology and scattering.

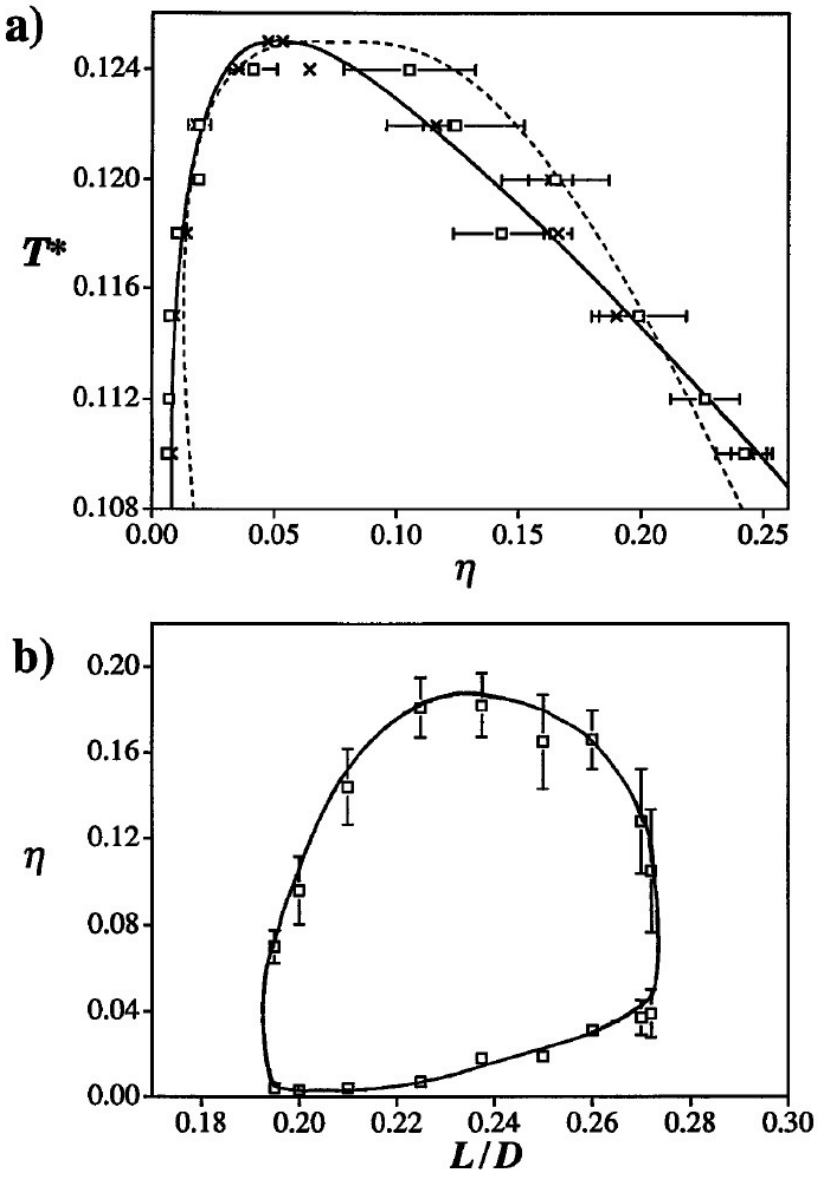

FIGURE 7.1. **Dipolar two-phase coexistence "islands"** — (*a*) The vapor-liquid coexistence curve for the dipolar hard sphero-cylinders of aspect ratio $L/D = 1/4$, obtained from Monte-Carlo simulations of McGrother and Jackson [96]. (*b*) The effect of the aspect ratio on the densities of the coexisting vapor and liquid phases for a fixed temperature of $T^* = 0.12$ (Note the similarity to the closed loops in the microemulsion system).

7.2 Conclusions

Our theory predicts that linearly aggregating systems, such as microemulsions or dipolar fluids, may self-assemble to form large-scale fluctuating networks (Figs. 1.2,1.3). This approach focuses on the topologically induced interactions within such networks and provides a unified understanding of both structure and thermodynamics over wide regions in the phase diagram. The junctions that connect the linear branches of the network may be considered as topological defects. The energetically favorable state of the amphiphile molecules or dipolar particles is one of chains or cylinders (the branches of the network). The formation of topological defects costs energy (curvature energy in the case of microemulsion or dipole interaction in dipolar fluids), while their presence increases the entropy of the system. It is exactly this interplay between the defect (i.e. the junction) energy and the network configurational entropy that determines the network topology.

Due to its universal, topological character, the fluctuating network model may be applied to various systems of different microscopic interactions. Our current work on dipolar fluids suggests that concepts and results derived for microemulsion systems can be generalized to other kinds self-assembling networks. The deep analogy between dipolar fluids and microemulsions, two systems of very different microscopic interactions, motivates us to suggest that these thermodynamic and structural features are generic to linearly aggregating systems and may therefore shed light on the basic properties of polar and network-forming fluids. Dipolar chaining at the single-molecule level was recently demonstrated by the observation of cyanide (HCN) chains in superfluid helium [105]. Similar linear and cyclic structures of small water clusters, connected by hydrogen bonds have been predicted by ab initio molecular calculations [106] and later have been spectroscopically verified [107]. The unusual thermodynamic features of water, such as the well-known density maximum at 4^oC [108], are attributed to the network formed by hydrogen bonds [109]. In addition, chaining and branching by dipolar forces or hydrogen bonds strongly modifies the nucleation of anisotropic fluids, leading to scaling laws that deviate off the predictions of classical, isotropic nucleation theory [110].

Another area that is worthy of further study are binary micellar solutions. Drye and Cates [98] have predicted that micellar solutions, under certain conditions of concentration, temperature and salinity, may form large-scale network, in accord with cryo-TEM measurements [111]. A recent set of experiments Bernheim-Grosswasser, Talmon and Wachtel has found direct evidence for the existence of micellar $C_{12}E_5$- in-water networks close to the lower critical point, which might relate the observed criticality to the network-induced criticality of microemulsions [112]. Similar network-induced mechanisms may play a role in the phase transitions observed in physical gels [113].

Formulating the self-assembling network model as a Heisenberg spin system with $n \to 0$ components provides a more rigorous vehicle to deeply explore properties of amphiphilic systems and dipolar fluids. This approach, which yields a free energy [88] very similar to the result of mean-field Flory model [98], has

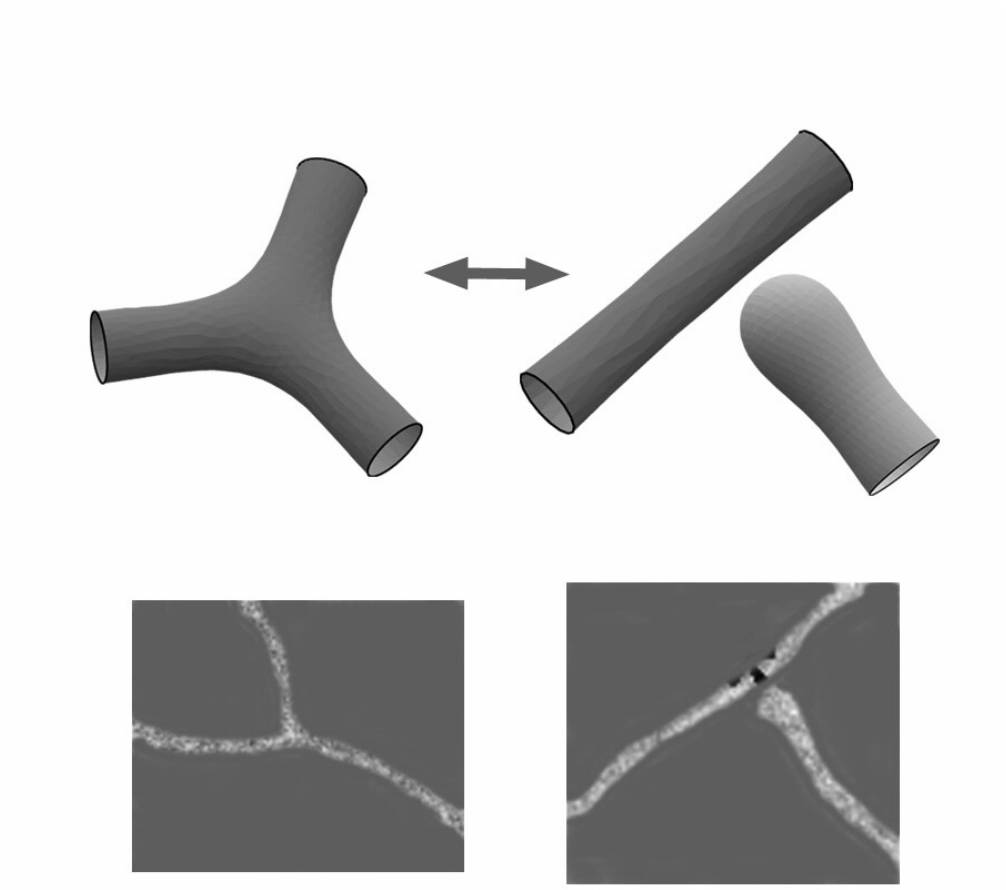

FIGURE 7.2. **Topological defects** — The connectivity transition, as a threefold Y-like junction forms from an end-cap. The theoretical shape of the junction, as calculated by numerical minimization, has a lamellar core, while the cylinder terminates with an enlarged spherical end cap (top). This prediction was verified by recent cryo-TEM measurements of Bernheim-Grosswasser and Talmon (bottom).

been recently used to calculate non-equilibrium properties of microemulsions, especially the correlation functions and the consequent scattering, $S(q)$ curve [101]. The spin $n \to 0$ approach seems like a natural candidate to treat the rheological properties of self-assembling networks, especially their viscoelastic characteristics. Another major advantage of the spin model is its ability to treat dense, sponge-like networks where junction-junction correlation and excluded-volume interactions are important. A main goal of this study is prediction of the evolution of the typical "sponge-peak" in the scattering curve as the sponge is diluted into a low-density network [101].

The spin model might be fruitful in the study of the field responsive properties of dipolar fluids [59, 60, 70], especially the non-linear dependence of the shear and the yield-strength of magneto- and electro-rheological fluids on the field magnitude [114]. Another related open question is the nature of the mechanism leading to the field-induced phase separation of dipolar fluids [115, 116].

References

[1] *Molecular Biology of the Cell*, B. Alberts et al. (Garland, New York 1994).

[2] *Molecular Cell Biology*, H. Lodish et al. (Freeman, 1998).

[3] *Statistical Thermodynamics of Surfaces, Interfaces and Membranes*, S. A. Safran (Addison-Wesley, 1994).

[4] W. H. Gilbert and A. Ben-Shaul, *J. Phys. Chem* **100,** 13169 (1996).

[5] *Complex Fluids,* MRS Symposium Proceedings **248**, E. B. Sirota, D. Weitz, T. Witten and J. Israelachvili, eds. (MRS 1991).

[6] *Introduction to Solid State Physics*, C. Kittel (Wiley, 1986). This range of elastic moduli refers to pure solids. However, under most realistic conditions, the deformability of matter is increased by the presence of defects and impurities. For the role of defects see [7]-[10] below.

[7] S. A. Safran, *Adv. Phys.* **48,** 395 (1999).

[8] *Theory of Elasticity,* L. D. Landau and E. M. Lifshitz (Oxford, 1986).

[9] *Defects and Geometry in Condensed Matter Physics,* D. R. Nelson (Cambridge University, 2002).

[10] *Principles of Condensed Matter Physics*, P. M. Chaikin and T. C. Lubensky (Cambridge University, 1995).

[11] T. A. Witten and L. M. Sander, *Phys. Rev. Lett.* **47**, 1400 (1981).

[12] T. A. Witten, in *Chance and Matter*, 46th Les Houches Summer School, eds. J. Vannimenus and R. Stora (North Holland, 1987).

[13] G. Gompper and M. Schick, *Self-Assembling Amphiphilic Systems* (Academic, New-York, 1994).

[14] *Curr. Op. Colloid and Interface*, **2** (1997), This issue contains discussion of self-assembly in theory and experiment (S. A. Safran and M. E. Cates, eds.).

[15] M. W. Matsen, F. S. Bates, *Macromolecules,* **29** (23), 7641 (1996).

[16] N. Koneripally, R. Levicky, F. S. Bates, M. W. Matsen, S. K. Satija, J. Ankner, H. Kaiser, *Macromolecules,* 31(11), 3498 (1998).

[17] F. S. Bates and G. H. Fredrickson, *Physics Today* 32 (February 1999).

[18] *Supramolecular Materials*, ed. J. S. Moore, MRS bulletin **25**(4), 26 (2000).

[19] E. Winfree, F. R. Liu, L. A. Wenzler, N. C. Seeman, *Nature* **394**, 539 (1998).

[20] W. Helfrich, *Z. Naturforsch* **33a**, 305 (1978).

[21] *Statistical Physics* Part 1, L. Landau and E. M. Lifshitz (Pergamon, Oxford, 1980), p. 537.

[22] *Micelles, Membranes and Microemulsions and Monolayers*, eds. W. M. Gelbart, A. Ben-Shaul and D. Roux (Springer, Berlin 1994).

[23] For reviews: *Statistical Mechanics of Membranes and Surfaces*, D. Nelson, S. Weinberg eds. (World Scientific, Singapore, 1989).

[24] *Modern Ideas and Problems in Amphiphilic Science*, W. M. Gelbart, D. Roux, A. Ben-Shaul eds. (Springer, Berlin, 1994).

[25] *Microemulsions - Proceedings of the International Discussion Meeting of the Deutsche Bunsen-Gesselschaft, Göttingen, 1995*, Ber. Bunsenges. Phys. Chem. **100** (3).

[26] *Fluctuating Geometries in Statistical Mechanics and Field Theory : Proceedings of the Les Houches Summer School, Session Lxii*, F. David, J. Zinn-Justin ,P. Ginsparg, eds. (Elsevier 1996).

[27] J. H. Schulman, W. Stoeckenius, and L. M. Prince, *J. Phys. Chem.* **63**, 1677 (1959), where the term **microemulsions** was suggested for the first time: "an optically isotropic transparent oil and water dispersion".

[28] For an updated review of scaterring techniques applied to microemulsions: O. Glatter, R. Strey, K. -V. Schubert, and E. Kaler, in Ref. [25], 323.

[29] W. Jahn and R. Strey, *J. Chem. Phys.* **92**, 2294 (1988).

[30] R. Strey, *Colloid Polym. Sci.* **272**, 1005 (1994).

[31] Discussion of state-of-the-art of transmission electron microscopy: Y. Talmon, in Ref. [25], 364.

[32] T. P. Hoar and J. H. Schulman, *Nature* **152**, 102 (1943).

[33] P. A. Winsor, *Trans. Faraday Soc.* **44**, 376 (1948).

[34] M. Kahlweit, *Science* **240**, 617 (1988).

[35] K. Shinoda and H. Saito, *Colloid Interface Sci.* **26**, 70 (1968).

[36] M. Kahlweit, R. Strey, and G. Busse, *Phys. Rev. E* **47** 4197 (1993).

[37] M. Kahlweit, R. Strey and P. Firman, *J. Phys. Chem.* **90** 671 (1986).

[38] M. Kahlweit, R. Strey, D. Hasse, and P. Firman, *Langmuir* **4**, 499 (1988).

[39] R. Strey, *Ber. Bunsenges. Phys. Chem.* **100**(3), 182 (1996).

[40] P. Kilpatrick et al., *J. Phys. Chem* **90**, 5292 (1986).

[41] M. Kahlweit, R. Strey and G. Busse, *J. Phys. Chem.* **94**, 3881 (1990).

[42] T. Sottmann, R. Strey, *J. Phys.: Cond. Mat.* **8** ,A39 (1996).

[43] T. Tlusty, R. Menes, S. A. Safran and R. Strey, *Phys. Rev. Lett.* **78**, 2616 (1997).

[44] M. Teubner and R. Strey, *J. Chem. Phys.*, **87**, 3195 (1987).

[45] P. G. de Gennes and C. Taupin, *J. Phys. Chem* **86**, 2294 (1982).

[46] P. Pieruschka and S. A. Safran, *Europhys. Lett.* **22**, 625 (1993).

[47] R. Aveyard and T. A. Lawless, J. Chem. Soc., Faraday Trans. 1, **82**, 2951 (1986).

[48] This decomposition process is termed "emulsification failure": S. A. Safran and L. A. Turkevich, *Phys. Rev. Lett.* **50**(24), 1930 (1983).

[49] M. Aratono, M. Kahlweit, *J. Chem. Phys.* **95**, 8578 (1991).

[50] T. Sottmann, R. Strey, *J. Chem. Phys.* **106**, 8606 (1997).

[51] T. Sottmann, R. Strey, *Ber. Bunsenges. Phys. Chem.* **100**(3), 237 (1996).

[52] T. Sottmann, R. Strey, S. -H. Chen, *J. Chem. Phys.* **106**, 6483 (1997).

[53] for a detailed review of microemulsion theories see Ref. [13].

[54] S. A. Safran, L. A. Turkevich and P. A. Pincus, *J. Phys. Lett.* **45** L-19 (1984).

[55] B. Widom, *Langmuir* **3**, **12** (1987).

[56] T. Tlusty, S. A. Safran and R. Strey, *Phys. Rev. Lett.* **84**, 1244 (2000).

[57] A. Bernheim-Grosswasser, T. Tlusty, S. A. Safran, Y. Talmon, *Langmuir* **15**, 5448 (1999).

[58] T. Tlusty, S. A. Safran, *J. Phys.: Cond. Mat.* **12**, A253 (2000).

[59] R. E. Rosensweig, *Science* **271**, 614 (1996).

[60] *Ferrohydrodynamics,* R. E. Rosensweig (Cambridge University , 1985).

[61] Q. A. Pankhurst, R. J. Pollard, *J.Phys.:Condens.Matter* **5,** 8487 (1993).

[62] T. C. Halsey, *Science* **258**, 761 (1992).

[63] For a detailed review of the history of the problem and current state of research : P. I. C. Teixeira, J. M. Tavares, M. M. Telo da Gama, *J.Phys.:Condens.Matter* **12**, R411 (2000).

[64] C. Menager, L. Bellony, V. Cabuil, M. Dubois, M. Gulik-Krzywicki, T. Zemb, *Langmuir* **12** ,3516 (1996).

[65] W. H. Keesom, *Phys. Z.* **22**, 129 (1921).

[66] K. Sano, M. Doi, *J. Phys. Soc. Japan* **52**, 2810 (1983).

[67] P. G. de Gennes, P. A. Pincus, *Phys. Kond. Mat.* **11**, 189 (1970).

[68] J. R. Thomas, *J. Appl. Phys.* **37**, 2914 (1966).

[69] A. P. Gast, C. F. Zukoski, *Adv. Colloid Interface Sci.* **30**, 153 (1989) .

[70] E. M. Furst and A. P. Gast, *Phys. Rev. E* **61**, 6732 (2000).

[71] H. Zhang, M. Widom, *Phys. Rev. E* **51,** 2099 (1995).

[72] An interesting example of chain formation in nature is exhibited by the magnetotatic bacteria which have backbones consisting of short, stiff chains of magnetite grains. The chains enable them to swim along the lines of the Earths magnetic field: R. P. Blakemore, *Science* **190** , 377 (1975).

[73] J. J. Weis, D. Levesque, *Phys. Rev. Lett.* **71**, 2729 (1993).

[74] M. E. van Leeuwan, B. Smit, *Phys. Rev. Lett.* **71**, 3991 (1993).

[75] M. J. Stevens, G. Grest, *Phys. Rev. Lett.* **72**, 3686 (1994).

[76] D. Levesque, J. J. Weis, *Phys. Rev. E* **49** 5131 (1994).

[77] R. P. Sear, *Phys. Rev. Lett.* **76**, 2310 (1996).

[78] R. van Roij, *Phys. Rev. Lett.* **76**, 3348 (1996).

[79] Y. Levin, *Phys. Rev. Lett.* **83**, 1159 (1999).

[80] C. Quillet, V. Ponsinet, V. Cabuil, *J. Phys. Chem.* **98**, 3566 (1994).

[81] M. A. Osipov, P. I. C. Texiera, M. M. Telo da Gama, *Phys. Rev. E* **54**, 2597 (1996).

[82] J. M. Tavares, M. M. Telo da Gama, M. A. Osipov, *Phys. Rev. E* **56**, 6252 (1997).

[83] S. H. L. Klapp, F. Forstmann, *J. Chem Phys.* **106**(23), 9742 (1997).

[84] J. M. Tavares, J. J. Weis, M. M. Telo da Gama, *Phys. Rev. E* **59**, 4388 (1999).

[85] M. S. Stevens and G. H. Grest, *Phys. Rev. E* **51**, 5962 (1995).

[86] M. S. Stevens and G. H. Grest, *Phys. Rev. E* **51**, 5976 (1995).

[87] I. Szalai, D. Handerson, D. Boda, K. -Y. Chen, *J. Chem. Phys.* **111**, 737 (1999).

[88] T. Tlusty, S. A. Safran, *Science* **290**, 1328 (2000).

[89] P. J. Camp, J. C. Shelley, G. N. Patey, *Phys. Rev. Lett.* **84**, 115 (2000).

[90] E. Dubois, V. Cabuil, F. Boué, R. Perzynski, *J. Chem. Phys.* **111**, 7147 (1999).

[91] J. C. Bacri, R. Perzynski, D. Salin, V. Cabuil, R. Massart, *J. Colloid Interface Sci.* **132**, 43 (1989).

[92] E. Dubois, R. Perzynski, F. Boué, V. Cabuil , Langmuir **16**, 5617 (2000).

[93] S. W. Davis et al., *Phys. Rev. E* 59, 2424 (1999).

[94] G. N. Coverdale et al., *J. Mag. Mag. Mat.* 188, **41** (1998).

[95] J. C. Bacri et al., *J. Coll. Int. Sci.* **132**, 43 (1988).

[96] S. C. McGrother and G. Jackson, *Phys. Rev. Lett.* **76**, 4183 (1996).

[97] J. C. Shelley, G. N. Patey, D. Levesque, J. J. Weis, *Phys. Rev. E* **59** 3065 (1999).

[98] T. J. Drye, M. E. Cates, *J. Chem. Phys.* **96**, 1367 (1992).

[99] *Scaling Concepts in Polymer Physics*, P. G. de Gennes (Cornell University, 1979).

[100] J. C. Wheeler, P. Pfeuty, *J. Chem. Phys.* **74**, 6415 (1981).

[101] A. J. Zilman, S. A. Safran, *to be published.*

[102] K. A. Brakke, *Phyl. Trans. Roy. Soc.* **A354** (1715) , 2143 (1996).

[103] M. S. Leaver and U. Olsson, *Langmuir* **10**, 3449 (1994).

[104] S. Banerjee, R. B. Griffiths, M. Widom, *J. Stat. Phys.* **93,** 109 (1998).

[105] K. Nauta and R. E. Miller, *Science* **283**, 1895 (1999).

[106] K. Liu, J. D. Cruzan, R. J. Saykally, *Science* **271**, 929 (1996).

[107] K. Nauta and R. E. Miller, *Science* **287**, 293 (2000).

[108] P. H. Poole, F. Sciortino, U. Essman, H. E. Stanley, *Nature* **360**, 324 (1992).

[109] P. H. Poole, F. Sciortino, T. Grande, H. E. Stanley, C. Austen Angell, *Phys. Rev. Lett.* **73**, 1632 (1994).

[110] P. R. Ten Wolde, D. W. Oxtoby, D. Frenkel, *Phys. Rev. Lett.* **81**, 3695 (1998).

[111] D. Danino, Y. Talmon, H. Levy, G. Beinert, R. Zana, Science **269,** 1420 (1995).

[112] A. Bernheim-Grosswasser, E. Wachtel, Y. Talmon, *Langmuir* **16**, 4131 (2000).

[113] M. Annaka, T. Tanaka, Nature 355, 430 (1992).

[114] *The Materials Science of Field Responsive Materials,* 1998, P. P. Phule and G. M. Gender, eds., MRS Bulletin **23** (8), 19 (1998).

[115] R. E. Rosensweig and J. Popllewell, in *Electromagnetic Forces and Applications*, J. Tani, T. Tagaki, eds. (Elsevier, Amsterdam 1992), pp. 83-86.

[116] M. S. Stevens and G. H. Grest, *Phys. Rev. Lett.* **72**, 3686 (1994).